THE
PHYSICAL REVIEW
A Journal of Experimental and Theoretical Physics Established by E. L. Nichols in 1893
VOL. 60, No. 4 AUGUST 15, 1941 SECOND SERIES

The Structure of Electronic Bands of Polyatomic Molecules

I. Prolate Approximation for XY_2 Molecules

N. METROPOLIS
Ryerson Physical Laboratory, University of Chicago, Chicago, Illinois
(Received June 18, 1941)

A study has been made of the rotational structure of electronic bands of polyatomic molecules whose moments of inertia are related approximately like those of a symmetrical top, with the object of facilitating the interpretation of observed (resolved or unresolved) structures. The present discussion concerns non-linear XY_2 molecules, but it is also valid for all polyatomic molecules that come approximately under the prolate symmetrical top classification. The four characteristic cases of changes in dimensions during the electronic transition are considered and yield four typically different band structures. The variation in band structure with bond distance and apex angle is worked out in detail for SO_2 molecules and theoretical quantitative diagrams of band structures are given, for a temperature of 200°K. The intensity distributions shown in these diagrams are valid (for some adjusted temperature) for any polyatomic molecules in which the moments of inertia of the ground state have the same ratio as those in SO_2. If, in addition, the same is true of the moments of inertia in the upper states, then the entire band structure is identical at some adjusted scale. The correlation between rotational structure and vibrational intensity distribution is worked out, from which conclusions about the changes in dimensions of the XY_2 molecule in the transition can be made. It is shown how a qualitative examination of the observed (resolved or unresolved) rotational structure may guide or confirm the associated vibrational analysis. Finally a comparison with the available data on SO_2 and ClO_2 is made.

INTRODUCTION

THE problem of analyzing electronic bands of non-linear molecules is, at best, a complicated one. One reason for this is the fact that the expressions for the rotational energy levels of non-linear, as compared to linear, molecules contain a second rotational quantum number. As is well known, the expressions are those derived by the quantum mechanics for a freely rotating top, either symmetrical or asymmetrical.[1] The most suitable approximations will depend, for a particular molecule, upon the relative values of its three principal moments of inertia. Following the notation used by Mulliken,[2] let these be I_a, I_b, I_c with $I_a \leq I_b \leq I_c$. For planar molecules, and in particular non-linear XY_2 molecules, $I_c = I_a + I_b$, so that, in general, non-linear triatomic molecules are of the asymmetrical top type. However, there is a particular value, say $2\alpha_{ob}$, of the YXY apex angle 2α, dependent only on the masses of the X and Y atoms, such that

$$I_a = I_b = \tfrac{1}{2} I_c$$

holds, yielding an oblate-symmetrical top. Now

[1] D. M. Dennison, Phys. Rev. **28**, 318 (1926); F. Hund, Zeits. f. Physik **43**, 805 (1927); H. A. Kramers and G. P. Ittmann, Zeits. f. Physik **58**, 217 (1929); O. B. Klein, Zeits. f. Physik **58**, 730 (1929); S. C. Wang, Phys. Rev. **34**, 243 (1929); D. M. Dennison, Rev. Mod. Phys. **3**, 280 (1931); W. H. Shaffer and H. H. Nielsen, Phys. Rev. **56**, 188 (1939).

[2] A complete discussion of top and species classifications of non-linear triatomic molecules has been given recently by R. S. Mulliken, Phys. Rev. **59**, 873 (1941).

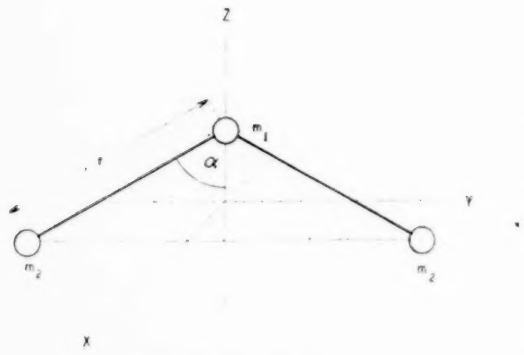

FIG. 1. XY_2 molecule.

then, if the actual value of 2α is near to $2\alpha_{ob}$, the molecule, strictly speaking, rotates like an asymmetrical top; nevertheless its wave functions and energy level patterns approximate those of the oblate-symmetrical top (see Fig. 4 of reference 2), and accordingly one may speak of the molecule as belonging to the near-oblate top classification. For 2α sufficiently far from $2\alpha_{ob}$, prolate top approximations to the wave functions and energy levels become valid. The acute near-prolate top or the obtuse near-prolate top case[2] obtains according as $\alpha \ll \alpha_{ob}$ or $\alpha \gg \alpha_{ob}$. For intermediate values of α, both symmetrical top approximations are poor.

The present discussion primarily concerns electronic spectra of non-linear XY_2 molecules in which the molecule in both upper and lower states belongs to the near-prolate top classification. Since, almost exclusively, the obtuse near-prolate case occurs in practice, the following discussion, for the most part, refers to this case. The changes necessary to cover the acute near-prolate case are quite simple and are given in the footnotes. A study of molecules which are of the near-oblate top classification in both states and of the mixed case where the top classification is different in the two states is in preparation.

For a particular XY_2 molecule, the values of the rotational constants [see Eqs. (2) below] depend, of course, on the values of the XY bond distance and of the apex angle. In an electronic transition the bond distance and angle will, in general, change. Two questions immediately arise: (1) How do the rotational constants depend upon the shape of the molecule? (2) What is the appearance of the resulting band structure for various possibilities as to shapes in upper and lower states? It was these points that had to be considered for SO_2, when the rotational spectrum of the λ3880 system was first photographed. Spectrograms of this system,[3] taken in first and second order of the 30-foot grating spectrograph, exhibited a curious shading toward both shorter and longer wave-lengths. Consideration of the above questions soon showed that an increase in bond distance and in angle could account for the two-sided shading. Because of the rather interesting results obtained, a systematic investigation has been carried through.

Hypothetical band structures for SO_2 have been computed and plotted, with symmetrical top formulas to approximate the rotational levels.[4] Electron diffraction values were used for the dimensions of the ground state and various reasonable assumptions were made about the dimensions in the excited state. Both parallel- and perpendicular-type bands have been considered.

A study of these plots showed that these band structures are examples of four general types whose qualitative aspects depend only on the signs of the changes in dimensions. Furthermore, such band structures are not limited to SO_2 and SO_2-like molecules, but must occur quite generally for XY_2 and other molecules, provided only that the moments of inertia in both states are related approximately like those of prolate symmetrical top.

For XY_2 molecules which satisfy the latter condition, it turns out that a qualitative treatment of the observed (resolved or unresolved) band structures may lead to definite conclusions concerning (1) relative values of bond distances and of angles of the molecule in upper and lower states; (2) direction of quantum-mechanical dipole moment; (3) intensity distribution to be expected in the associated vibrational structure in case the latter has not yet been analyzed: for there exist definite relations, based on the Franck-Condon principle, between the rotational and vibrational structures; or on the other hand,

[3] N. Metropolis and H. Beutler, Phys. Rev. **57**, 1078A (1940).

[4] G. H. Dieke and G. B. Kistiakowsky, Phys. Rev. **45**, 4 (1934), and L. Harris and G. W. King, J. Chem. Phys. **8**, 775 (1940).

a vibrational analysis already made can be confirmed.

Rotational Structures and Band Shading

In infra-red band spectra of diatomic molecules, the equilibrium nuclear separation, r_e, remains nearly constant in transitions to higher vibrational and rotational states. As a result, each band appears as a series of nearly evenly spaced lines on both sides of the origin. In rare cases, heads may be formed. In marked contrast, electronic bands are transitions in which the equilibrium nuclear separations are usually different in the two states, so that heads are formed. For diatomic molecules, it is well known that the bands degrade toward the ultraviolet or the red according as $r_e' < r_e''$ or $r_e' > r_e''$.

In polyatomic molecules, there is greater complexity in band structures, together with a greater variety of possibilities in band shading. To a good approximation, the rotational terms of an asymmetrical top molecule, if two moments of inertia are even roughly equal and differ markedly from the third (unique) moment, may be written

$$F = BJ(J+1) + CK^2 \tag{1}$$

where, for the near-prolate case,[5]

$$\begin{aligned} B &= (h/8\pi^2 c)\tfrac{1}{2}(1/I_b + 1/I_c); \\ C &= (h/8\pi^2 c)[1/I_a - \tfrac{1}{2}(1/I_b + 1/I_c)]. \end{aligned} \tag{2}$$

J is the total angular momentum quantum number, and K is the approximately valid quantum number associated with the component of the total angular momentum along the axis of the unique moment of inertia (quasi-symmetrical-top axis). Necessarily $J \geq K$.

The rotational levels of the normal and excited states in a spectroscopic transition are given by Eq. (1) with B', C' for the upper levels and B'', C'' for the lower. The allowed transitions[1] are given by $\Delta J = 0, +1, -1$, which correspond respectively to the Q, R and P branches of the "J structure," and by $\Delta K = 0, \pm 1$, which correspond to the q, r and p branches of the "K structure." The two cases, $\Delta K = 0$ and $|\Delta K| = 1$, which usually occur only in separate vibrational or electronic transitions, are referred to as "parallel-type" and "perpendicular-type" transitions because of the orientation of the quantum-mechanical dipole moment parallel or perpendicular to the unique axis of the symmetrical or quasi-symmetrical top.

It is convenient to write

$$\nu_{KJ} = \nu_0 + \nu_K + \nu_J, \tag{3}$$

where ν_0 is the band origin, and where

$$\nu_K = C'K'^2 - C''K''^2, \tag{4}$$

giving the K structure, and

$$\nu_J = B'J'(J'+1) - B''J''(J''+1), \tag{5}$$

giving the J structure. Usually the distance between lines is much smaller for one structure than for the other. This fact makes it convenient

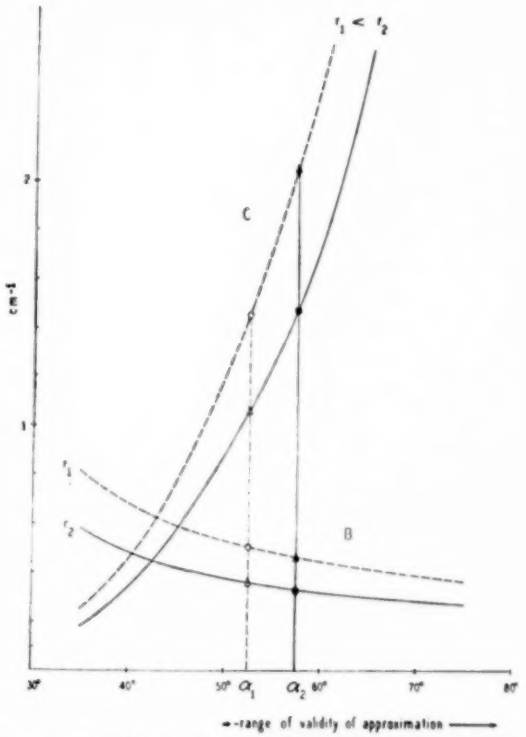

FIG. 2. Graphs showing the behavior of the rotational constants B and C of Eq. (1) as functions of the half-angle α at the apex for *constant bond distance*. The solid curves are for a state having a bond distance r_2, the dashed curves are for a state having $r_1 = 0.85 r_2$. Other r_1/r_2 ratios would give similar curves. α_1 and α_2 are two sample values of α. The scale for ordinates applies to SO_2; the value of r_2 is 1.43A, the experimental value for the normal state. For any other XY_2 molecule belonging to the obtuse near-prolate top classification, the curves have approximately the same shape. Although no sharply defined limit exists for the range of validity, this extends approximately to 50°. As α approaches 90°, C tends toward infinity, while B approaches $\hbar/8\pi^2 c(2m_2 r^2)$; all C curves cross the α-axis at $\alpha = \tan^{-1}[\sqrt{2}(1+2m_2/m_1)]^{-\frac{1}{2}}$.

[5] It is easily seen that for XY_2 molecules $I_b = 2m_2 r^2 \sin^2\alpha$, and $I_a = (2m_1 m_2/m_1 + 2m_2) r^2 \cos^2\alpha$.

to regard the frequencies of the coarser structure as giving the positions of sub-band origins, e.g., the frequencies $\nu_0+\nu_K$ of Eq. (4) if the K structure is the coarser, as for molecules like SO_2.[6] The sub-bands themselves are made up of sets of lines constituting fine structure, the frequencies being given by ν_J of Eq. (5).

In infra-red studies, the coefficients B' and B'' are nearly equal in the two states, just as in the diatomic case. Similarly C' and C'' are nearly equal. Hence the series of lines and sub-bands forming the band structure due to $|\Delta K|=1$ or $|\Delta J|=1$ exhibit slow convergence, if any, while series corresponding to $\Delta K=0$ or $\Delta J=0$ exhibit little if any *divergence*. On the other hand, the values of B and C may be quite different in the two states if a transition involves a change in the electronic state. This is the case in which we are interested.

Dependence of Rotational Coefficients upon Bond Distance and Apex Angle

Special cases to be treated

The available experimental data show that a number of non-linear XY_2 molecules belong to the obtuse near-prolate top type. This follows from the fact that 2α (see Fig. 1) is usually large enough so that $I_c \approx I_b > I_a$. Thus in the normal states of SO_2, NO_2 and ClO_2, the values of 2α from electron diffraction studies and spectroscopic data are approximately 120°, 154° and 122° respectively. For these values of the angles, the following ratios are obtained

	SO_2	NO_2	ClO_2
I_c/I_a	7.00	7.16	7.23
I_c/I_b	1.17	1.16	1.16

(In Fig. 1 for XY_2, the moments of inertia I_c, I_b and I_a are those about the x, y and z axes respectively.)

As an aid to analyzing actual spectra, it is useful to work out the band structures for the four following cases:

$$\begin{aligned} &\text{I. } \alpha'>\alpha'', \quad r'=r'' \\ &\text{II. } \alpha'<\alpha'', \quad r'=r'' \\ &\text{III. } \alpha'=\alpha'', \quad r'>r'' \\ &\text{IV. } \alpha'=\alpha'', \quad r'<r''. \end{aligned} \tag{6}$$

Table I. *Character of band structures in four special cases for XY_2 molecules belonging to the obtuse near-prolate top classification.*

	Case	B	C	J Structure Degrades Toward	K Structure Degrades Toward
I	$\alpha'>\alpha'', r'=r''$	$B'<B''$	$C'>C''$	red	violet
II	$\alpha'<\alpha'', r'=r''$	$B'>B''$	$C'<C''$	violet	red
III	$\alpha'=\alpha'', r'>r''$	$B'<B''$	$C'<C''$	red	red
IV	$\alpha'=\alpha'', r'<r''$	$B'>B''$	$C'>C''$	violet	violet

In a discussion of these cases, it is useful to consider Fig. 2. The solid curves show the behavior of B and C [cf. Eq. (2)] for SO_2 as functions of the half-angle at the apex, for a *constant bond distance* $r_2=1.43$A. The dashed curves are similar functions for a bond distance $r_1=0.85r_2$. Curves for other XY_2 molecules are qualitatively the same as these for SO_2; the C curves are always monotonic increasing and the B curves monotonic decreasing functions.[6a] In Fig. 2, α_1 and α_2 are two sample values of α such that $\alpha_1<\alpha_2$.

For cases I and II, where only the angle changes in the transition, the behavior of B and C is immediately apparent; if α increases in an absorption transition (suppose $\alpha''=\alpha_1$, $\alpha'=\alpha_2$) C increases markedly but B decreases slightly, whereas for $\alpha'<\alpha''$, the directions of the changes in B and C are reversed.

For cases III and IV, where only the bond distance changes in the transition, it is easy to show that $B'=[(r''/r')^2]B''$ and $C'=[(r''/r')^2]C''$. Hence a change in bond distance alone increases both B and C if $r'<r''$, decreases both if $r'>r''$. If, for example, in Fig. 2, $\alpha''=\alpha'=\alpha_2$ and $r''=r_2$ and $r'=r_1$, all that is necessary is to move along the vertical from the solid circles to the solid triangles. The foregoing relations are summarized in Table I; the direction toward which each

[6] A convenient qualitative method for comparing the relative coarseness of spacing of J and K structures is the following: (i) For parallel-type bands, the span of, say, the first ten Q lines from the head may be compared with that of the first ten q transitions. (ii) For perpendicular-type transitions, the span of the first ten lines from the head of the J structure (P or R branch) in some strong sub-band may be compared with that of the first ten transitions from the head of the K structure (p or r branch). Using this criterion for case II in SO_2 (see Fig. 4) one finds that the K structure is about five and seven times as coarse as the J structure for the parallel- and perpendicular-types, respectively.

[6a] The corresponding curves for the acute near-prolate top case are approximately those obtained by reflecting the curves in Fig. 2 at $\alpha=45°$. Consequently the present discussion applies to the acute form provided the inequality signs in $\alpha'<\alpha''$ and in $\alpha'>\alpha''$, wherever used, are reversed.

structure degrades in each of the four cases is also indicated.

Characteristic patterns of bands

The four representative cases considered above yield four characteristic band structures.[7] For case I, where $\alpha' > \alpha''$ results in $C' > C''$ and $B' < B''$, the K structure degrades toward the violet, whereas the J structure goes off toward the red. Case II with $\alpha' < \alpha''$ reverses both directions of shading. Cases I and II will thus exhibit a shading of K structure to one side with a superposition of J structure shaded to the other. The band as a whole will not have a

[7] Explicit band formulas for the two types of transitions are as follows. For the perpendicular type ($\Delta K = \pm 1$), the formula [cf. Eq. (3)] may be written

$$\nu = \nu_0 + \tfrac{1}{2}(C' - C'') + (C' + C'')k + (C' - C'')k^2 + \begin{cases} (B' + B'')m + (B' - B'')m^2 \\ (B' - B'')J + (B' - B'')J^2 \end{cases}.$$

Here k is a convenient index number with the value $k = K + \frac{1}{2}$ for the r branch and $k = -K + \frac{1}{2}$ for the p branch of the K structure [cf. Eq. (4)]. The bracketed expressions represent ν_J of Eq. (5). The lower expression for ν_J corresponds to the Q branch; in the upper expression, the index number m with $m = J + 1$ gives the R branch, and with $m = -J$ the P branch. For parallel-type transitions, the formula may be written

$$\nu = \nu_0 + (C' - C'')K^2 + \begin{cases} (B' + B'')m + (B' - B'')m^2 \\ (B' - B'')J + (B' - B'')J^2 \end{cases}.$$

In all the foregoing formulas, K means K'', J means J''.

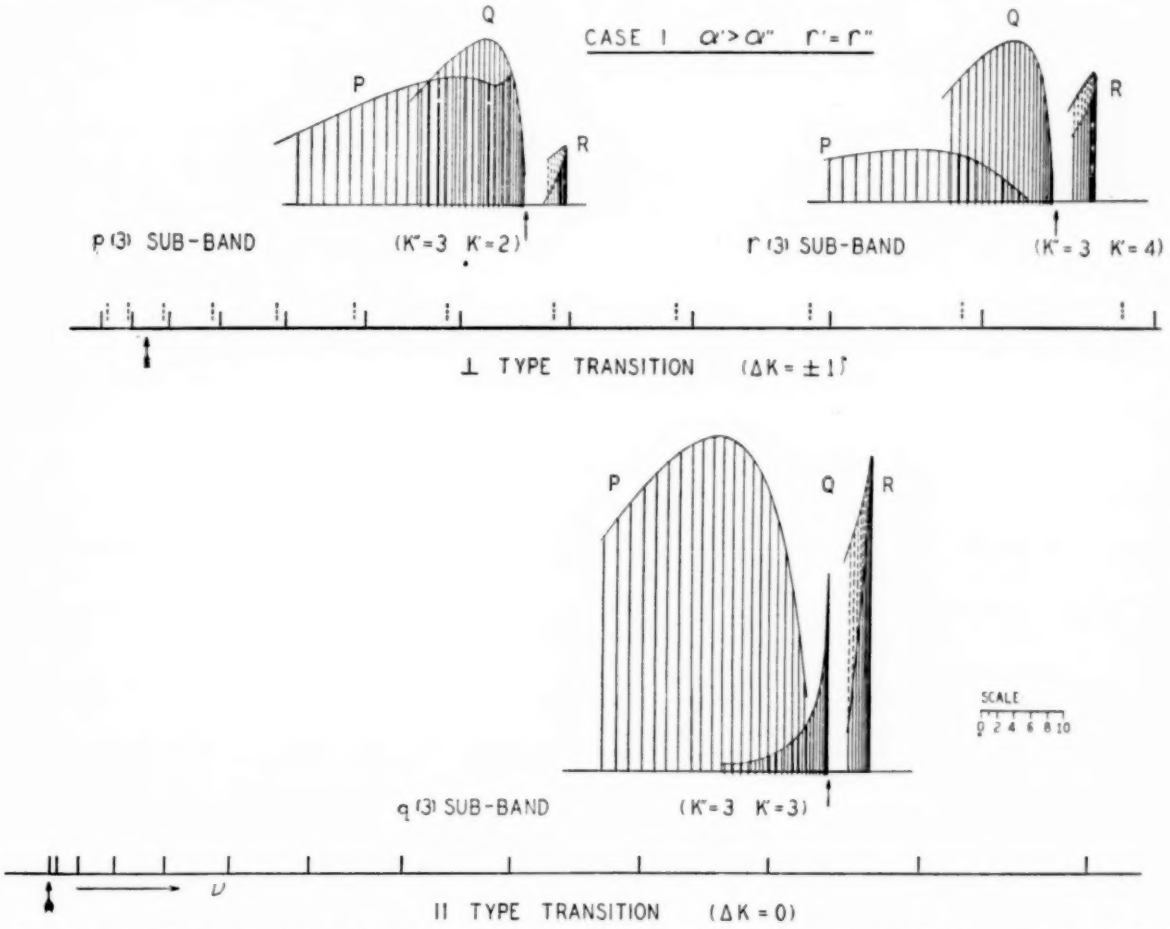

FIG. 3. Schematic representation of typical band structures of SO_2-like molecules, showing the "component parts" of both parallel- and perpendicular-type transitions when the only change in dimensions is (for absorption) an increase in the apex angle (case I). The K structure, which forms a set of origins for the sub-bands (J structure), is shown by lines of uniform height. Returning branches in the perpendicular-type K structures and in the J structures are shown by dashed lines. Lines of the Q branches are drawn below the axis. The feathered arrows correspond to origins of bands, unfeathered arrows to sub-band origins. The intensities correspond to a temperature of 200°K for the case of SO_2. For any other XY_2 molecule having the same ratio of moments of inertia I_b/I_c as SO_2, a change in scale combined with an appropriate temperature T' would yield an identical plot; T' is given by $T'(I_b/I_b')$. Since $K'' = 3$ has been chosen for all three sub-bands exhibited here, the first lines in the P, Q and R branches shown are $P(3)$, $Q(3)$ and $R(3)$ where, as usual, the numbers in parentheses refer to J''. The J'' values run to 25.

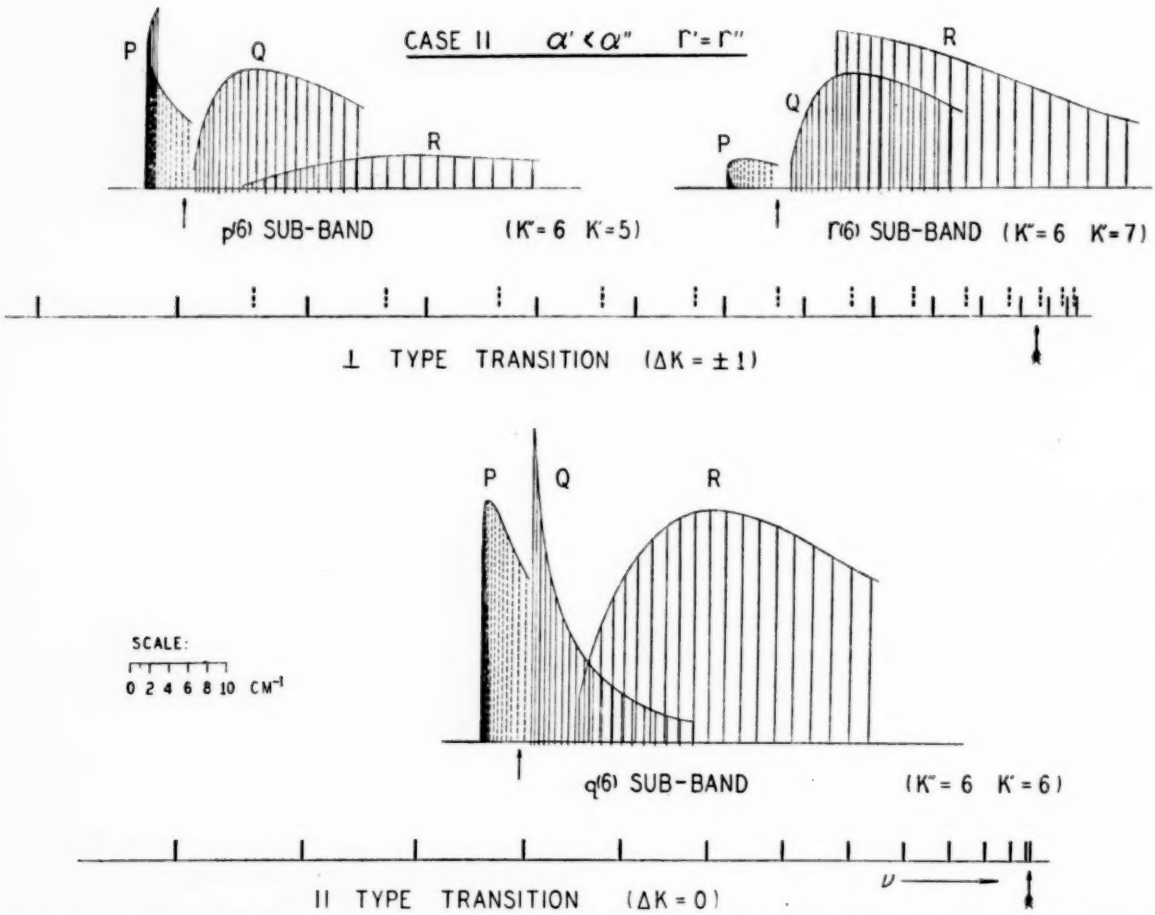

FIG. 4. Band structures for the case (in absorption) of a decrease in angle without change in bond distance (case II). In this instance the J and K structures degrade toward the ultraviolet and red respectively. See Fig. 3 for other details.

characteristic sharp edge, but will spread out on both sides.

In distinct contrast to the foregoing, cases III and IV will exhibit a shading of both J and K structures in the same direction; the whole band will possess a characteristic edge[8]—rather sharp in most instances—on the violet or red side according as $r' > r''$ or $r' < r''$.

The foregoing applies equally to parallel- and perpendicular-type transitions; in fact, it is only with some difficulty that one can expect to distinguish between these two types by observing the qualitative features of the bands. A returning branch of the K structure would distinguish a ⊥ from a || type transition, the latter having no returning branch. However, the considerable overlapping should make it difficult to ascertain whether or not a returning branch of the K structure is present (cf. K structures of Figs. 3–6 where returning branches are shown by dashed lines); both ⊥ and || types exhibit a convergence in the K structure. However, a plot of subband intensities should be of considerable aid.

[8] It may, of course, happen that the convergence in both structures is rather slow so that the intensity is small at the heads.

More general cases

The four cases just treated are, of course, very special; in general, both angle and bond distance change in going from one electronic state to another. In the preceding sections, the discussion of the coefficients was limited to a change in only one parameter (either α or r). To understand the effects of a change in both parameters, one considers first the effect of a change in one parameter, and using the results as a starting

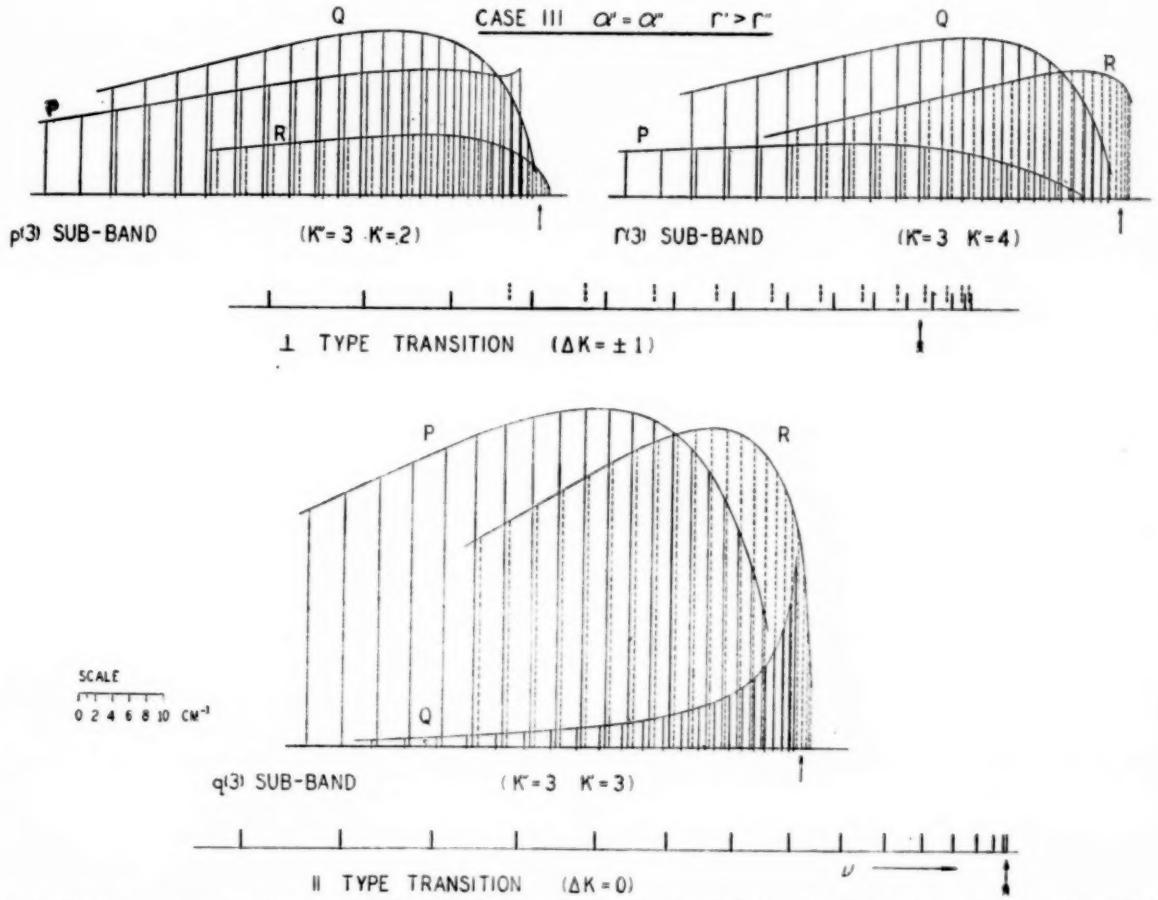

FIG. 5. Band structures for the case (in absorption) of an increase in bond distance without change in angle (case III). Note that both J and K structures degrade toward the red.

point, one may study the effect of a change in the second parameter.

From Fig. 2 one may obtain an insight into a variety of cases. As an example, let $\alpha'' = \alpha_2$, $r'' = r_2$ and $\alpha' = \alpha_1$, $r' = r_1$, and consider an absorption transition. B'' and C'' values are given by solid circles in Fig. 2, B' and C' by open circles. The effect of the decrease in angle alone (from α_2 to α_1) would be a movement along the solid curves from the solid circles to the open triangles. To obtain also the change in bond distance $r_2 \rightarrow r_1$, a shift is now necessary along the vertical at α_1 from the solid to the dashed curves, i.e., from the open triangles to the open circles. The net result is seen to be a considerable increase in B and a slight decrease in C for the example selected.

The fact that B and C change in opposite directions for a change in angle alone affords some interesting possibilities. In the example just given, $C' \approx C''$ resulted, yielding non-convergent K structure. This might suggest that $\alpha' \approx \alpha''$, $r' \approx r''$. However, inspection of the J structure, which (in our example) forms heads at relatively small quantum numbers, indicates $B' > B''$ definitely, since $-\Delta\alpha$, $-\Delta r$ both decrease B.

If the dimensions of the molecule should be practically unchanged in a transition, this fact would be immediately evident by the absence of heads in *both* J and K structures.

TYPICAL ELECTRONIC BANDS

Detailed diagrams of spectra of SO_2 and SO_2-like molecules have been worked out for each of the four special cases [Eqs. (6)] treated above, for values of J up to twenty-five and of K up to fifteen, for temperatures of 200° and of 300°K. Equations (1) and (2) were used to calculate the positions of lines, and the intensities were calcu-

lated from formulas taken from Dennison's review;[1] the frequency factor ν for absorption (or ν^4 for emission) was, however, omitted.

Since the oxygen nucleus has zero resultant spin, only one of the two possible levels associated with $|K|$ exists for $K>0$; for $K=0$, lines with alternate J values are missing.

Representative parts of the spectra of SO_2-like molecules for the four special cases are shown in Figs. 3–6. The ground state dimensions, $\alpha''=60°$, $r''=1.43$A, were taken to agree with electron diffraction values for SO_2;[9] for the excited states the following assumptions were made:

$$\begin{aligned} &\text{Case} \quad \text{I.} \quad \alpha'=65°, \quad r'=r'', \\ &\qquad \text{II.} \quad \alpha'=55°, \quad r'=r'', \\ &\qquad \text{III.} \quad \alpha'=\alpha'', \quad r'=1.15r'', \\ &\qquad \text{IV.} \quad \alpha'=\alpha'', \quad r'=0.85r''. \end{aligned} \tag{7}$$

In each figure, the K (coarser) structure is shown for a parallel-type transition ($\Delta K=0$) and gives the origins of a set of sub-bands [cf. Eqs. (3)–(5)]; in addition, the structure of one sample sub-band is shown to the same scale. In each figure also, the K structure of a perpendicular-type transition ($\Delta K=\pm 1$) is similarly exhibited together with one sample sub-band from each of the two K branches (p and r). (A sub-band origin, shown by unfeathered arrow in the sample sub-band, should be brought into coincidence with the line representing each K transition.) It is, of course, necessary to make appropriate changes in relative intensity for the various sub-bands and to delete lines with $K>J$.

As a supplement to Figs. 3–6, Figs. 7 and 8 have been constructed to help in visualizing the change in intensity from one sub-band to the next. In the cases of both parallel- and perpendicular-type transitions, the intensity of the *most intense line* for each branch of the J structure has been plotted as a function of K. The dashed segments at $K=0$ have been inserted to remind one that the sub-bands having either K'' or K' equal to zero contain only half as many lines as other sub-bands, since lines with alternate J values are missing.

Returning to Figs. 3–6, one observes that in cases I and II, the J and K structures degrade in opposite directions, whereas in cases III and IV the two structures are shaded in the same direction; it is clear that the bands in the latter two

[9] V. Schomaker and D. P. Stevenson, J. Am. Chem. Soc. **62**, 1270 (1940).

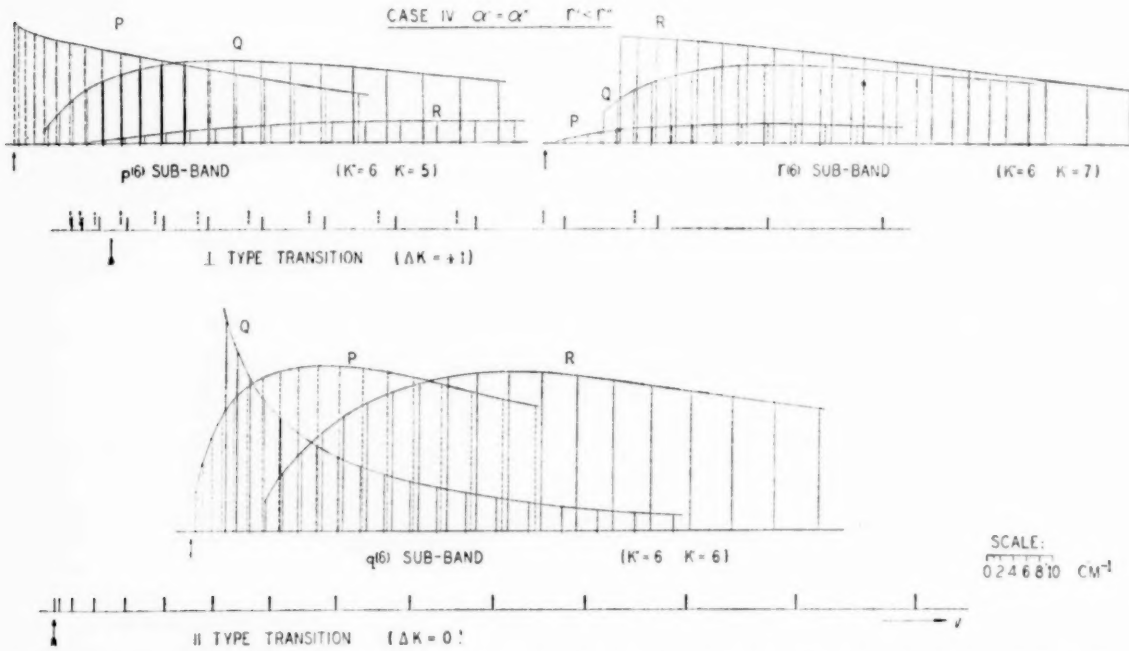

FIG. 6. Band structures typical of a decrease in bond distance without change in angle in an absorption transition (case IV). As in case III (Fig. (5)), J and K structures both degrade in the same direction, but here the direction is toward the ultraviolet.

cases must have a characteristic sharp edge.[8] In view of the considerable overlapping of the sub-bands and the usually large moments of inertia, the band may be so complicated that the only characteristic feature is the presence or absence of a sharp edge. However, even such meager information as the qualitative shape of the band envelope is valuable both for itself and as a help in the corresponding vibrational analysis; this latter point is discussed in the next section.

Application to Vibrational Analysis

In this last section the correlation of the qualitative characteristics of electronic bands with the intensity distribution in the associated vibrational structure is discussed. As a result of the interrelations that exist between rotational and vibrational structures, it is convenient to carry out the two analyses side by side. In the following, only absorption bands arising from the vibrationless level of the ground state will be considered. The fundamental frequencies of the normal state are usually known (mostly from infra-red and Raman work), so that transitions from excited vibrational levels in the ground state are easily recognized. However, in the event that these frequencies are not known, the temperature-sensitiveness of such bands makes them easy to pick out; or they can be made quite faint by lowering the temperature.

In making (or confirming) a vibrational analysis for an XY_2 molecule, two factors are to be considered: (1) the direction toward which the K structure (here the coarser) and the J (here the sub-band) structure degrade, (2) the intensity distribution in the vibrational structure. These two factors can be correlated by means of the Franck-Condon principle.

In the simplest instance there is one strong band, the vibrationless transition, accompanied by a few weaker ones. This intensity distribution is expected if the dimensions of the molecule are not appreciably changed in the transition to the excited state; the latter relation would be confirmed by slow convergence, if any, of both J and K structures.

If, on the other hand, there is one prominent series of quite evenly spaced bands, then by the Franck-Condon principle one may conclude that

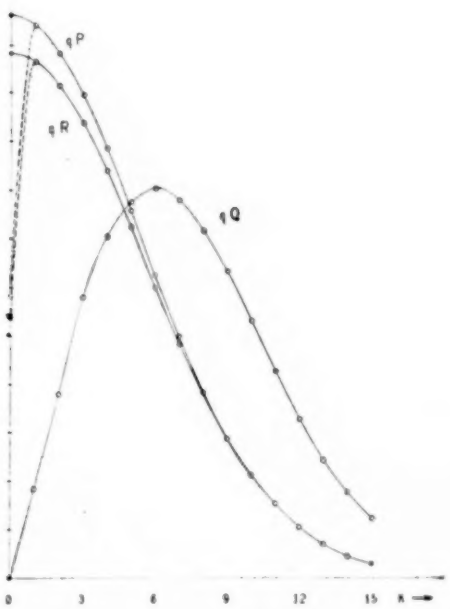

Fig. 7. The intensity of the strongest line of each branch (branches P, Q, R) of each sub-band is plotted as a function of K (i.e., K'') for a parallel-type transition, for SO_2 and SO_2-like molecules. The dashed segments from $K=1$ to $K=0$ are to remind one that only lines with alternate J values are present for $K=0$, so that the total intensity of each sub-band with $K=0$ is halved.

either the angle or bond distance has changed. If the bands exhibit a two-sided shading (cf. Figs. 3–4), it is primarily a change in angle that has occurred; but if both J and K structures degrade in the same direction so that the band as a whole possesses a sharp edge (cf. Figs. 5–6), then it is principally a change in bond distance that has taken place.

If the intensity distribution is more complicated, then the bond distance and angle must both have suffered appreciable changes, Δr (i.e., $r'-r''$) and $\Delta\alpha$ ($\alpha'-\alpha''$) in the electronic transition. Before attempting to discuss the interpretation of such cases with complicated intensity relations in terms of molecular changes, it is useful to consider first the converse problem of determining the directions toward which the J and K structures degrade for each of four possible types of transition in respect to the signs of the changes in r and α. For convenience let J and K with the subscripts $+$ or $-$ be used to denote whether the J or K rotational structure degrades toward the violet or the red. Referring to Table II, one observes that to each of the four types of changes in molecular dimensions (A, B, C, D)

there correspond two rotational-structure subtypes. In type A, the J structure is necessarily J_-; for, referring to Fig. 2, one observes that an increase in either α or r decreases B, hence certainly $B'<B''$. On the other hand, the K structure may be either K_+ or K_-, giving the two subtypes A_1 and A_2. This follows from the fact that an increase in α tends to increase C but an increase in r tends to decrease it; if the effect of the increase in r more than compensates that of the change in α, K is K_-; if not, then it is K_+. The discussion of the other types proceeds in similar fashion.

Returning to the original problem, one desires to determine the signs of the changes in molecular dimensions for a given type of band shading. Referring to Table III, one sees that for each of the K and J shading cases, there are two possible interpretations in terms of molecular changes. To ascertain which of the two possibilities is at hand, it would be necessary to determine which structure, J or K, converges more rapidly to form a head. This could be done easily if both structures are resolved. Usually the J structure is not completely resolved; however, the second differences in the J structure may be evaluated from resolved lines with high J values far from the head. From these evaluations, combined with a knowledge of B'', one can determine B'. Analogously, the second differences in the K structure can be determined, and finally C', since C'' is usually known. Hence the expressions

TABLE II. *Possibilities for shading of K and J structures for various $\Delta\alpha$, Δr types where $\Delta\alpha$ and Δr are changes in molecular dimensions. ($\Delta\alpha=\alpha'-\alpha''$, $\Delta r=r'-r''$.) The signs in column 3 indicate directions of shading (+, toward ultraviolet, −, toward red).*

			Band Shading	
Type	$\Delta\alpha$	Δr	K struc.	J struc.
A_1	+	+	+	−
A_2			−	−
B_1	−	−	−	+
B_2			+	+
C_1	+	−	+	−
C_2			+	+
D_1	−	+	−	+
D_2			−	−

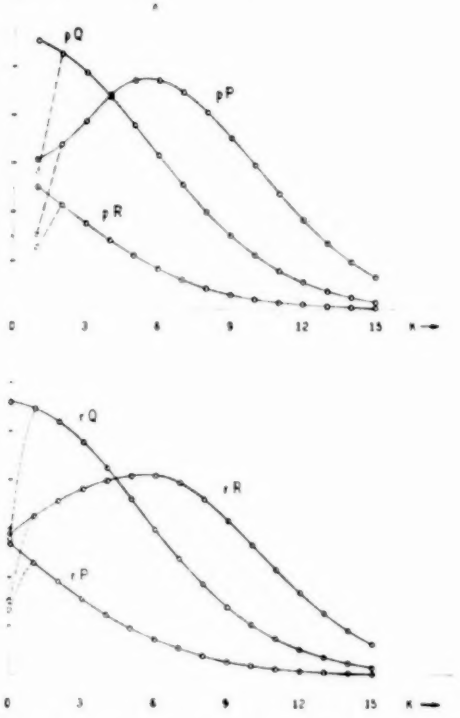

FIG. 8. Analogous to Fig. 7. Here a perpendicular-type transition is considered.

$|(B'-B'')/(B'+B'')|$ and $|(C'-C'')/(C'+C'')|$ can be evaluated. Their numerical values indicate the rate of convergence (or divergence) in the respective structures. A comparison of these serves as a criterion to distinguish between the two possibilities in Table III.

However, in practice it is usually not necessary to use this quantitative method because many spectra show such markedly dissimilar rates of divergence of the two structures that a mere inspection suffices. This situation occurs when both α and r change considerably. In the absence of marked differences, one has recourse to another criterion, taken from the vibrational intensity distribution. This situation arises from a change principally in only one of the two parameters, α and r (cf. p. 291).

As an example, suppose the spectrum observed is the case J_-K_-. Then definitely the bond distance has increased, but it remains to determine whether α has increased or decreased. If the J structure converges relatively more rapidly than the K, then $\alpha'>\alpha''$; if the opposite is observed, then $\alpha'<\alpha''$.

If one succeeds in determining the signs of the changes in dimensions, one is interested in know-

ing more explicitly how these changes are correlated with the vibrational intensity distribution. As yet, a quantitative treatment of the Franck-Condon principle for triatomic molecules is lacking, but some conclusions may be reached if simplifying assumptions are made.

Suppose, first, that the equilibrium bond distance increases by an amount Δr as a result of the electronic transition. Qualitative application of the Franck-Condon principle then shows that a pure v_1 vibrational progression should be developed (ν_1=breathing frequency). Let us denote the quantum number of the strongest band in this series by $(v_1)_{max}$. Evidently $(v_1)_{max}$ is larger the larger is Δr.[10]

Again, suppose that $\Delta r=0$ but that the equilibrium angle increases by an amount $\Delta\alpha$. In this event, a pure v_2 progression should be developed, whose strongest member may be designated by $(v_2)_{max}$ (ν_2=deformation frequency). Finally, suppose both Δr and $\Delta\alpha$ differ from zero. Then both pure v_1 and pure v_2 progressions should be developed; and in addition mixed progressions. Further, for any given Δr value there is some corresponding $\Delta\alpha$ value such that $(v_1)_{max}$ and $(v_2)_{max}$ are equal.

If now a plane is defined by plotting $\Delta\alpha$ as ordinate against $\Delta r/r'$ as abscissa (it is found that $\Delta r/r'$ is more convenient for this purpose than Δr itself), then curves can be plotted in this plane passing through points where Δr and $\Delta\alpha$ are so related that $(v_1)_{max}=(v_2)_{max}$: see Fig. 9. If some simple assumptions are made,[10] it turns out that these curves are approximately straight lines passing through the origin (dashed lines in Fig. 9), given roughly by

$$\Delta\alpha=\pm 2^{\frac{1}{2}}(\Delta r/r').$$

These lines evidently divide the plane into four regions, in two of which $(v_2)_{max}>(v_1)_{max}$ (dotted regions in Fig. 9), while in the other two $(v_1)_{max}>(v_2)_{max}$ (undotted regions in Fig. 9).

The $\Delta\alpha$, Δr plane can be divided into regions not only with respect to vibrational intensity distribution in the manner just discussed, but also with respect to rotational structure types. The rotational structure regions, like the vibrational distribution regions, are four in number. In the terminology introduced earlier, the four rotational regions may be labeled J_+K_+, J_+K_-, J_-K_+, and J_-K_-. The boundary between any two of these regions corresponds either to $B'=B''$ (J_+, J_- boundary) or to $C'=C''$ (K_+, K_- boundary). These boundaries can be located with the help of considerations used in plotting Fig. 2, and are given, for the case of absorption by SO_2 in its normal state, in Fig. 9.

Now then, if it is known which mode of vibration is more strongly excited and if the J, K shading can be determined, the possible changes in dimensions are limited to a region of the

TABLE III. *Interpretation of various K and J shading cases in terms of changes in molecular dimensions $\Delta\alpha$ and Δr.*

	Band Shading			
Case	*K* struc.	*J* struc.	$\Delta\alpha$	Δr
I	+	−	+	+
			+	−
II	−	+	−	−
			−	+
III	−	−	+	+
			−	+
IV	+	+	−	−
			+	−

[10] It is to be expected that for a given total intensity the number of bands in a v_1 progression (pure breathing series) is greater the larger the change in bond distance. If harmonic motion is assumed, one can estimate $(v_1)_{max}$, the quantum number of the strongest band in such a series. It turns out that $(v_1)_{max}$ is related to the frequency and the change in bond distance approximately according to

$$(v_1)_{max}=c(\Delta r)^2\nu_1. \quad (a)$$

where ν_1 is the symmetrical valence or breathing frequency and c is a constant factor. It is interesting to observe that some deformation vibration is excited even though only the bond distance changes. If the angular change in a transition is $\Delta\alpha$, the distance of the Y atom in its normal state position, measured perpendicularly to the X−Y bond distance, from the excited state equilibrium position is approximately $\Delta s=r'\Delta\alpha$, where r' is the bond distance in the excited state. Then

$$(v_2)_{max}=c(\Delta s)^2\nu_2, \quad (b)$$

where v_2 is the quantum number associated with ν_2, the deformation frequency, and c is the same as in Eq. (*a*). Empirically, $\nu_1=2\nu_2$ is found to be roughly true for the normal states of several XY_2 molecules. Hence from Eqs. (a) and (b)

$$(v_1)_{max}=(v_2)_{max} \quad (c)$$

provided

$$(\Delta s)=\sqrt{2}(\Delta r).$$

In other words, Eq. (a) is true in case the change in α has the special value $\Delta_s\alpha$ given by

$$\Delta_s\alpha=\sqrt{2}(\Delta r)/r'. \quad (d)$$

diagram where these properties overlap. For example, suppose the v_1 vibration is the stronger and the rotational structure is J_-K_-, then the possible changes in dimensions are represented by the area common to the vertically shaded region and the undotted region in the neighborhood of the positive $\Delta r/r'$ axis. At first it may appear that there still remains a considerable range of allowed changes in dimensions. However, a closer study should confine the region still more. For clearly, near the lower boundary (dashed line) of the region in the foregoing example, $(v_1)_{max} \approx (v_2)_{max}$. In addition, the J structure converges relatively slowly. For changes corresponding to points near the $\Delta r/r'$ axis, $(v_1)_{max} > (v_2)_{max}$ definitely, and both J and K structures degrade approximately at the same rate. Finally, in the vicinity of the upper boundary (solid line) the coarse K structure should degrade rather slowly, if at all.

A more favorable case occurs when the v_2 vibration is the more prominent and both J and K structures degrade in the same direction. In this instance, the overlapping regions are quite small.

If, for some molecule, the dotted region should coincide with the vertically-shaded region, one could determine from the J, K shading which vibration would be more prominent. Conversely, if the vibrational intensity were known, the J, K shading could be determined. Finally, from the figure the remarks made in connection with Tables II and III can be confirmed.

Some actual cases may be considered. Recent photographs of the absorption spectrum of ClO_2 taken on the 30-foot grating spectrograph by J. B. Coon in this laboratory[11] provide an interesting example to show the correlation between vibrational and rotational analysis. Here the structure is J_-K_- and both structures converge approximately at the same rate. On the basis of the present work it was seen that this indicates an increase in bond distance as the principal change in the transition and identifies the long series of some twenty bands as belonging to the breathing rather than the deformation frequency. The subsequent analysis proved this.

Photographs of the λ3880 system of SO_2 taken by Metropolis and Beutler[3] show quite other characteristics. Here the structure is J_-K_+. Of the two possibilities, case C_1 of Table II $(+\Delta\alpha, -\Delta r)$ is excluded because long progressions of the deformation frequency are not evident. Hence it must be case A_1 $(+\Delta\alpha, +\Delta r)$, and this is confirmed by the fact that the K structure converges more slowly than the J. That the changes are small is confirmed by the fact that the combination band having one quantum of each of the totally symmetrical vibrations is the strongest.

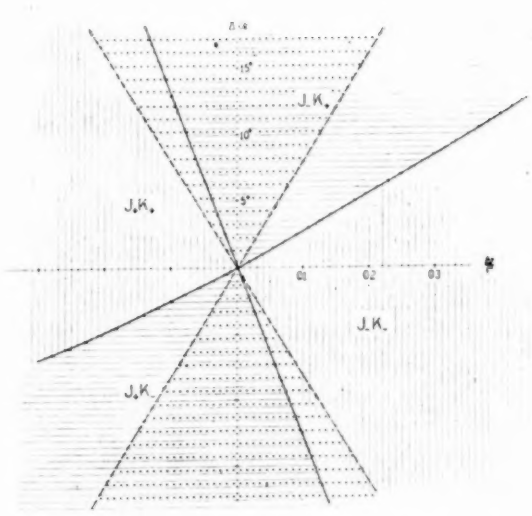

FIG. 9. A schematic diagram showing the directions of shading of the J and K structures for simultaneous changes in angle and in bond distance. As before, the subscripts indicate direction of shading (+, toward ultraviolet; −, toward red). Change in the value of the apex half-angle in degrees is plotted as ordinate, and $\Delta r/r'$ as abscissa, where $\Delta r = r' - r''$. The whole field is divided by two intersecting full heavy curved lines into four regions J_+K_+, J_-K_+, J_-K_-, J_+K_- indicated by horizontal or vertical hatching. The field is also divided in another way into four regions by two intersecting dashed lines: in the dotted region, the deformation is more prominent than the symmetrical valence vibration, whereas the opposite is true in the undotted region.

ACKNOWLEDGMENTS

The author is indebted to Professor Robert S. Mulliken, Dr. Hans G. Beutler and Dr. Wave H. Shaffer for their suggestions and encouragement and for many helpful discussions. Dr. Shaffer was also kind enough to help with the calculations of the intensity factors which were used for Figs. 3–6.

[11] J. B. Coon, Phys. Rev. **58**, 926(L) (1940).

Vibrational Analysis of the Absorption System of Sulphur Dioxide at λ3400–2600

N. METROPOLIS
Ryerson Physical Laboratory, University of Chicago, Chicago, Illinois

(Received June 18, 1941)

Photographs of the bands of sulphur dioxide in the region of λ3400–2600 have been taken under low, medium and high dispersion, both at room temperature and at 200°K; the pressure of the absorbing gas was varied from 0.3 mm to 480 mm. Thirty bands can be represented by the formula

$$\nu = 29622 + 770v'_1 + 320v'_2 + 813v'_3 - 6v'^2_1 - 2.5v'^2_2 - 20v'_1v'_2 - 25v'_2v'_3 - 15v'_1v'_3,$$

where v'_1, v'_2, v'_3, are the quantum numbers of the symmetrical valence, the deformation and the antisymmetrical vibrations respectively. The three fundamental frequencies for infinitesimal vibrations in the upper electronic state are $\nu'_1 = 794$, $\nu'_2 = 345$ and $\nu'_3 = 833$ cm^{-1}. In addition, twelve bands have been identified that correspond to transitions from excited vibrational levels in the normal state. The relatively long v'_1 and v'_2 progressions indicate that both the bond distance and the angle have changed considerably in the transition to the excited electronic state. The vibrationless transition at 29622 cm^{-1} is weak, as one would have expected from considerations of the Franck-Condon principle. Substituting the three fundamental frequencies in the formula based on a valence force model, one obtains a value of 100° for the apex angle in the excited state, as compared with 120° in the normal state. The absence of any regularity in the rotational structure supports the resulting conclusion that the molecule in its upper state has become a more asymmetrical top.

INTRODUCTION

THE vibrational structure of the absorption bands of sulphur dioxide in the region λ3900–2600 has been studied in recent years by several investigators.[1–5] Previously Henri[6] had reported three main absorption regions in the near ultraviolet, (1) λ3900–3400, weak; (2) λ3370–2450, moderately strong; (3) λ2300–2000 and beyond, very strong. There was no evidence that these absorbing regions corresponded to three different electronic transitions except that the absorption intensities varied so widely. Watson and Parker[2] and Clements[4] investigated the absorption in regions (1) and (2) and concluded that both regions constitute one system; the bands at longer wave-lengths (λ3900–3400) were considered as transitions from excited vibrational states of the normal electronic state. Clements identified a moderately strong band at 31945 cm^{-1} as the band origin.

Retaining the assumption of a single upper electronic state, Samuel and Asundi[5] proposed two alternative analyses, the first a modification of the analysis of Clements, the second entirely new, with the vibrationless transition at 33303 cm^{-1}, one of the most intense bands. However, the proposals of Samuel and Asundi are not free from objections, as they themselves have remarked. In particular, their second analysis does not contain any bands with deformation vibration in the excited state. In addition, doubt is cast upon their assignment of the origin since there is no band at the position corresponding to the transition $(000)' \leftarrow (001)''$, although bands corresponding to higher vibrational levels of the normal state are assigned. Further comments on their analysis have been made by Price and Simpson.[7]

More recently, with the object of investigating the rotational band structure, the spectrum of sulphur dioxide has been photographed under low, medium and high dispersion in the region λ3900–2600 at various pressures from 0.3 mm to two atmospheres and at 800°, 300° and 200°K. As a result of this survey Metropolis and Beutler[8] established definitely that the electronic transition connected with the weak absorption around λ3800 is distinct from that associated with the stronger contiguous absorption toward shorter wave-lengths. Furthermore, even at pressures of a few millimeters and a dry ice temperature,

[1] A. K. Dutta, Acad. Sci. U. P. Bull. **1**, 89 (1931).
[2] W. W. Watson and A. E. Parker, Phys. Rev. **37**, 1484 (1931).
[3] A. Jonescu, Comptes rendus **197**, 35 (1933).
[4] J. H. Clements, Phys. Rev. **47**, 224 (1935).
[5] R. K. Asundi and R. Samuel, Proc. Ind. Acad. Sci. **A2**, 30 (1935).
[6] V. Henri, Nature **125**, 275 (1930).
[7] W. C. Price and D. M. Simpson, Proc. Roy. Soc. **A165**, 272 (1938).
[8] N. Metropolis and H. Beutler, Phys. Rev. **57**, 1078 (1940).

considerable structure was evident on the long wave-length side of the origin assigned by Clements (which is itself further toward the red than the origin assumed by Samuel and Asundi). This latter fact suggested that the origin must lie at still longer wave-lengths. Finally, the large number of bands excited indicated that the dimensions of the molecule have changed considerably in the electronic transition, so from considerations based on the Franck-Condon principle, one would expect the vibrationless transition to be quite weak.

In view of the foregoing, it was thought advisable to reconsider the vibrational structure of the system around λ3200; the results obtained form the basis of the present work.

Experimental

Sulphur dioxide obtained commercially was distilled twice before being admitted to a reservoir. The Pyrex absorption tube was 4.5 cm in diameter and 1 m in length with flanges at each end. Cylindrical quartz cells of the same diameter as the absorption tube and of 2-cm length with two quartz windows as bases were sealed onto the flanges with Picein. When these cells were evacuated, no water vapor condensed on the windows at low temperatures. From one end of the absorption tube, a side arm was connected to a mercury diffusion pump. At the other, the following were connected in series: stopcock A, a small cell whose volume was very nearly 15.9 cc (1/100 the volume of the absorption tube), stopcock B, a vertical U-tube, and finally a reservoir.

The U-tube was surrounded by a dry ice-acetone bath. At the equilibrium temperature of CO_2-acetone, the pressure of SO_2 is 8 mm. To obtain pressures less than 8 mm, the small cell was filled with SO_2 at 8 mm pressure, stopcock A being kept closed. Then stopcock B was closed and A opened, allowing the gas to expand into the absorption tube. Thus one could obtain any desired pressure between 0.008 mm and 8.0 mm simply by repeating the operation the required number of times. For higher pressures, crushed dry ice was slowly added to acetone in a thermos flask and sufficiently agitated to obtain a uniform temperature. The absorption tube was then filled at the temperature corresponding to the desired pressure. A pentane thermometer was used (sufficiently accurate here). Finally, a

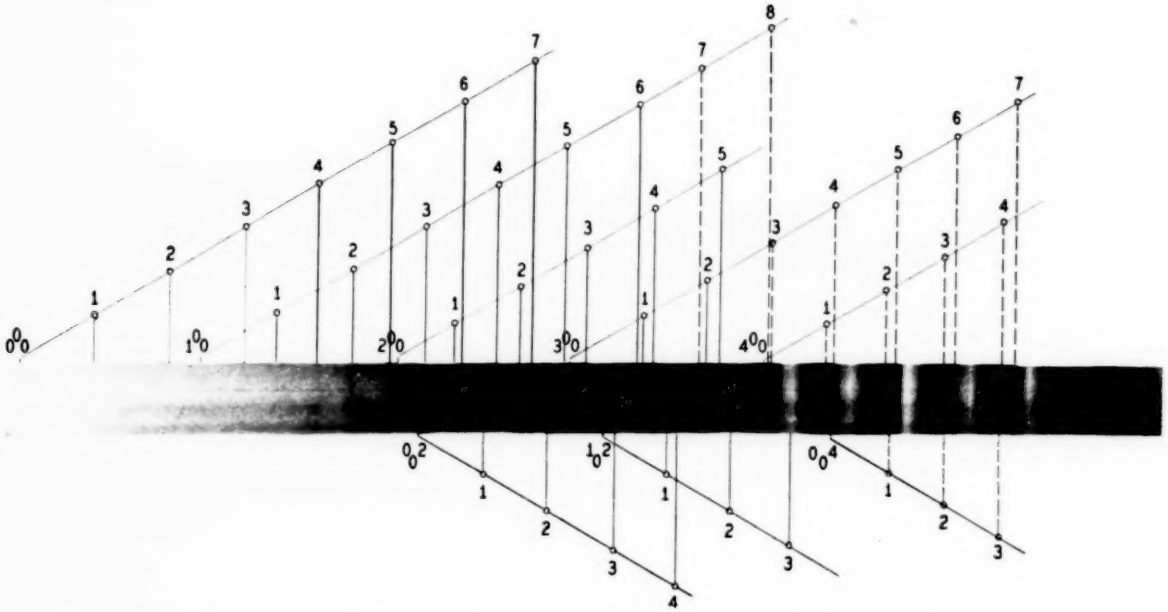

Fig. 1. Spectrogram of SO_2 at 5 mm pressure and 200°K in the region λ3400–2900, taken on the Hilger E1 spectrograph. The vibrational analysis is indicated at the sides of the spectrum; the quantum numbers v'_1, v'_2, v'_3, correspond to the symmetrical valence, the deformation, and the antisymmetrical vibrations respectively. The running numbers are for v'_2. The positions of bands near the system origin have been taken from spectrograms of SO_2 made at higher pressures. The dashed lines correspond to bands calculated by Eq. (1), which is based on bands marked by solid lines.

thermally insulated metal trough, which could be packed with dry ice, surrounded the absorption tube.

For studying the gross features of the electronic system, photographs were taken with a Hilger E3 spectrograph having a dispersion of 15.8A/mm at λ3200 and a Hilger E1 having a dispersion of 5.2A/mm in the same region. The light source used for these photographs was a conventional hydrogen discharge tube carrying 0.8 ampere at 5000 volts. In addition, it was desirable to have photographs taken on the 30-foot grating spectrograph to guide and confirm the vibrational analysis (cf. later discussion and preceding paper[9]). For this purpose a high power tungsten light source[10] was used. For the low dispersion photographs, the exposure time was about three minutes; for medium dispersion, exposures ranged from twenty minutes to an hour. In the region of λ3100 the high dispersion photographs required twenty hours with a slit width of twelve microns. In some cases where it was desired to observe the shape of the band envelopes, the maximum resolving power of 300,000 in the second order of the grating spectrograph was not necessary, and a wide slit of forty microns was used. The high dispersion photographs then required only three hours. Process and Eastman 33 plates were used. An iron arc provided the comparison spectrum.

Description and Analysis of Spectrum

A series of exposures taken under low dispersion at various increasing pressures of SO_2 exhibits a maximum absorption intensity around λ2900 with gradual fading out on both sides. (A photograph of a similar set of SO_2 exposures has been published by Watson and Parker.[2]) As the pressure is increased, the region of marked absorption increases toward both longer and shorter wave-lengths; at atmospheric pressure of SO_2, the long wave-length limit is nearly λ3400. The weaker electronic band system at longer wave-lengths appears at about 50 mm and is well developed at 760 mm. The latter system is more or less clearly separated from the strong absorption region under investigation.

From a study of the vibrational intensity distribution, one may conclude that both apex angle and bond distance have changed considerably in the transition. Consequently, from considerations based on the Franck-Condon principle, the vibrationless transition should be weak. Thus the system origin must lie at longer wave-lengths than the relatively strong bands identified by previous investigators as the vibrationless transition, that is, greater than λ3125. That it does is indeed confirmed by a comparison of spectrograms taken on the Hilger E1 spectrograph at pressures of 0.8 mm, 1.6 mm and 5.0 mm both at room temperature and at dry ice-acetone equilibrium temperature. They show conclusively that the bands lying at wave-lengths longer than λ3125 are definitely *not* from excited vibrational levels but from the vibrationless level in the normal state. The Boltzmann factor for one quantum of the deformation vibration is about 3.5 times smaller at 200° than at 300°K, for two quanta the ratio is 12.25; for one quantum of the ν_1 frequency the ratio is about 15.5. No such changes in intensity were observed for the bands mentioned when the temperature was lowered from 300° to 200°K.

At first it was suspected that the band corresponding to the vibrationless transition, although weak, would be among the bands that appear on the spectrogram taken with 5.0 mm pressure of SO_2 at 200°K. The band of longest wave-length under these conditions is at 30685 cm^{-1}. From this band a progression of quite evenly spaced bands proceeds toward higher frequencies at intervals of approximately 300 cm^{-1}, a spacing which is to be identified with the deformation, or bending, frequency. In addition to the latter progression, another progression, starting approximately in the middle of the first interval of the first progression, proceeds toward shorter wave-lengths with the same intervals. The obvious conclusion is that these two progressions differ by one quantum of the symmetrical valence, or breathing, frequency, and that the origin lies at still longer wave-lengths.

The relative positions of the two progressions indicate that the symmetrical valence frequency ν'_1 is some odd multiple of one-half the deformation frequency ν'_2. It is easily seen that a value near 450 cm^{-1} for ν'_1 is incompatible with the

[9] N. Metropolis, Phys. Rev. **60**, 283 (1941).
[10] H. Beutler and N. Metropolis, J. Opt. Soc. Am. **30**, 115 (1940).

TABLE I. *Absorption bands of sulphur dioxide. Observed bands and their associated vibrational quantum numbers. The bands without letters or * arising from the vibrationless level of the normal state have been used to determine the coefficients in Eq. (1). The intensity values are those of Clements. In the last column, the mean effective heights of the lower state vibrational levels above the vibrationless level are given as determined by Clements using a temperature variation method. The differences between observed and calculated bands are also given. The calculated values are from Eqs. (1) and (2). All data are for maxima of observed bands. The frequencies of bands labeled with letters or marked with * are taken from Clements, all others are from new measurements. Brackets on left of quantum numbers indicate overlapping bands. Brackets on right indicate that the intensity is to be divided between them. Intensity values in Parentheses are estimated by the author.*

ν	$v'_1v'_2v'_3$	$v''_1v''_2v''_3$	I†	Temp. Variation (cm^{-1})	Obs. ν − Calc. ν
29439	0 1 0	0 1 0	0.3	200	24
29622	0 0 0	0 0 0	0.3		0
29648	1 1 0	0 2 0	0.5		15
29742	0 2 0	0 1 0	0.8		18
29940	0 1 0	0 0 0	1.4	0	0
29994	2 0 0	1 0 0	1.2	1000	−12
30048	0 3 0	0 1 0	1.2	1000	18
	0 7 0	1 1 0			−16
30175	1 1 0	0 1 0	(1.2)		16
30249	0 2 0	0 0 0	3	150	0
30280	2 1 0	1 0 0			20
30386	1 0 0	0 0 0	6	300	0
	0 6 0	0 2 0			− 7
30435	0 0 1	0 0 0	(1.5)		− 3
30465	1 2 0	0 1 0	(3.0)		15
30551	0 3 0	0 0 0	10	70	− 4
30685	1 1 0	0 0 0	15	50	1
30721	0 1 1	0 0 0	20	0	− 6
30760	1 3 0	0 1 0	(10)		22
30848	0 4 0	0 0 0	25	60	− 8
30980	1 2 0	0 0 0	40	40	4
31037	1 4 0	0 1 0	40	40	17
31125	2 0 0	0 0 0	40	0	−10
31140	0 5 0	0 0 0			−12
31258	0 0 2	0 0 0	(30)		10
31275	1 3 0	0 0 0	(30)		12
31405	2 1 0	0 0 0	60	500	− 8
31430	0 6 0	0 0 0			−13
	2 3 0	0 1 0			− 3
31520	0 1 2	0 0 0	65		4
31567	1 4 0		60		22
31675	2 2 0		120		−10
31717	0 7 0		100		−21
31778	0 2 2		80		0
31840	1 5 0		90		16
31855	3 0 0				−14
31940	2 3 0			0	−13
31991	1 0 2		(20)	0	3
32033	0 3 2		(25)	0	− 3
32119	1 6 0		(30)	0	24
32140	3 1 0		(40)	0	9
32198	2 4 0	0 0 0		0	−17
32235	1 1 2		(25)	0	0
32276	0 4 2		(15)	0	−12
32377*C*	1 7 0		600	0	15
	3 2 0				− 6
32438	2 5 0		(120)	0	−34
32479	1 2 2		(15)	0	1
32607*D*	1 8 0		600	0	−18
	3 3 0				−21
	4 0 0				7
32713	1 3 2		(5)	0	− 3
32850*E*	3 4 0		1200	0	−23
	4 1 0				12
	0 0 4				−18
	3 5 0				−30
33080*F*	4 2 0		1700	0	10
	0 1 4				− 6
33313*G*	3 6 0		2000	0	−30
	4 3 0				15
	5 0 0				− 3
	0 2 4				15
33547*H*	3 7 0		1900	0	−23
	4 4 0				27
	5 1 0				13
	0 3 4				15
33760*J*	3 8 0		2000	0	−33
	4 5 0				22
	5 2 0				14
33960*K*	4 6 0		1700	0	10
	5 3 0				6
34030*L*	3 9 0		1600	0	20
	6 0 0				7
34241*	6 1 0[1]		700	0	20
34180*M*	4 7 0[1]		1600	0	22
	5 4 0[1]				24
34396*N*	6 2 0[1]		1600	0	7
34620*O*	6 3 0[1]		1700	0	19
34724*	7 0 0[1]		200	0	3
34785*	6 4 0[1]		1000	0	2
34970*	6 5 0[1]		500	0	9

† Intensity values from Clements (presumably at room temperature).
[1] Possibilities for superposed bands have not been exhausted.

experimental findings. For instance, it is difficult to explain the absence of many bands in case that $\nu'_1 = 450$ cm^{-1} is assumed. In addition, other considerations make this value unlikely. Using 750 cm^{-1} for ν'_1, however, one can identify not only a v'_1 progression but also combination overtones in harmony with the vibrational intensity distribution. Finally, the extrapolated pure v'_1 and pure v'_2 progressions have a common point at 29622 cm^{-1}, which must then be the origin of the band system. The photographs taken at higher pressures of SO_2 confirmed the positions of the origin and of the bands that were too weak on the low pressure photographs.

A band at 31258 cm^{-1} is moderately strong and comparable in intensity to its immediate neighbors. This band cannot be fitted into the scheme of the symmetrical vibrations, and temperature variation data of Clements[4] indicate that it is not from excited levels in the normal

state. Assuming that this band corresponds to two quanta of the antisymmetrical frequency ν'_3, one can also explain eight additional bands as combinations of the symmetrical vibrations with two quanta of the antisymmetrical. In addition, a very weak band is found at 30432 cm^{-1}, corresponding to one quantum of the ν'_3 frequency. Although this transition is forbidden by electronic selection rules,[11] it may, nevertheless, be permitted by vibronic selection rules.[12] In a later section, we shall discuss the possibilities for the electronic character of the upper state.

Figure 1 is a reproduction of a spectrogram taken at 200°K and at 5 mm pressure of SO_2, marked with a schematic representation of the vibrational analysis. Bands from excited vibrational levels of the normal state are not labeled in this photograph.

Table I contains a list of the bands according to increasing wave number, with their vibrational quantum number assignments. The wave numbers of the bands labeled A, B, C, $\cdots$ and of those marked with * are taken from the work of Clements, together with their absorption intensities. However, from only the present measurements, it is found that the vibrational energy levels of the excited state can be represented by the formula

$$\nu = 29622 + 770v'_1 + 320v'_2 + 813v'_3 - 6v'^2_1 - 2.5v'^2_2 - 20v'_1v'_2 - 25v'_2v'_3 - 15v'_1v'_3, \quad (1)$$

where v'_1, v'_2, v'_3 are the symmetrical valence, deformation, and antisymmetrical vibrational quantum numbers respectively. The three fundamental frequencies for the normal state as determined from Raman and infra-red data[13] are

$$\nu''_1 = 1152 \text{ cm}^{-1}, \quad \nu''_2 = 525, \quad \nu''_3 = 1361. \quad (2)$$

In order to account for the prominent series called A, B, C, $\cdots$ by Clements, Eq. (1) plus the term $+0.15v'^3_1$ have been used to calculate higher members of several progressions, and the results are indicated in Fig. 2 by dashed lines. Thus it is possible to explain the strong progression of Clements, not as a simple v'_2 progression as he did, but by superpositions of various higher combination bands. By application of the Franck-Condon principle, one expects that the pure v'_1 and v'_2 progressions, although of considerable length, do not contain the most intense bands. The latter are found among the combination overtones. Thus the individual bands have already considerable intensity and their superposition effects even higher absorption intensities.

Table I also contains a comparison of the observed and calculated positions of the bands. In the region where the overlapping of intense bands creates a fortuitous appearance of a simple progression, no attempt has been made to identify the various superposed bands individually; instead, the values of the observed maxima are taken from Clements. Better agreement between observed and calculated values cannot be expected for the following reasons: (1) The position of the maximum intensity is used since the location of the band origin is not known; (2) no account is made of resonance

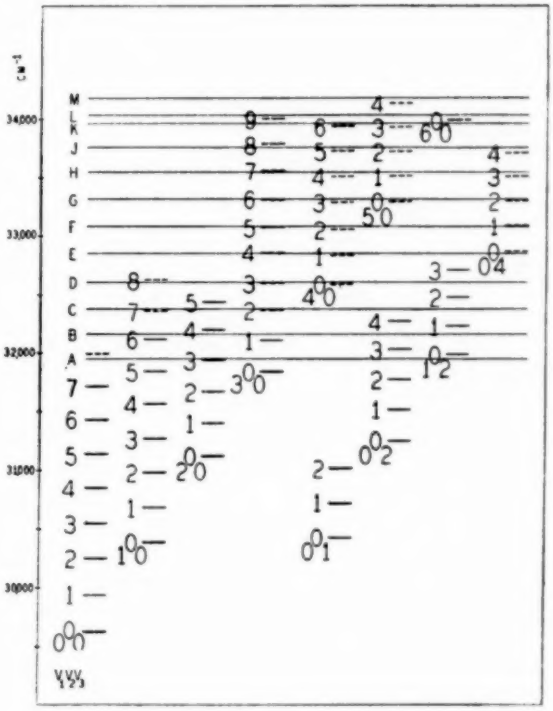

FIG. 2. Vibrational term scheme of the upper electronic state. The bands represented by short solid lines have been used to evaluate the coefficients in Eq. (1). The dashed lines correspond to bands calculated by this equation. Thus the A, B, C, $\cdots$ absorption regions can be interpreted as superpositions of several bands rather than as a pure v'_2 progression.

[11] G. Herzberg and E. Teller, Zeits. f. physik. Chemie **B21**, 410 (1938).
[12] Cf. R. S. Mulliken, Phys. Rev. **59**, 873 (1941).
[13] Cf. H. Sponer, *Molekülstruktur* (Julius Springer, Berlin, 1934).

interactions between superposed vibrational levels; (3) overlapping bands arising from low lying excited vibrational levels of the ground state may distort the intensity distribution of a given band appreciably.

Included in Table I are eleven bands which arise from excited levels of the normal state and whose positions are in agreement with what may be calculated from Eq. (1) combined with Eqs. (2).

It was hoped that the photographs taken under high dispersion would exhibit some characteristic feature in the rotational structure, as does the system at λ3880, so that analogous positions in each band could be measured and used instead of the intensity maxima under low dispersion. Unfortunately this was not the case.

Discussion of Results

When the values of the three upper state fundamental frequencies, $\nu'_1 = 794$ cm^{-1}, $\nu'_2 = 345$ cm^{-1}, $\nu'_3 = 833$ cm^{-1}, are substituted in theoretical formulas based on a valence force model,[14] one obtains two solutions, 100.3° and 79.7°, as possible values for the apex angle. Since there are only seven members of appreciable intensity in the pure v'_2 progression, one is strongly inclined to favor the value of 100.3°.[15] Jonescu[16] from a study of rotational structures in the region λ3000, using the first and second orders of a twenty-one foot grating spectrograph (resolving power not given), reports in a brief communication an apex angle of 96° in the excited and 120° in the normal state. He calculated and plotted band structures assuming various values for α, but keeping the assumed bond distance always fixed at $r = 1.36$A for both electronic states, and compared the results with observed structures. Because, however, of the considerable superposition of bands shown by the present work to exist in the region Jonescu studied, it is very doubtful that any single band can be present there under favorable conditions for investigating the rotational structure; furthermore, calculation shows that the most intense lines for room temperature must be around $J = 20$. Consequently Jonescu's results do not appear to be conclusive, even though there is good agreement of his α' with the value calculated from the fundamental frequencies obtained here.

That the angle has decreased in the upper state is, however, confirmed by the present high dispersion photographs, where the irregular band structures indicate quite definitely that the molecule becomes a more asymmetrical top (see below). The type of structure which would have been expected if the angle had remained unchanged or increased slightly in the transition can be judged from a study of the high dispersion photographs of the λ3880 system of SO_2 and of the figures of the preceding paper.

Clements developed a temperature variation method for determining the heights of initial vibration levels above the vibrationless level. The determination is based on photometric measurements of absorption at two temperatures not too widely separated. The method was first applied to SO_2, and it is interesting to see whether his results are in harmony with the present analysis. Since the various contiguous regions of the spectrum, in which he applied the method, did not overlap, it was possible only for him to compare bands in each region with reference to a fiducial band in that region. However, the present analysis shows that the fiducial bands for all the regions are from the vibrationless level of the normal state. Thus it is possible to compare various regions directly. Referring to the last column of Table I, one sees that the present assignments are in harmony with Clements' data, except, perhaps, for the value of 200 cm^{-1} for $(010)' \leftarrow (010)''$, which lies on the long wave-length side of the vibrationless transition. Very likely, however, an absorption band (arising from the vibrationless level) of the adjacent electronic system overlaps $(010)' \leftarrow (010)''$, giving effectively a value of 200 cm^{-1}.

The considerable overlapping in the absorption regions *A*, *B*, *C*, ··· may explain why Kusch and Loomis[17] obtained such widely varying magnetic rotation spectra for these "bands."

[14] C. R. Bailey and A. B. D. Cassie, Proc. Roy. Soc. **A137**, 630 (1932).

[15] Cf. J. B. Coon, Phys. Rev. **58**, 926(L) (1940). He reported only two bands in a v'_2 progression in ClO_2 corresponding to a change in apex angle from 122° to 114°.

[16] A. Jonescu, Comptes rendus **196**, 1476 (1933).

[17] P. Kusch and F. W. Loomis, Phys. Rev. **55**, 850 (1939).

The electronic character of the excited state is indicated as singlet by the strong absorption intensity. The presence of two bands in which definitely one quantum of the antisymmetrical vibration is excited, taken in connection with a consideration of the vibronic selection rules, show that the excited state must be either $^1A_1$ or $^1B_2$ (cf. reference 12, Table XI). Were it possible to determine whether the bands under discussion are of the perpendicular or parallel type, one could determine uniquely the nature of the upper electronic state ($^1B_2$ if these bands are of the parallel type, $^1A_1$ if they are perpendicular).

In conclusion, a few remarks may be made concerning the prospects of a rotational analysis of this system. As a result of a decrease in the apex angle ($2\alpha' = 100°$) in the transition, the regularity of symmetric top levels must be entirely lost (cf. Fig. 4 of reference 12), thus rendering the analysis more difficult. In addition, there should be greater overlapping of sub-band structure. Another point is the scarcity of bands free from overlapping; those bands which are intense enough at low pressures, where low temperatures could then be used to reduce the complexity, are considerably overlapped, as we have seen. Those near the system origin require higher pressures to obtain sufficient absorption. The increased pressure precludes work at low temperatures, tends to broaden the rotational lines and makes probable the presence of overlapping, low lying excited vibrational levels of the normal state.

The author is indebted to Professor Robert S. Mulliken and Dr. Hans G. Beutler for helpful suggestions.

AUGUST 15, 1941 PHYSICAL REVIEW VOLUME 60

Spectra of Argon in the Extreme Ultraviolet

L. W. PHILLIPS AND W. L. PARKER
Department of Physics, University of Illinois, Urbana, Illinois

(Received June 23, 1941)

A simple method for the excitation of spectra of higher stages of ionization of rare gases is described. Applied to argon, the method has yielded spectra of all stages of ionization from A III to A IX. Classified lines in the extreme ultraviolet and term tables for the ions V to IX are given. Some minor additions and corrections to previous analyses of Cl V and Cl VI are pointed out.

GENERAL AND EXPERIMENTAL

THE extreme ultraviolet spectra of argon have been studied by a number of investigators, the latest work being that of Boyce.[1] References to earlier work may be found in his paper. As a result of these investigations, the spectra of the first four stages of ionization are quite well known. Two multiplets in A V due to transitions from the first excited configuration to the ground state configuration were found by Boyce, but nothing else was known in V or in higher stages. The present investigation was undertaken in the hope of extending the analysis to higher stages of ionization. A preliminary report has already been published.[2]

The method of excitation used is simple and effective. It consists of introducing the gas directly into the space between the two electrodes of an ordinary vacuum spark such as is usually used for the excitation of the spectra of other highly ionized elements. To accomplish this a one-eighth-inch hole is drilled axially into the lower electrode. The gas is fed into the bottom of this hole through a small bronze capillary, which passes through the bottom of the lower electrode holder and is connected to a reservoir in which

[1] J. C. Boyce, Phys. Rev. **48**, 396 (1935).

[2] W. L. Parker and L. W. Phillips, Phys. Rev. **58**, 93 (1940).

the gas is kept at low pressure. The gas then passes up into the spark gap where it is excited. Mercury diffusion pumps operating continually keep the gas from accumulating in the spark chamber and building up the pressure to a point where an arc discharge could occur.

In the original installation the rate of flow of argon was controlled both by the reservoir pressure and by a needle valve placed between the reservoir and the spark chamber. In later work the needle valve was removed and the flow controlled entirely by adjustment of the reservoir pressure. With an electrode separation of from four to six millimeters, argon was admitted from the storage bulb into the reservoir until a pressure was reached at which sparking occurred at a rate of from 60 to 100 sparks per minute. The optimum flow of argon was about 1 cc per minute.

The condensed discharge was obtained by means of a condenser bank consisting of nine General Electric pyranol capacitors arranged three in series, three in parallel, to give a combination having a capacity of 0.35 microfarad. The pictures were taken on the twenty-one-foot grazing incidence vacuum spectrograph at voltages ranging from 100 to 120 kilovolts. A three-quarter-inch air gap in series with the vacuum gap kept the spark from passing before the condensers were charged to full potential.

The pictures were taken with aluminum or carbon electrodes; the exposures ranged from 15,000 to 25,000 sparks. Commercial tank argon, contaminated with oxygen and nitrogen, was used for all but one exposure, which was made

TABLE I. *Classified lines of* A V.

INT.	λ(VAC.)	ν(CM^{-1})	CLASSIFICATION
2*	836.126	119,599	$3s^23p^2\ {}^3P_2-3s3p^3\ {}^3D_1$
1*	835.792	119,647	${}^3P_2-\ {}^3D_2$
4*b*	834.878	119,778	${}^3P_2-\ {}^3D_3$
3*	827.349	120,868	${}^3P_1-\ {}^3D_1$
5*	827.055	120,911	${}^3P_1-\ {}^3D_2$
4*	822.159	121,631	${}^3P_0-\ {}^3D_1$
3*	715.645	139,734	$3s^23p^2\ {}^3P_2-3s3p^3\ {}^3P_2$
4*	715.599	139,743	${}^3P_2-\ {}^3P_1$
5*	709.195	141,005	${}^3P_1-\ {}^3P_{0,1,2}$
3*	705.353	141,773	${}^3P_0-\ {}^3P_1$
5	558.481	179,057	$3s^23p^2\ {}^1D_2-3s3p^3\ {}^1P_1$
6	527.693	189,504	$3s^23p^2\ {}^3P_2-3s3p^3\ {}^3S_1$
5	524.189	190,771	${}^3P_1-\ {}^3S_1$
3	522.090	191,538	${}^3P_0-\ {}^3S_1$
0	517.250	193,330	$3s^23p^2\ {}^3P_2-3s3p^3\ {}^1P_1$
1	513.914	194,585	${}^3P_1-\ {}^1P_1$
0	511.886	195,356	${}^3P_0-\ {}^1P_1$
7	463.938	215,546	$3s^23p^2\ {}^3P_2-3s^23p3d\ {}^3P_2$
3	462.415	216,256	${}^3P_2-\ {}^3P_1$
6*b*	461.227	216,813	${}^3P_1-\ {}^3P_2$
1	459.728	217,520	${}^3P_1-\ {}^3P_1$
2	458.975	217,877	${}^3P_1-\ {}^3P_0$
3	458.121	218,283	${}^3P_0-\ {}^3P_1$
1	450.079	222,183	$3s^23p^2\ {}^3P_2-3s^23p3d\ {}^3D_1$
4	449.493	222,473	${}^3P_2-\ {}^3D_2$
18	449.065	222,685	${}^3P_2-\ {}^3D_3$
4	447.527	223,450	${}^3P_1-\ {}^3D_1$
8	446.949	223,739	${}^3P_1-\ {}^3D_2$
5	445.997	224,217	${}^3P_0-\ {}^3D_1$
3	350.878	284,999	$3s^23p^2\ {}^1D_2-3s^23p4s\ {}^1P_1$
3	339.886	294,216	$3s^23p^2\ {}^3P_2-3s^23p4s\ {}^3P_1$
3	339.009	294,977	${}^3P_1-\ {}^3P_0$
2	338.426	295,486	${}^3P_1-\ {}^3P_1$
6	337.998	295,860	${}^3P_2-\ {}^3P_2$
3	337.555	296,248	${}^3P_0-\ {}^3P_1$
3	336.555	297,128	${}^3P_1-\ {}^3P_2$

* Classified by Boyce, reference 1.

TABLE II. A V *term values.*

CONFIGURATION	J	RELATIVE TERM VALUE
$3s^2p^2\ {}^3P$	0	0
	1	765
	2	2,032
${}^1D$	2	16,301
$3s3p^3\ {}^3D$	1	121,632
	2	121,678
	3	121,810
${}^3P$	2	141,764
	1, 0	141,773
${}^3S$	1	191,537
${}^1P$	1	195,356
$sp3d\ {}^3P$	2	217,578
	1	218,286
	0	218,642
${}^3D$	1	224,216
	2	224,505
	3	224,717
$sp4s\ {}^3P$	0	295,742
	1	296,249
	2	297,893
${}^1P$	1	301,300

TABLE III. *Observed nebular lines.*

OBSERVER	$^3P_1-{}^1D_2$	$^3P_2-{}^1D_2$
Stoy[3]	6435.0	7007
Bowen[6]	6435	7005
Bowen and Wyse[7]		
NGC 7662	6435.2	
NGC 7027	6434.6	
Average λ	6435	7006
$\nu-\text{cm}^{-1}$	15,536	14,270
From term table	15,536	14,269

TABLE IV. *Classified lines of* A VI.

INT.	λ(VAC.)	ν(CM⁻¹)	CLASSIFICATION
4	596.694	167,590	$3s^23p\ ^2P_{3/2}-3s3p^2\ ^2S_{1/2}$
5	588.921	169,802	$^2P_{1/2}-\ ^2S_{1/2}$
3	594.096	168,323	$3s3p^2\ ^4P_{5/2}-3p^3\ ^4S_{3/2}$
2	589.783	169,554	$^4P_{3/2}-\ ^4S_{3/2}$
1	587.006	170,356	$^4P_{1/2}-\ ^4S_{3/2}$
4	555.639	179,973	$3s^23p\ ^2P_{3/2}-3s3p^2\ ^2P_{1/2}$
8	551.371	181,366	$^2P_{3/2}-\ ^2P_{3/2}$
5	548.905	182,181	$^2P_{1/2}-\ ^2P_{1/2}$
4	544.731	183,577	$^2P_{1/2}-\ ^2P_{3/2}$
4	466.932	214,164	$3s3p^2\ ^4P_{5/2}-3s3p3d\ ^4P_{5/2}$
2	465.586	214,783	$^4P_{5/2}-\ ^4P_{3/2}$
4	464.257	215,398	$^4P_{3/2}-\ ^4P_{5/2}$
1	461.898	216,498	$^4P_{3/2}-\ ^4P_{1/2}$
6[b]	461.227	216,813	$^4P_{1/2}-\ ^4P_{3/2}$
1	460,202	217,296	$^4P_{1/2}-\ ^4P_{1/2}$
4	462.146	216,382	$3s^23p\ ^2P_{3/2}-3s^23d\ ^2D_{3/2}$
25	462.007	216,447	$^2P_{3/2}-\ ^2D_{5/2}$
20[b]	457.475	218,591	$^2P_{1/2}-\ ^2D_{3/2}$
1	460.058	217,364	$3s3p^2\ ^4P_{5/2}-3s3p3d\ ^4D_{3/2}$
3	459.603	217,579	$^4P_{5/2}-\ ^4D_{5/2}$
10	459.320	217,713	$^4P_{5/2}-\ ^4D_{7/2}$
1	458.039	218,322	$^4P_{3/2}-\ ^4D_{1/2}$
20[b]	457.475	218,591	$^4P_{3/2}-\ ^4D_{3/2}$
5	457.007	218,815	$^4P_{3/2}-\ ^4D_{5/2}$
3	456.375	219,118	$^4P_{1/2}-\ ^4D_{1/2}$
2	455.813	219,388	$^4P_{1/2}-\ ^4D_{3/2}$
6	294.052	340,076	$3s^23p\ ^2P_{3/2}-3s^24s\ ^2S_{1/2}$
5	292.154	342,285	$^2P_{1/2}-\ ^2S_{1/2}$
3	283.164	353,152	$3s3p^2\ ^4P_{3/2}-3s3p4s\ ^4P_{1/2}$
1	282.556	353,912	$^4P_{3/2}-\ ^4P_{3/2}$
6	282.423	354,079	$^4P_{5/2}-\ ^4P_{5/2}$
4	281.915	354,717	$^4P_{1/2}-\ ^4P_{3/2}$
3	281.433	355,324	$^4P_{3/2}-\ ^4P_{5/2}$
5	220.946	452,600	$3s^23p\ ^2P_{3/2}-3s^24d\ ^2D_{5/2}$
3	219.896	454,760	$^2P_{1/2}-\ ^2D_{3/2}$
3	180.719	553,345	$3s^23p\ ^2P_{3/2}-3s^25d\ ^2D_{5/2}$
2	180.074	555,327	$^2P_{1/2}-\ ^2D_{3/2}$

[b] Blend.

with s.p. argon. The oxygen and nitrogen lines in the region are all well known and were, in many cases, used as standards. In addition, carbon and aluminum lines, and in some instances copper lines from an overlapping picture, were used as standards.

The argon spectrograms were quite rich in lines. All stages of ionization from III to IX appear on the plates. The spectrum of argon VI appears to have been the most strongly excited, with V, VII, and VIII less intense but still quite strong. Known lines of argon IV in the region are quite weak, and only the strongest argon III lines given by Boyce appear. The spectrum of argon II seems to be definitely absent.

ARGON V

Argon V is isoelectronic with silicon I. The spectra of all other ions in the sequence through titanium IX are known, and references to the work on these ions may be found in the bibliography recently published by Boyce.[3] The ground state of silicon-like ions is $3s^23p^2$, giving a normal ^3P ground state with ^1D and ^1S lying above it. In phosphorus II and succeeding ions the first excited configuration is $3s3p^3$, giving $^{5,3}(S)$ and $^{3,1}(P, D)$ terms. The next configurations are $3s^23p3d$ and $3s^23p4s$. Boyce classified the $^3P-{}^3D$ and $^3P-{}^3P$ multiplets coming from the $3s^23p^2-3s3p^3$ transition. Most of the other lines coming from this transition, and the triplet multiplets arising from the transitions $3s^23p^2-3s^23p3d$, $3s^23p4s$, have now been identified. The intercombination lines $3s^23p^2\ ^3P_{0,1,2}-3s3p^3\ ^1P_1$ have been found, hence it is possible to tie the singlet and triplet systems together. A complete list of all the argon V lines so far classified is given in Table I, and the term values in Table II.

TABLE V. A VI *term values.*

CONFIGURATION	J	RELATIVE TERM VALUE
	Doublets	
$3s^23p\ ^2P$	1/2	0*
	3/2	2,210
$3s3p^2\ ^2S$	1/2	169,801
^2P	1/2	182,182
	3/2	183,577
$3s^23d\ ^2D$	3/2	218,592
	5/2	218,657
$3s^24s\ ^2S$	1/2	342,286
$3s^24d\ ^2D$	3/2	454,760
	5/2	454,810
$3s^25d\ ^2D$	3/2	555,330
	5/2	555,555
	Quartets	
$3s3p^2\ ^4P$	1/2	0**
	3/2	802
	5/2	2,034
$3p^3\ ^4S$	3/2	170,356
$sp3d\ ^4P$	5/2	216,199
	3/2	216,815
	1/2	217,298
^4D	1/2	219,121
	3/2	219,393
	5/2	219,615
	7/2	219,747
$sp4s\ ^4P$	1/2	353,954
	3/2	354,716
	5/2	356,115

* (721,300±300) cm⁻¹ below ground state of A VII.
** Estimated (100,000±1000) cm⁻¹ above $3s^23p\ ^2P$.

[3] J. C. Boyce, Rev. Mod. Phys. **13**, 1 (1941).

Robinson[4] has suggested that the pair of nebular lines at 6435 and 7005A are due to transitions from the metastable $3s^23p^2\ ^1D_2$ to $3s^23p^2\ ^3P_{1,2}$. This suggestion can now be verified. Taking 6434.8 and 7005A as averages of values given by Stoy,[5] Bowen,[6] and Bowen and Wyse[7] for the wave-lengths of the nebular lines (see Table III), one obtains wave numbers of 15,536 cm^{-1} and 14,270 cm^{-1}, respectively. These are in good agreement with the values of 15,536 cm^{-1} and 14,269 cm^{-1} derived from the term table.

No series have been discovered so the only estimate of the ionization potential which is possible is a rough one based on data for the earlier members of the isoelectronic sequence. Boyce's value of 78 volts is still retained.

Argon VI

Argon VI is isoelectronic with aluminum I. The spectra of all other ions in the sequence are quite well known through scandium IX and references to previous work on these ions are given by Boyce.[3] Beyond scandium IX, Edlén[8] has identified the transition $3s^23p\ ^2P-3s^24d\ ^2D$ in the ions titanium X to cobalt XVI. The ground state configuration of aluminum-like ions is $3s^23p$, giving a normal ^2P ground state. The $3p$ electron may be excited to higher states giving a system of doublet levels similar to those of the alkali metals. Another series of levels is obtained by excitation of one of the $3s$ electrons. The resulting configurations of the type $3s3pnl$ give rise to quartet as well as doublet terms. The first excited configuration of this type is $3s3p^2$, which gives rise to $(^3P)\ ^{2,4}P$, $(^1D)\ ^2D$ and $(^1S)\ ^2S$. Of these, the $(^3P)\ ^4P$ lies deepest and is the ground state of the quartet system. A third possibility is the excitation of both $3s$ electrons, giving rise to the states $3p^3\ ^4S$, $^2(P, D)$.

All of the lines so far identified in the spectrum of argon VI are given in Table IV. Terms are listed in Table V. No intercombinations have been found, so the doublet and quartet systems cannot be tied together accurately. Accordingly, the two systems of terms are listed separately. The location of $3s3p^2\ ^4P_{1/2}$ is estimated to be $100{,}000\pm1000$ cm^{-1} above $3s^23p\ ^2P_{1/2}$.

Table VI. *Classified lines of* A VII.

Int.	λ(Vac.)	ν(cm⁻¹)	Classification
2	644.388	155,186	$3s3p\ ^3P_2-3p^2\ ^3P_1$
2	641.318	155,929	$^3P_1-\ ^3P_0$
1	637.466	156,871	$^3P_1-\ ^3P_1$
4	637.052	156,973	$^3P_2-\ ^3P_2$
2	634.208	157,677	$^3P_0-\ ^3P_1$
2	630.306	158,653	$^3P_1-\ ^3P_2$
15	585.754	170,720	$3s^2\ ^1S_0-3s3p\ ^1P_1$
2	479.485	208,557	$3s3p\ ^3P_2-3s3d\ ^3D_2$
12	479.379	208,603	$^3P_2-\ D_3$
2	475.733	210,202	$^3P_1-\ D_1$
8	475.656	210,236	$^3P_1-\ D_2$
4	473.938	210,998	$^3P_0-\ D_1$
6	297.701	335,907	$3s3d\ ^3D_3-3s4f\ ^3F_4$
4	297.658	335,956	$^3D_2-\ ^3F_3$
3	297.621	335,998	$^3D_1-\ ^3F_2$
7	250.940	398,502	$3s3p\ ^3P_2-3s4s\ ^3S_1$
5	249.886	400,183	$^3P_1-\ ^3S_1$
2	249.384	400,988	$^3P_0-\ ^3S_1$
7	192.635	519,116	$3s3p\ ^3P_2-3s4d\ ^3D_3$
5	192.041	520,722	$^3P_1-\ ^3D_2$
3	191.759	521,489	$^3P_0-\ ^3D_1$
10	176.566	566,362	$3s^2\ ^1S_0-3s4p\ ^1P_1$
3	152.259	656,775	$3s3p\ ^3P_2-3s5d\ ^3D_3$
2	151.876	658,430	$^3P_1-\ ^3D_2$
1	151.698	659,205	$^3P_0-\ ^3D_1$

Table VII. A VII *term values.*

Configuration	J	Relative Term Value
	Singlets	
$3s^2\ ^1S$	0	0*
$3s3p\ ^1P$	1	170,720
$3s4p\ ^1P$	1	566,362
	Triplets	
$3s3p\ ^3P$	0	0**
	1	805
	2	2,486
$3p^2\ ^3P$	0	156,734
	1	157,675
	2	159,459
$3s3d\ ^3D$	1	211,002
	2	211,041
	3	211,089
$3s4s\ ^3S$	1	400,988
$3s4d\ ^3D$	1	521,489
	2	521,527
	3	521,602
$3s4f\ ^3F$	2, 3, 4	546,997
$3s5d\ ^3D$	1	659,205
	2	659,230
	3	659,260

* Estimated 1,005,000 cm^{-1} below ground state of A VIII.
** Estimated 114,000 cm^{-1} above $3s^2\ ^1S_0$.

[4] H. A. Robinson, Nature **137**, 992 (1936).
[5] R. H. Stoy, Lick Obs. Bull. No. 480, 179 (1935).
[6] I. S. Bowen, Rev. Mod. Phys. **8**, 55 (1936).
[7] I. S. Bowen and A. B. Wyse, Lick Obs. Bull. No. 495, 1 (1939).
[8] B. Edlén, Zeits. f. Physik **103**, 536 (1936).

TABLE VIII. *Classified lines of* A VIII.

INT.	λ(VAC.)	ν(CM⁻¹)	CLASSIFICATION
*	713.990	140,058	$3s\ ^2S_{1/2}-3p\ ^2P_{1/2}$
*	700.398	142,776	$^2S_{1/2}-\ ^2P_{3/2}$
1	526.870	189,800	$3p\ ^2P_{3/2}-3d\ ^2D_{3/2}$
5	526.457	189,949	$^2P_{3/2}-\ ^2D_{5/2}$
3	519.429	192,519	$^2P_{1/2}-\ ^2D_{3/2}$
0*d*	338.222	295,664	$3d\ ^2D_{3/2}-4p\ ^2P_{1/2}$
2*d*	337.257	296,510	$^2D_{5/2}-\ ^2P_{3/2}$
6	260.332	384,125	$3d\ ^2D_{5/2}-4f\ ^2F_{7/2}$
4	260.253	384,242	$^2D_{3/2}-\ ^2F_{5/2}$
7	230.875	433,135	$3p\ ^2P_{3/2}-4s\ ^2S_{1/2}$
5	229.437	435,850	$^2P_{1/2}-\ ^2S_{1/2}$
5	184.315	542,550	$3d\ ^2D_{5/2}-5f\ ^2F_{7/2}$
3	184.273	542,672	$^2D_{3/2}-\ ^2F_{5/2}$
15	180.254	554,772	$3p\ ^2P_{3/2}-4d\ ^2D_{5/2}$
10	179.400	557,413	$^2P_{1/2}-\ ^2D_{3/2}$
5	159.175	628,240	$3s\ ^2S_{1/2}-4p\ ^2P_{1/2}$
8	158.923	629,236	$^2S_{1/2}-\ ^2P_{3/2}$
3	149.333	669,644	$3p\ ^2P_{3/2}-5s\ ^2S_{1/2}$
2	148.725	672,385	$^2P_{1/2}-\ ^2S_{1/2}$
5	138.440	722,335	$3p\ ^2P_{3/2}-5d\ ^2D_{5/2}$
3	137.926	725,025	$^2P_{1/2}-\ ^2D_{3/2}$
1	123.033	812,790	$3p\ ^2P_{3/2}-6d\ ^2D_{5/2}$
0	122.624	815,500	$^2P_{1/2}-\ ^2D_{3/2}$
1	120.157	832,250	$3s\ ^2S_{1/2}-5p\ ^2P_{1/2}$
2	120.093	832,690	$^2S_{1/2}-\ ^2P_{3/2}$

* Calculated from the term table.

The $3s^25d\ ^2D$ term may be open to question because of the anomalously large separation. However, both in Cl V[9] and Ca VIII[10] the 5*d* separation is found to be larger than the 4*d* separation, though not as much larger proportionately. The values for the $4d\ ^2D$, $5d\ ^2D$ separations are, respectively, 33 and 73 cm⁻¹ in chlorine, 50 and 225 cm⁻¹ in argon, and 191 and 210 cm⁻¹ in calcium. These are the only ions beyond aluminum for which both separations are known.

A calculation of the series limit, based on three members of the $3s^23p-3s^2nd$ series, gives 721,300±300 cm⁻¹. This corresponds to an ionization potential of 89.00±0.05 volts for argon VI.

ARGON VII

Argon VII is isoelectronic with magnesium I. The spectra of all other ions in the sequence through cobalt XVI are known and references to the work on these ions are given by Boyce.[3] The ground state of the magnesium-like ions is $3s^2\ ^1S$. The first excited state is $3s3p$, giving a ^1P, and a ^3P which is the deepest term of the triplet system. Above these states are terms of the type $3snl$, giving rise to $^{1,3}L$ levels. Other series of terms come from the excitation of both electrons, i.e., configurations of the type $3pnl$, etc. The lowest of these is $3p^2$, giving ^3P, ^1D and ^1S terms.

A few of the strong singlet lines and a number of triplets have been identified and are listed in Table VI. Term values are given in Table VII. No intercombinations have been found. A series limit calculation based on three members of the series $3s3p-3snd$ yields 891,000±200 cm⁻¹ for $3s3p\ ^3P_0$ with respect to the ground state of A VIII. The $3s^2\ ^1S_0-3s3p\ ^3P_1$ interval can be estimated by extrapolation of data on other ions in the sequence, or can be calculated by Houston's

TABLE IX. A VIII *term values and effective quantum numbers.*

CONFIGURATION	*J*	ABSOLUTE TERM VALUES	*n**
$3s\ ^2S$	1/2	1,157,400	2.4633
$3p\ ^2P$	1/2	1,017,342	
	3/2	1,014,624	2.6310
$3d\ ^2D$	3/2	824,824	
	5/2	824,673	2.9183
$4s\ ^2S$	1/2	581,490	3.4753
$4p\ ^2P$	1/2	529,160	
	3/2	528,163	3.6466
$4d\ ^2D$	3/2	459,929	
	5/2	459,852	3.9080
$4f\ ^2F$	5/2	440,582	
	7/2	440,548	3.9927
$5s\ ^2S$	1/2	344,978	4.5120
$5p\ ^2P$	1/2	325,155	
	3/2	324,709	4.6507
$5d\ ^2D$	3/2	292,316	
	5/2	292,289	4.9019
$5f\ ^2F$	5/2	282,152	
	7/2	282,123	4.9894
$6d\ ^2D$	3/2, 5/2	201,840	5.8989

TABLE X. *Classified lines and term values of* A IX.

CONFIGURATION			$2p^53s\ ^3P_1$	$2p^53s\ ^1P_1$
	TERM VALUE		2,033,350	2,052,120
		Int.	(5)	(5)
		λ(vac.)	49.180	48.730
$2p^6\ ^1S_0$	0	ν(cm⁻¹)	2,033,350	2,052,120

[9] See Table XII.
[10] L. W. Phillips, Phys. Rev. **55**, 708 (1939).

TABLE XI. *$sp^2\ ^4P-sp3d\ ^4P$ multiplet in* Cl V.

TERM		$sp3d\ ^4P$													
	J	1/2				3/2					5/2				
$sp^2\ ^4P$	1/2	184,746	[3]		322	184,424	[8]								
		539				539									
	3/2	184,207	[4]		322	183,885	[1]		437		183,448	[10]			
		181,450	*(2)*	*[7]*	*173*	*181,277*	*(1)*	*[1]*	*415*		*180,862*	*(2B)*	*[1]*		
						845					843				
						840					*839*				
	5/2					183,040	[6]		435		182,605	[10]			
						180,437	*(1)*	*[6]*	*414*		*180,023*	*(1)*	*[10]*		

method. An average of 114,000 cm^{-1} is found for the interval $3s^2\ ^1S_0-3s3p\ ^3P_0$. The final value for $3s^2\ ^1S_0$ with respect to the ground state of A VIII is 1,005,000±1000 cm^{-1}. The ionization potential of argon VII is 124.0±0.1 volts.

ARGON VIII

Argon VIII is isoelectronic with sodium I. The spectra of all other ions in the sequence, through copper XIX, are known and references may be found in Boyce's report and in a previous paper from this laboratory.[11] The ground state of sodium-like ions is $3s\ ^2S$. Excitation of the single valence electron yields the well-known doublet spectrum.

Table VIII gives all the lines which have been identified in argon VIII. The resonance lines, $3s\ ^2S-3p\ ^2P$, are just out of the range of the spectrograph. The $3d-4p$ transition has been found, and this serves to tie the whole term table together. Calculated wave-lengths and wave numbers for the resonance lines have been entered in the list of classified lines for convenience. Four members of the series $3p-nd$ have been identified, so that a more accurate calculation of absolute term values is possible. The ionization potential is 142.82±0.05 volts. Absolute term values and effective quantum numbers are given in Table IX.

TABLE XII. *Classified lines and term values of* Cl V.

INT.	λ(VAC.)	(CM^{-1})	CLASSIFICATION		TERM VALUES*	
10	547.630	182,605	$sp^2\ ^4P_{5/2}-sp3d\ ^4P_{5/2}$			
6	546.329	183,040	$^4P_{5/2}$	$^4P_{3/2}$		
10	545.114	183,448	$^4P_{3/2}$	$^4P_{5/2}$		
1	543.818	183,885	$^4P_{3/2}$	$^4P_{3/2}$	$sp3d\ ^4P$	
4	542.868	184,207	$^4P_{3/2}$	$^4P_{1/2}$	5/2	277,014
8	542.229	184,424	$^4P_{1/2}$	$^4P_{3/2}$	3/2	276,577
3	541.284	184,746	$^4P_{1/2}$	$^4P_{1/2}$	1/2	276,255
3	537.461	186,060	$sp^2\ ^4P_{3/2}-sp3d\ ^4D_{1/2}$			
2	237.231	421,530	$s^2p\ ^2P_{3/2}-s^25d\ ^2D_{5/2}$		$s^25d\ ^2D$	
1	236.435	422,949	$^2P_{1/2}$	$^2D_{3/2}$	3/2	124,051
					5/2	123,978

* See Table VI, reference 11.

TABLE XIII. *Classified lines and term values of* Cl VI.

INT.	λ(VAC.)	(CM^{-1})	CLASSIFICATION		TERM VALUES	
2	580.444	172,282	$3p^2\ ^3P_2-3p3d\ ^3P_2$			
1	577.444	173,177	$^3P_2$	$^3P_1$	$3p3d\ ^3P$**	
2	576.419	173,485	$^3P_1$	$^3P_2$	2	310,932
1	571.376	175,016	$^3P_0$	$^3P_1$	1	311,828
0	570.881	175,168	$^3P_1$	$^3P_0$	0	312,615
0	571.435	174,998	$3p^2\ ^3P_2-3p3d\ ^3D_1$			
2	570.529	175,276	$^3P_2$	$^3D_2$	$3p3d\ ^3D$	
4	570.025	175,431	$^3P_2$	$^3D_3$	1	313,655
1	567.479	176,218	$^3P_1$	$^3D_1$	2	313,928
2	566.630	176,482	$^3P_1$	$^3D_2$	3	314,081
6*	565.480	176,841	$^3P_0$	$^3D_1$		

* Blend with Cl III line.
** See Table V, reference 13.

ARGON IX

Argon IX is isoelectronic with neon I. References to work on the spectra of neon I—silicon V, chlorine VIII, and potassium X—cobalt XVIII are given in Boyce's bibliography. The ground state of neon-like ions is $2p^6\ ^1S$. The first excited configuration is $2p^53s$, giving $^{1,3}P$, of which $^3P_1$ and $^1P_1$ combine with the ground state. The two lines which have been identified as arising from these transitions in argon IX, together with term values calculated therefrom, are given in Table X. The lines were measured with respect to nearby Cl VIII lines, and may be in error by as much as 100 cm^{-1} (equivalent to 0.002 angstrom).

[11] P. G. Kruger and L. W. Phillips, Phys. Rev. **55**, 352 (1939).

Note on Chlorine Spectra

From consideration of data on isoelectronic sequences involving the above argon ions, it was possible to make some minor additions and corrections to previous analyses of chlorine V and chlorine VI spectra.

The latest and most complete report on the spectrum of chlorine V was given by Bowen.[12] Work done in this laboratory confirms all of his results except for the multiplet $sp^2\ {}^4P-sp3d\ {}^4P$. Table XI shows Bowen's classification (in italics) and the alternative classification. Intensities in parentheses are Bowen's; those in brackets are taken from our plates. The new identifications seem better for several reasons. (1) One should be able to find transitions to the $sp^2\ {}^4P_{1/2}$ level, but no such lines can be found to accompany Bowen's values. (2) The separations of the $spd\ {}^4P$ levels (Fig. 1(a)) are more in line with corresponding separations for other ions in the sequence. (3) Figure 1(b), showing the trend of the $spd\ {}^4(P, D)$ term values for several ions of the sequence, supports the new identification. The fact that three of Bowen's lines show an increase in intensity on our plates, while two do not, may indicate that the five lines identified by Bowen do not all belong to the same stage on ionization. The necessity for classifying 552.908 as a blend with $s^2p^3\ {}^2D_{5/2}-s^2p^2({}^1D)3d\ {}^2P_{3/2}$ of Cl III is now removed. The multiplet $sp^2\ {}^4P-spd\ {}^4D$ is found to be more intense on our plates than on Bowen's, as is evidenced by the fact that ${}^4P_{3/2}-{}^4D_{1/2}$ appears. The above-mentioned lines, together with two lines which are tentatively identified as $s^2p\ {}^2P-s^25d\ {}^2D$, are listed in Table XII. Term values given there are adjusted to fit Bowen's Table VI.

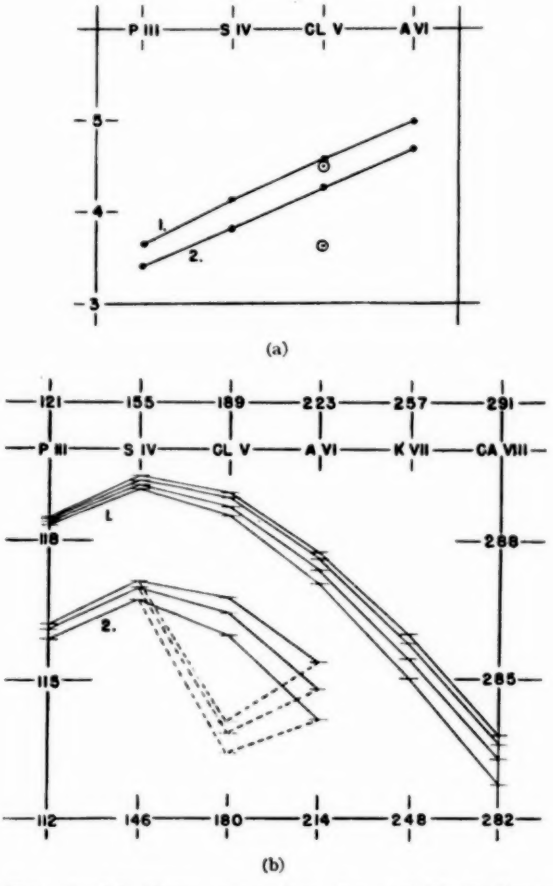

FIG. 1. (a) Term separations for $spd\ {}^4P$. Ordinate-$[\Delta\nu]^{\frac{1}{3}}$. Curve 1. ${}^4P_{5/2}-{}^4P_{3/2}$. Curve 2. ${}^4P_{3/2}-{}^4P_{1/2}$. Bowen's data indicated by ⊙. (b) Term values for (1) $spd\ {}^4D$, (2) $spd\ {}^4P$ states with respect to $sp^2\ {}^4P_{1/2}$. Scale in thousands of cm^{-1}. Bowen's data indicated by dotted lines.

Two additional multiplets in chlorine VI have now been identified. Classifications and term values are given in Table XIII. We wish to take this opportunity to point out a typographical error in Table V of a previous report on magnesium-like spectra.[13] The term value for $sp^2\ {}^3P_0$ of Cl VI should read 136,813 instead of 136,713.

[12] I. S. Bowen, Phys. Rev. **45**, 401 (1934).

[13] W. L. Parker and L. W. Phillips, Phys. Rev. **57**, 140 (1940).

On the Fermi Theory of β-Radioactivity

II. The "Forbidden" Spectra

E. J. KONOPINSKI, *Department of Physics, Indiana University, Bloomington, Indiana*

AND

G. E. UHLENBECK, *Department of Physics, University of Michigan, Ann Arbor, Michigan*

(Received June 24, 1941)

Fermi's theory of the energy distribution of β-particles is extended to first and second forbidden transitions for arbitrarily charged nuclei. The calculations are done not only for Fermi's original "polar vector" form of the theory but also for the scalar, tensor, axial vector and pseudo-scalar forms. Selection rules appropriate for these are given in Table I. The final results are given in the form of a "correction factor" C, by which the allowed distribution must be multiplied to give a forbidden spectrum. They are listed in §4. The energy dependence of the correction factors was found to be completely independent of knowledge concerning the details of the nuclear states only for the scalar and pseudo-scalar interactions (which give identical results) and for certain special selection rules in the other interactions. Comparison with experimental data on Na^{24}, P^{32} and RaE seems to eliminate the scalar, pseudo-scalar and axial vector possibilities, all of which yield results independent of detailed knowledge concerning the nuclear states involved in these cases. The polar vector and tensor results depend on the unknown ratio of the magnitudes of certain nuclear matrix elements. Arbitrary adjustment of the unknown ratios allows fairly good fitting of the data. Especially striking is the reproduction of a "K-U type" shape for the RaE spectrum. Although the tensor and polar vector theories are equally favored by the evidence of the energy distributions, the fact that the tensor theory leads to Gamow-Teller selection rules perhaps make it preferable.

§1. INTRODUCTION

THE distinction between "allowed" and "forbidden" β-decay was first made by Sargent[1] on an empirical basis. By plotting the decay constants of the naturally β-radioactive elements as a function of the maximum energy of the β-rays, Sargent showed that there is no one-to-one correspondence between the two quantities, but that for a given energy release the decay constant may have any one of a discrete set of order of magnitudes. Fermi's[2] theory attributes these differences between equally energetic transitions to differences in the change of angular momentum and parity which occur during each, in analogy to the emission of dipole, quadrupole, etc. radiation in atomic spectra. The class of β-emitters with the largest decay constants as a function of the energy release are said to undergo "allowed" transitions; the transitions with a decay rate a distinct order of magnitude smaller (it turns out to be ~100) are "first forbidden"; the next class is "second forbidden," and so on. When the Sargent plot is extended to lighter, artificially radioactive atoms, the distinctions between the classes become obscured, although certain groups can still be distinguished if care is taken to compare only atoms of comparable size.[3] This happens because the decay constants depend also on the nuclear charge and on the complexity of the nucleus.

A formula for the energy distribution $P(W)dW$ of the β-particles emitted in "allowed" transitions was given by Fermi.[4] He obtained:

$$P(W)dW=(G^2/2\pi^3)C_0F(Z,W)pW\times(W_0-W)^2dW, \quad (1)$$

in which W is the electron energy, $p=(W^2-1)^{\frac{1}{2}}$ is its momentum, W_0 is the maximum energy of the β-spectrum, and G is the "Fermi constant" having the order of magnitude 5×10^{-12}. The function

$$F(Z,W)=\frac{4}{\Gamma^2(1+2s)}(2p\rho)^{2s-2}e^{\pi\alpha ZW/p}\times|\Gamma(s+i\alpha ZW/p)|^2 \quad (2)$$

represents the influence of the nuclear charge Z; ρ is the nuclear radius and $s=(1-\alpha^2Z^2)^{\frac{1}{2}}$;

[1] B. W. Sargent, Proc. Roy. Soc. **139**, 659 (1933).
[2] E. Fermi, Zeits. f. Physik **88**, 161 (1934).
[3] L. W. Nordheim and F. L. Yost, Phys. Rev. **51**, 942 (1937); compare also E. J. Konopinski, *Advances in Nuclear Physics* (Interscience Publishers, Inc., in press).
[4] The usual relativistic units will be used throughout; unit of energy is mc^2, of time $\hbar/mc^2$ and of length $\hbar/mc$. All formulas will be written for electron emission; for positron emitters one has to change the sign of the nuclear charge Z.

$F(0, W)=1$. The quantity C_0 (for which exact expressions will be given later) contains a matrix element of the initial and final nuclear states and is independent of the energy W. The formula (1) seems to be adequately confirmed by the best experimental measurements of various β-spectra. Most notable are Lawson and Cork's[5] In^{114} spectrum, Tyler's[6] spectra of the Cu^{64} positrons and electrons, and the measurements[7] on N^{13} and C^{11}.

The authors[8] made a criticism of Fermi's formula (1) on the basis of a comparison with older experimental data and advanced a modification of the Fermi theory which seemed to represent those data better. The technical improvements in the most recent measurements, particularly in eliminating scattering, have withdrawn the basis for the criticism. Further, these measurements have confirmed the values of the maximum energy W_0 as derived from the nuclear masses. The so-called K-U modification had led to values of W_0 which were distinctly too large.[9]

Fermi's formula (1) however still does not represent a great number of observed β-spectra. Many of these disagreements are undoubtedly due to the superposition of several spectra, as has lately again been emphasized by Bethe, Hoyle and Peierls.[10] Nevertheless, all the disagreements cannot be explained in this way. The very well investigated[11] spectra of RaE and P^{32} show definite deviations from Fermi's formula. No evidence of the γ-radiation to be expected if these spectra were complex has been found. The feeble γ-radiation which has been observed can be completely accounted for as internal bremsstrahlung.[12] Now, according to the Sargent relation both P^{32} and RaE seem to belong to the "second forbidden" class. There is, therefore, no *a priori* reason to expect them to obey the "allowed" formula (1). Accordingly, it will be of interest to see whether an extension of Fermi's calculations to forbidden transitions can account for such cases. Attempts in this direction have been made already by Hoyle[13] and by Berestetzky.[14] These authors however have confined themselves to the K-U modification of the theory and moreover have made no systematic examination of the possible forms of the forbidden β-spectra.

The calculation of the form of forbidden spectra may also have importance for the general theory of β-decay. As is well known, the Fermi theory can be formulated in several different ways, all of which lead to the same shape for allowed spectra, but can be expected to yield distinct results for forbidden transitions. These various ways can be expressed in terms of five independent forms, listed by Bethe and Bacher.[15] We have especially investigated the shape of the forbidden spectra for each of these forms separately. The method of calculation is illustrated in §§2, 3 for the one of these forms originally adopted by Fermi. The results for all the forms are listed in §§4, 5. In §6, a comparison of these results with the limited accurate experimental data available, namely the P^{32} and RaE spectra, has been made. This seems already able to eliminate some of the possible forms.

§2. The Forbidden Spectra for the Fermi Interaction ($Z=0$)

The result of Fermi's formulation for the number of electrons $P(W)dW$ emitted into the energy range dW at W may be written:

$$P(W)dW=G^2/(2\pi)^5\int d\omega_e\int d\omega_n\left|\int d\tau\sum_k\{(V^*Q_kU)(\psi^*\varphi)_k-(V^*\boldsymbol{\alpha}_kQ_kU)\cdot(\psi^*\boldsymbol{\alpha}\varphi)_k\}\right|^2\cdot q^2pWdW. \quad (3)$$

[5] J. L. Lawson and J. M. Cork, Phys. Rev. **57**, 982 (1940).
[6] A. W. Tyler, Phys. Rev. **56**, 125 (1939).
[7] E. M. Lyman, Phys. Rev. **55**, 1123A (1939); Y. Watase and J. Itoh, Proc. Phys. Math. Soc. Japan **22**, 639 (1940); A. A. Townsend, Proc. Roy. Soc. **177**, 357 (1941).
[8] E. J. Konopinski and G. E. Uhlenbeck, Phys. Rev. **48**, 7 (1935). (To be referred to as I.)
[9] Kurie, Richardson, and Paxton, Phys. Rev. **49**, 368 (1936); Bonner, Delsasso, Fowler, and Lauritsen, Phys. Rev. **49**, 203 (1936); J. D. Cockcroft and W. B. Lewis, Proc. Roy. Soc. **154**, 261 (1936).
[10] Bethe, Hoyle and Peierls, Nature **143**, 200 (1939).
[11] J. L. Lawson, Phys. Rev. **56**, 131 (1939); A. Flammersfeld, Zeits. f. Physik **112**, 727 (1939); G. J. Neary, Proc. Roy. Soc. **175**, 71 (1940); L. M. Langer and M. D. Whitaker, Phys. Rev. **51**, 713 (1937); Alichanian and Nikitin, J. Phys. Acad. Sci. USSR **3**, 243 (1940).
[12] E. Stahel and J. Guillissen, J. de phys. et rad. **1**, 12 (1940); Sizoo, Eykman and Groen, Physica **6**, 1057 (1939); Chien-Shiung Wu, Phys. Rev. **59**, 481 (1941).
[13] F. Hoyle, Proc. Roy. Soc. **166**, 249 (1938).
[14] Berestetzky, Comptes rendus Acad. Sci. USSR **23**, 450 (1939).
[15] H. A. Bethe and R. F. Bacher, Rev. Mod. Phys. **8**, 82 (1936).

The integral over the coordinates of all the nucleons, $\int d\tau \cdots$ represents the matrix element of the interaction between the nucleons and the electron-neutrino field. U and V are the wave functions of the initial and final nuclei; Q_k is an operator which by definition replaces U with a wave function describing a nucleus in which the kth neutron is replaced by a proton; ψ and φ are the wave functions of the emitted electron and anti-neutrino, respectively, normalized to one particle per unit volume and evaluated at the position of the transforming nucleon. All the wave functions are assumed to be of the four-component Dirac type and the $\boldsymbol{\alpha}$'s are the usual Dirac matrix operators; q is the neutrino momentum, in our units numerically equal to the neutrino energy K, since, at the outset, we assume the neutrino mass to be zero. The integrals over ω_e and ω_n represent integrations over the directions of the electron and the neutrino momenta and a summation over their spin directions. Accordingly, the formula (3) is written appropriately for the case in which the forces on the electron and the neutrino are neglected, so that their wave functions can be taken as plane waves:

$$\psi = A \exp[i(\mathbf{p}\cdot\mathbf{r})], \quad \varphi = B \exp[-i(\mathbf{q}\cdot\mathbf{r})].$$

Since the de Broglie wave-lengths of the electron and the neutrino are, in general, large compared to nuclear dimensions, one can evaluate the matrix element in (3) in successive approximations, corresponding to an expansion of ψ and φ in successive powers of $(\mathbf{p}+\mathbf{q})\cdot\mathbf{r}$:

$$(\psi^*\varphi)_k = (A^*B)[1 - i(\mathbf{p}+\mathbf{q}\cdot\mathbf{r}_k) - \tfrac{1}{2}(\mathbf{p}+\mathbf{q}\cdot\mathbf{r}_k)^2\cdots], \quad (4a)$$

$$(\psi^*\boldsymbol{\alpha}\varphi)_k = (A^*\boldsymbol{\alpha}B)[1 - i(\mathbf{p}+\mathbf{q}\cdot\mathbf{r}_k)\cdots]. \quad (4b)$$

If only the first term of (4a) is kept one is led to a nuclear matrix element in (3), which we shall represent by the symbol $\int 1$:

$$\int 1 = \int d\tau \sum_k (V^* Q_k U). \quad (5)$$

Since this is the matrix element of a scalar quantity it can be different from zero only when the initial and final states have the same angular momentum J and parity. When this is the case we shall call the transition "allowed." By carrying out the further operations in (3) we are then led to Eq. (1) with $Z=0$ and

$$C_{0V}(Z=0) = \left|\int 1\right|^2. \quad (6)$$

The index V is added to C_0 to distinguish the Fermi interaction from the other four forms to be discussed later.

The first term in (4b) leads to a nuclear matrix element in (3):

$$\int \boldsymbol{\alpha} = \int d\tau \sum_k (V^* \boldsymbol{\alpha}_k Q_k U), \quad (7)$$

which has the selection rules appropriate for a polar vector:

$$\Delta J = 0, \pm 1 (\text{no } 0 \to 0); \text{ yes} \quad (8)$$

where the "yes" signifies that the parity must change in the transition. These same selection rules are likewise characteristic of the nuclear matrix element which arises from the second term of (4a):

$$\int \mathbf{r} = \int d\tau \sum_k (V^* \mathbf{r}_k Q_k U). \quad (9)$$

We must, therefore, take the second term of (4a) and the first term of (4b) together. Whether the matrix elements $\int \boldsymbol{\alpha}$ and $\int \mathbf{r}$ are also of the same order of magnitude will be discussed in §5. Together they lead to the formulas for what we shall call the "first forbidden" transitions. The result can be expressed in the same form as (1) except that C_0 is now replaced by the "correction factor":

$$C_{1V}(Z=0) = \left|\int \mathbf{r}\right|^2 (a+b) + \left|\int \boldsymbol{\alpha}\right|^2 + i\left\{\left(\int \boldsymbol{\alpha}\right)\cdot\left(\int \mathbf{r}\right)^* - \text{c.c.}\right\} c, \quad (10)$$

in which a, b, c are abbreviations for:

$$a = \tfrac{1}{3}(p^2+q^2), \quad b = -\frac{2}{9}\frac{p^2q^2}{WK}, \quad c = -\frac{1}{3}\left(\frac{p^2}{W} + \frac{q^2}{K}\right). \quad (11)$$

To obtain the formulas for the "second forbidden" transitions, we proceed in an analogous fashion. We consider together the third

term of (4a) and the second term of (4b), since each will yield nuclear matrix elements containing products of two polar vectors. These tensors can always be written as combinations of the scalars

$$\int r^2 \quad \text{and} \quad \int (\boldsymbol{\alpha}\cdot\mathbf{r}), \tag{12}$$

the axial vector

$$\int \boldsymbol{\alpha}\times\mathbf{r}, \tag{13}$$

and the symmetrical tensors with spur zero:

$$R_{ij}=\int (x_i x_j-\tfrac{1}{3}\delta_{ij}r^2), \tag{14}$$

$$A_{ij}=\int (\alpha_i x_j+\alpha_j x_i-\tfrac{2}{3}\delta_{ij}(\boldsymbol{\alpha}\cdot\mathbf{r})). \tag{15}$$

Each of these matrix elements has characteristic selection rules. For the scalars (12), these will be the same as for the "allowed" transition (i.e., $\Delta J=0$, no) and their contribution will, therefore, constitute only a presumably small correction to the "allowed" formula. In addition to these (except for $0\to 0$ and $\frac{1}{2}\to\frac{1}{2}$) the axial vector and the tensors give really new selection rules. They are

$$\Delta J=\pm 1;\ \text{no} \tag{16}$$

for the axial vector and

$$\Delta J=\pm 1,\ \pm 2(\text{no } 1\leftrightarrow 0);\ \text{no} \tag{17}$$

for each tensor. Only the contributions of the axial vector and the tensors are, therefore, of interest for the "second forbidden" formula. They give the correction factor,

$$C_{2V}(Z=0)=\sum_{ij}|R_{ij}|^2(\tfrac{1}{6}d+\tfrac{3}{5}ab)+\sum_{ij}|A_{ij}|^2\cdot\tfrac{1}{4}a$$
$$+i(\sum_{ij}A_{ij}R^*_{ij}-\text{c.c.})f+\left|\int\boldsymbol{\alpha}\times\mathbf{r}\right|^2(\tfrac{1}{2}a-b), \tag{18}$$

with the additional abbreviations,

$$d=\tfrac{1}{5}(p^4+q^4)+\tfrac{2}{3}p^2q^2,$$
$$f=\frac{1}{30}\left(\frac{p^4}{W}+\frac{q^4}{K}\right)+\frac{1}{4}W_0 b. \tag{19}$$

The derivation of (18) is greatly facilitated by taking advantage of the fact that the nuclear matrix elements can only occur in the invariant combinations indicated in (18). Just as in deriving Eq. (10) it was sufficient to compute only the coefficient of one of the components in each of the expressions $|\int\mathbf{r}|^2$, $|\int\boldsymbol{\alpha}|^2$ and $(\int\mathbf{r})\cdot(\int\boldsymbol{\alpha})^*$, so in deriving (18) it is enough to consider only certain representative terms. The only complication arises from the fact that in the terms with A_{ij}, $\int\boldsymbol{\alpha}\times\mathbf{r}$ and $\int\boldsymbol{\alpha}\cdot\mathbf{r}$ the same combinations of the $\boldsymbol{\alpha}$ and $\mathbf{r}$ components occur. One must, therefore, compute the coefficients of more than one representative term in each of the invariant expressions, in order to obtain enough simultaneous linear equations to determine the coefficients with which each invariant occurs.

§3. The Forbidden Spectra for the Fermi Interaction ($Z\neq 0$)

When the influence of the Coulomb field on the wave function of the electron is taken into account, it becomes necessary to use spherical coordinates, at least for the electron. The formula (3) is now replaced by:

$$P(W)dW=G^2/4\pi^3\int d\omega_n\sum_{j,l,m}\left|\int d\tau\sum_k\{(V^*Q_kU)(\psi^*\varphi)_k-(V^*\boldsymbol{\alpha}_kQ_kU)\cdot(\psi^*\boldsymbol{\alpha}\varphi)_k\}\right|^2\cdot(q^2W/p)dW. \tag{20}$$

ψ is now the solution of the Dirac equations in the Coulomb field,[16] corresponding to the energy W and the angular momentum quantum numbers j, l, m, normalized to one particle in a sphere of unit radius. For φ we still keep the plane wave solution in Cartesian coordinates.

We try now to divide the matrix element occurring in (20) into parts with characteristic selection rules, as in the preceding section. To do this we write the spherical harmonics occurring in ψ as polynomials in x/r, y/r, z/r. When the plane wave φ is also developed in powers of x, y, z, for each

[16] Compare M. E. Rose, Phys. Rev. **51**, 484 (1937). His notation will be followed in this paper.

set of values of j, l, m one obtains formulas for $(\psi^*\varphi)$ and $(\psi^*\boldsymbol{\alpha}\varphi)$ analogous to (4a) and (4b), except that the coefficients still depend on the coordinate r. One should evaluate these coefficients at the place of the transforming nucleon. The difficulty then arises that they contain the radial wave functions of the electron, which are singular at the origin. However, this is without physical significance since the Coulomb field undoubtedly breaks down within the nucleus. Following Fermi, we avoid the difficulty by evaluating the radial functions at a value ρ of r, which has the order of magnitude of the nuclear radius. It is now possible to select the terms appropriate for the allowed, the first forbidden, etc., transitions, just as in the preceding section.

The result for the allowed spectrum becomes

$$P(W)dW=(G^2/\pi^2)\left|\int 1\right|^2((g_0^2+f_{-2}^2)/4\pi)(q^2W/p)dW, \tag{21}$$

where g_0 and f_{-2} are radial wave functions in the notation of reference 16. Evaluating these functions by keeping only the largest terms in their series expansions in powers of ρ, one obtains:

$$(g_0^2+f_{-2}^2)/4\pi=(p^2/2\pi)F(Z,W)(1+s)/2. \tag{22}$$

This leads to formula (1) with[17]

$$C_{0V}=\left|\int 1\right|^2(1+s)/2. \tag{23}$$

For the first forbidden transitions one obtains analogously:

$$P(W)dW=dW\frac{G^2}{\pi^2}\frac{q^2W}{p}\left[\left|\int \mathbf{r}\right|^2\left\{\frac{q^2}{3}\frac{g_0^2+f_{-2}^2}{4\pi}+\frac{f_0^2+g_{-2}^2}{4\pi\rho^2}+\frac{g_1^2+f_{-3}^2}{2\pi\rho^2}-\frac{q^2}{3K}\frac{g_0f_0-g_{-2}f_{-2}}{2\pi\rho}\right\}\right.$$
$$\left.+\left|\int\boldsymbol{\alpha}\right|^2\frac{g_0^2+f_{-2}^2}{4\pi}+i\left\{\left(\int\boldsymbol{\alpha}\right)\cdot\left(\int\mathbf{r}\right)^*-\text{c.c.}\right\}\left\{\frac{q^2}{3K}\frac{g_0^2+f_{-2}^2}{4\pi}-\frac{g_0f_0-g_{-2}f_{-2}}{4\pi\rho}\right\}\right]. \tag{24}$$

Here new radial wave functions appear which again are to be evaluated from their series expansions. The expansions will always be carried to high enough powers in ρ to give non-vanishing results in the limit of $Z\to 0$, which can then be checked against the formulas of §2. The explicit results are listed in §5, together with those for the second forbidden transitions and for other forms of interaction.

§4. The Forbidden Spectra for Other Forms of Interaction

In constructing the matrix elements in (3) and (20), Fermi used a combination of ψ and φ which behaves like a polar four-vector in Lorentz transformations. The natural generalization of this special form is to include in the consideration the four additional combinations which transform, respectively, like a scalar, a tensor, an axial vector and a pseudo-scalar. For each of these the curly brackets in the integrands of expressions (3) and (20) are replaced by[15]

$$\text{Scalar:}\quad \{(V^*\beta_kQ_kU)(\psi^*\beta\varphi)_k\}, \tag{25a}$$

$$\text{Tensor:}\quad \{(V^*\beta_k\boldsymbol{\sigma}_kQ_kU)\cdot(\psi^*\beta\boldsymbol{\sigma}\varphi)_k+(V^*\beta_k\boldsymbol{\alpha}_kQ_kU)\cdot(\psi^*\beta\boldsymbol{\alpha}\varphi)_k\}, \tag{25b}$$

$$\text{Axial V.:}\quad \{(V^*\boldsymbol{\sigma}_kQ_kU)\cdot(\psi^*\boldsymbol{\sigma}\varphi)_k-(V^*\gamma_{5k}Q_kU)(\psi^*\gamma_5\varphi)_k\}, \tag{25c}$$

$$\text{Pseudo-S.:}\quad \{(V^*\beta_k\gamma_{5k}Q_kU)(\psi^*\beta\gamma_5\varphi)_k\}. \tag{25d}$$

In these expressions the β's are the usual Dirac matrices, $\gamma_5=-i\alpha_x\alpha_y\alpha_z$ and the $\boldsymbol{\sigma}$'s are the familiar Pauli matrices doubled to four rows and four columns; $\boldsymbol{\sigma}=\gamma_5\boldsymbol{\alpha}$.

[17] This differs from Fermi's original result by the factor $(1+s)/2$, which has no effect on the energy distribution.

TABLE I. *Selection rules.*

		ALLOWED	FIRST FORBIDDEN			SECOND FORBIDDEN		
Scalar	Matrix	$\int 1$	$\int \mathbf{r}$			R_{ij}		
	ΔJ	0	0, ± 1 (no $0 \to 0$)			± 1, ± 2 (no $1 \leftrightarrow 0$)		
	Parity Change	no	yes			no		
Polar V.	Matrix	$\int 1$	$\int \mathbf{r}$, $\int \boldsymbol{\alpha}$			R_{ij}, A_{ij}	$\int \boldsymbol{\alpha} \times \mathbf{r}$	
	ΔJ	0	0, ± 1 (no $0 \to 0$)			± 1, ± 2 (no $1 \leftrightarrow 0$)	± 1	
	Parity Change	no	yes			no	no	
Tensor	Matrix	$\int \boldsymbol{\sigma}$	$\int \boldsymbol{\sigma} \cdot \mathbf{r}$	$\int \boldsymbol{\sigma} \times \mathbf{r}$, $\int \boldsymbol{\alpha}$	B_{ij}	$\int \boldsymbol{\alpha} \cdot \mathbf{r}$	T_{ij}, A_{ij}	S_{ijk}
	ΔJ	0, ± 1 (no $0 \to 0$)	0	0, ± 1 (no $0 \to 0$)	0, ± 1, ± 2 (no $0 \to 0$, $\frac{1}{2} \to \frac{1}{2}$, $1 \leftrightarrow 0$)	$0 \to 0$	± 2	± 2, ± 3 (no $2 \leftrightarrow 0$)
	Parity Change	no	yes	yes	yes	no	no	no
Axial V.	Matrix	$\int \boldsymbol{\sigma}$	$\int \boldsymbol{\sigma} \cdot \mathbf{r}$, $\int \gamma_5$	$\int \boldsymbol{\sigma} \times \mathbf{r}$	B_{ij}	T_{ij}		S_{ijk}
	ΔJ	0, ± 1 (no $0 \to 0$)	0	0, ± 1 (no $0 \to 0$)	0, ± 1, ± 2 (no $0 \to 0$, $\frac{1}{2} \to \frac{1}{2}$, $1 \leftrightarrow 0$)	± 2		± 2, ± 3 (no $2 \leftrightarrow 0$)
	Parity Change	no	yes	yes	yes	no		no
Pseudo-S.	Matrix	$\int \gamma_5$	$\int \gamma_5 \mathbf{r}$			R_{ij}^{γ}		
	ΔJ	0	0, ± 1 (no $0 \to 0$)			± 1, ± 2 (no $1 \leftrightarrow 0$)		
	Parity Change	yes	no			yes		

All the forms (25) lead to exactly the same formula (1) for allowed spectra except for differences in the nuclear matrix elements, and, therefore, in the selection rules. The scalar leads to the same "allowed" selection rules as Fermi's polar vector because β_k is a scalar operator just as the unity in $\int 1$. Since the β_k is a mere scalar, it is ignored in all the further considerations. For the pseudo-scalar interaction the nuclear matrix element $\int \gamma_5$ replaces Fermi's $\int 1$ in allowed transitions, and, therefore, its selection rules differ only in that parity is required to change. The axial vector and the tensor interactions each consist of a pair of terms, as does the Fermi interaction. It can be made plausible (for further discussion see §5), that again only the first terms play a role in allowed transitions. However, they lead to completely different selection rules because they involve the matrix element $\int \boldsymbol{\sigma}$ which is non-vanishing only for

$$\Delta J = 0, \pm 1 \text{ (no } 0 \to 0); \text{ no.} \tag{26}$$

The difference from (8) is, of course, due to the fact that $\boldsymbol{\sigma}$ is an axial whereas $\boldsymbol{\alpha}$ is a polar vector. The rules (26) for allowed transitions are referred to as the Gamow-Teller rules because evidence for their correctness was first adduced by these authors.[18]

Still further types of nuclear matrix elements must be introduced when the results of the interactions (25) for forbidden transitions are investigated. The scalar interaction brings in elements which differ from $\int \mathbf{r}$ and R_{ij} only in that the operator β_k also appears in the integrands; as already mentioned, this distinction is unimportant and will be ignored. The effect of γ_{5k} in the matrix elements needed with the pseudo-scalar interaction,

$$\int \gamma_5 \mathbf{r} \quad \text{and} \quad R_{ij}^{\gamma} = \int \gamma_5 (x_i x_j - \tfrac{1}{3}\delta_{ij} r^2), \tag{27}$$

is to require parity changes opposite to those required by $\int \mathbf{r}$ and R_{ij}. The axial vector interaction

[18] G. Gamow and E. Teller, Phys. Rev. **49**, 895 (1936).

will, for first forbidden transitions, introduce $\int \gamma_5$ and combinations of $\boldsymbol{\sigma}$ with $\mathbf{r}$:

$$\int \boldsymbol{\sigma}\cdot\mathbf{r}, \quad \int \boldsymbol{\sigma}\times\mathbf{r}, \quad B_{ij}=\int (\sigma_i x_j+\sigma_j x_i-\tfrac{2}{3}\delta_{ij}(\boldsymbol{\sigma}\cdot\mathbf{r})). \tag{28}$$

For the second forbidden transitions $\int \gamma_5 \mathbf{r}$ and combinations of $\boldsymbol{\sigma}$, $\mathbf{r}$, and $\mathbf{r}$ are needed. The irreducible forms consist of two vectors $\int r^2\boldsymbol{\sigma}$ and $\int(\boldsymbol{\sigma}\cdot\mathbf{r})\mathbf{r}$, one symmetrical tensor of the second rank and with zero spur

$$T_{ij}=\int ([\boldsymbol{\sigma}\times\mathbf{r}]_i x_j+[\boldsymbol{\sigma}\times\mathbf{r}]_j x_i), \tag{29}$$

and finally a completely symmetrical tensor of the third rank with diagonal "spurs" zero,

$$S_{ijk}=\int \{\sigma_{(i}x_j x_{k)}-\tfrac{1}{5}\delta_{(ij}[\sigma_{k)}r^2+2k_{k)}(\boldsymbol{\sigma}\cdot\mathbf{r})]\}, \tag{30}$$

where enclosing indices in parenthesis signifies a sum of terms for all permutations of the indices. Except for the trivial β_k, it is easy to see that the tensor interaction requires all the matrix elements already introduced which contain $\boldsymbol{\sigma}$ or $\boldsymbol{\alpha}$.

The selection rules characteristic of the various matrix elements are presented in Table I. Just as in §2, all matrix elements introduced in the second forbidden approximation which only repeat the allowed selection rules are left out; also, for the matrix elements which are admitted, only those rules are quoted which are not also "allowed."

It can be seen from Table I that 0→0 transitions possess a special property. The scalar and polar vector interaction do not allow 0→0 transitions with parity change in any approximation. The axial vector and pseudo-scalar interaction similarly forbid completely 0→0 transitions with no parity change. The table shows this only up to the second forbidden approximation, but it is easy to convince oneself that this property extends to all approximations.

The calculations proceed as illustrated in §§2, 3. The final results for the energy distributions are always expressible in the form (1), with new correction factors taking the place of C_0. The subscripts S, V, T, A will refer to the scalar, vector, tensor and axial vector interactions, respectively. The "1" and "2" will distinguish the first forbidden and second forbidden formulas. The pseudo-scalar gives exactly the same results as the scalar, except for the appearance of γ_5 in the matrix element itself. The calculations were always done first for $Z=0$ and then for arbitrary Z, so that a check was available by going to the limit $Z\to 0$. The results for the first forbidden transitions are:

$$C_{1S}=\left|\int \mathbf{r}\right|^2(\tfrac{1}{3}K^2L_0+2L_1+M_0+\tfrac{2}{3}KN_0),$$

$$C_{1V}=\left|\int \mathbf{r}\right|^2(\tfrac{1}{3}K^2L_0+2L_1+M_0-\tfrac{2}{3}KN_0)+\left|\int \boldsymbol{\alpha}\right|^2 L_0+i\left\{\left(\int \boldsymbol{\alpha}\right)\cdot\left(\int \mathbf{r}\right)^*-\text{c.c.}\right\}(\tfrac{1}{3}KL_0-N_0),$$

$$C_{1T}=\left|\int (\boldsymbol{\sigma}\cdot\mathbf{r})\right|^2(\tfrac{1}{5}K^2L_0+M_0+\tfrac{2}{3}KN_0)+\left|\int \boldsymbol{\alpha}\right|^2 L_0+\left|\int \boldsymbol{\sigma}\times\mathbf{r}\right|^2(\tfrac{1}{6}K^2L_0+\tfrac{1}{2}L_1+M_0-\tfrac{2}{3}KN_0)$$
$$-\left\{\left(\int \boldsymbol{\sigma}\times\mathbf{r}\right)\cdot\left(\int \boldsymbol{\alpha}\right)^*+\text{c.c.}\right\}(\tfrac{1}{3}KL_0-N_0)+\sum_{ij}|B_{ij}|^2(\tfrac{1}{12}K^2L_0+\tfrac{3}{4}L_1),$$

$$C_{1A}=\left|\int \boldsymbol{\sigma}\cdot\mathbf{r}\right|^2(\tfrac{1}{9}K^2L_0+M_0-\tfrac{2}{3}KN_0)+\left|\int \gamma_5\right|^2 L_0-i\left\{\left(\int \boldsymbol{\sigma}\cdot\mathbf{r}\right)\left(\int \gamma_5\right)^*-\text{c.c.}\right\}(\tfrac{1}{3}KL_0-N_0)$$
$$+\left|\int \boldsymbol{\sigma}\times\mathbf{r}\right|^2(\tfrac{1}{6}K^2L_0+\tfrac{1}{2}L_1+M_0+\tfrac{2}{3}KN_0)+\sum_{ij}|B_{ij}|^2(\tfrac{1}{12}K^2L_0+\tfrac{3}{4}L_1).$$

For the second forbidden transitions one obtains:

$$C_{2S}=\sum_{ij}|R_{ij}|^2\{\tfrac{1}{30}K^4L_0+\tfrac{2}{15}K^3N_0+\tfrac{1}{3}K^2(2L_1+M_0)+2KN_1+\tfrac{9}{2}L_2+3M_1\},$$

$$C_{2V}=\sum_{ij}|R_{ij}|^2\{\tfrac{1}{30}K^4L_0-\tfrac{2}{15}K^3N_0+\tfrac{1}{3}K^3(2L_1+M_0)-2KN_1+\tfrac{9}{2}L_2+3M_1\}$$
$$+\sum_{ij}|A_{ij}|^2(\tfrac{1}{12}K^2L_0+\tfrac{3}{4}L_1)-i\{\sum_{ij}R_{ij}A^*_{ij}-\text{c.c.}\}(\tfrac{1}{30}K^3L_0-\tfrac{1}{6}K^2N_0+\tfrac{1}{2}KL_1-\tfrac{3}{2}N_1)$$
$$+\left|\int\boldsymbol{\alpha}\times\mathbf{r}\right|^2(\tfrac{1}{6}K^2L_0+\tfrac{2}{3}KN_0+\tfrac{1}{2}L_1+M_0),$$

$$C_{2T}=\sum_{ijk}|S_{ijk}|^2\cdot\tfrac{1}{72}(\tfrac{1}{15}K^4L_0+2K^2L_1+15L_2)+\sum_{ij}|T_{ij}|^2\cdot\tfrac{1}{12}\{\tfrac{1}{15}K^4L_0-\tfrac{2}{5}K^3N_0+K^2(L_1+M_0)$$
$$-6KN_1+6L_2+9M_1\}+\sum_{ij}|A_{ij}|^2(\tfrac{1}{12}K^2L_0+\tfrac{3}{4}L_1)-\{\sum_{ij}T_{ij}A^*_{ij}+\text{c.c.}\}$$
$$\times\tfrac{1}{4}(\tfrac{1}{15}K^3L_0-\tfrac{1}{3}K^2N_0+KL_1-3N_1)+\left|\int\boldsymbol{\alpha}\cdot\mathbf{r}\right|^2(\tfrac{1}{9}K^2L_0+\tfrac{2}{3}KN_0+M_0),$$

$$C_{2A}=\sum_{ijk}|S_{ijk}|^2\cdot\tfrac{1}{72}(\tfrac{1}{15}K^4L_0+2K^2L_1+15L_2)+\sum_{ij}|T_{ij}|^2$$
$$\cdot\tfrac{1}{12}\{\tfrac{1}{15}K^4L_0+\tfrac{2}{5}K^3N_0+K^2(L_1+M_0)+6KN_1+6L_2+9M_1\}.$$

Here the quantities L, M, and N represent combinations of radial wave functions. They are listed below, together with their values, computed as explained in §3. Following the arrows are given expressions which are good approximations for the case $\alpha Z\ll 1$.

$$L_0=\left(\frac{p^2}{2\pi}F\right)^{-1}\frac{g_0^2+f_{-2}^2}{4\pi}=\frac{1+s}{2}\qquad\rightarrow 1,$$

$$L_1=\left(\frac{p^2}{2\pi}F\right)^{-1}\frac{g_1^2+f_{-3}^2}{4\pi\rho^2}=\frac{F_1}{F}\frac{p^2}{9}\frac{2+s_1}{4}\rightarrow\frac{p^2}{9},$$

$$L_2=\left(\frac{p^2}{2\pi}F\right)^{-1}\frac{g_2^2+f_{-4}^2}{4\pi\rho^4}=\frac{F_2}{F}\frac{p^4}{225}\frac{3+s_2}{6}\rightarrow\frac{p^4}{225},$$

$$M_0=\left(\frac{p^2}{2\pi}F\right)^{-1}\frac{f_0^2+g_{-2}^2}{4\pi\rho^2}=\frac{1-s}{2\rho^2}+\frac{\alpha Z}{\rho}\frac{1}{2s+1}\left\{(2s-1)W-\frac{s}{W}\right\}+\frac{1}{(2s+1)^2}\{\alpha^2Z^2+(4s^2-3)sp^2\}$$
$$\rightarrow\frac{1}{9}p^2+\frac{\alpha^2Z^2}{4\rho^2}+\frac{\alpha Z}{3\rho}\left(W-\frac{1}{W}\right),$$

$$M_1=\left(\frac{p^2}{2\pi}F\right)^{-1}\frac{f_1^2+g_{-3}^2}{4\pi\rho^4}=\frac{F_1}{F}\frac{p^2}{36}\left[\frac{2-s_1}{\rho^2}+\frac{\alpha Z}{\rho}\frac{1}{2s_1+1}\left\{2W(2s_1-3)-\frac{s_1}{W}\right\}+\frac{1}{(s_1+1)(2s_1+1)^2}\{2s_1(s_1^2-1)p^2\right.$$
$$\left.+\alpha^2Z^2(2s_1+1)^2+2\alpha^2Z^2W^2(3+s_1-4s_1^2)\}\right]\rightarrow\frac{p^4}{225}+\frac{p^2}{36}\left\{\frac{\alpha^2Z^2}{4\rho^2}+\frac{2\alpha Z}{5\rho}\left(W-\frac{1}{W}\right)\right\},$$

$$N_0=\left(\frac{p^2}{2\pi}F\right)^{-1}\frac{f_0g_0-f_{-2}g_{-2}}{4\pi\rho}=-\frac{\alpha Z}{2\rho}-\frac{1}{2s+1}\left(\frac{sp^2}{W}-2\alpha^2Z^2W\right)\qquad\rightarrow-\frac{p^2}{3W}-\frac{\alpha Z}{2\rho},$$

$$N_1=\left(\frac{p^2}{2\pi}F\right)^{-1}\frac{f_1g_1-f_{-3}g_{-3}}{4\pi\rho^3}=\frac{F_1}{F}\frac{p^2}{18}\left[-\frac{\alpha Z}{2\rho}-\frac{1}{2s_1+1}\left(\frac{s_1p^2}{W}-2\alpha^2Z^2W\right)\right]\rightarrow-\frac{p^4}{45W}-\frac{p^2}{18}\frac{\alpha Z}{2\rho}.$$

Above are used the abbreviations:

$$s_1=(4-\alpha^2Z^2)^{\frac{1}{2}},\quad s_2=(9-\alpha^2Z^2)^{\frac{1}{2}},$$

$$F_1(Z,W)=\frac{(4!)^2}{\Gamma^2(2s_1+1)}(2p\rho)^{2s_1-4}e^{\pi\alpha ZW/p}\,|\,\Gamma(s_1+i\alpha ZW/p)\,|^2,$$

$$F_2(Z,W)=\frac{(6!)^2}{4\Gamma^2(2s_2+1)}(2p\rho)^{2s_2-6}e^{\pi\alpha ZW/p}\,|\,\Gamma(s_2+i\alpha ZW/p)\,|^2.$$

§5. General Discussion of the Formulas

The characteristic features of the formulas can be seen completely by using the $\alpha Z\ll 1$ approximations for L, M, and N. For example, one then obtains:

$$C_{1V}=\left|\int\mathbf{r}\right|^2\left\{a+b+\frac{\alpha^2Z^2}{4\rho^2}+\frac{\alpha Z}{3\rho}\left(W_0-\frac{1}{W}\right)\right\}+\left|\int\boldsymbol{\alpha}\right|^2+i\left\{\left(\int\boldsymbol{\alpha}\right)\cdot\left(\int\mathbf{r}\right)^*-\text{c.c.}\right\}\left(c+\frac{\alpha Z}{2\rho}\right),$$

$$C_{2V}=\sum_{ij}|R_{ij}|^2\left[\tfrac{1}{6}d+\tfrac{3}{5}ab+\frac{\alpha^2Z^2}{12\rho^2}(q^2+\tfrac{1}{4}p^2)+\frac{\alpha Z}{3\rho}\left\{\left(W-\frac{1}{W}\right)(\tfrac{1}{3}q^2+\tfrac{1}{10}p^2)+K(\tfrac{1}{5}q^2+\tfrac{1}{6}p^2)\right\}\right]$$

$$+\sum_{ij}|A_{ij}|^2\cdot\tfrac{1}{4}a+i\left\{\sum_{ij}A_{ij}R^*_{ij}-\text{c.c.}\right\}\left\{f+\frac{\alpha Z}{6\rho}(q^2+\tfrac{1}{2}p^2)\right\}+\left|\int\boldsymbol{\alpha}\times\mathbf{r}\right|^2$$

$$\cdot\left\{\tfrac{1}{2}a-b+\frac{\alpha^2Z^2}{4\rho^2}+\frac{\alpha Z}{3\rho}\left(2W-W_0-\frac{1}{W}\right)\right\},$$

where a, b, c, d, and f are defined as in §2 (Eqs. (11) and (19)).

The first characteristic of these formulas which stands out immediately is that, in contrast to the allowed formulas, these involve more than one nuclear matrix element. The only exceptions to this are the scalar and pseudo-scalar correction factors, and, for certain special cases of selection rules, also some of the other factors. When more than one matrix element is thus involved, one

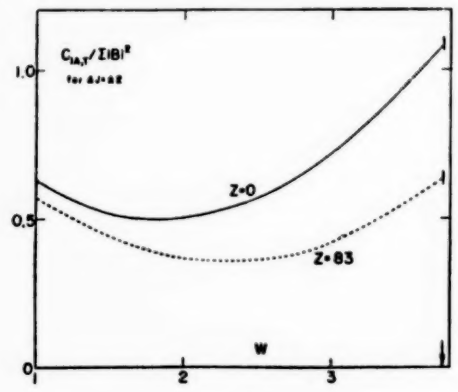

FIG. 1. The first forbidden correction factors C_{1A} and C_{1T} for the axial vector and tensor interactions with $\Delta J=\pm 2$, divided by the nuclear matrix element expression $\Sigma|B_{ij}|^2$, as functions of the electron energy W. The arrow indicates the end point used, $W_0=3.75$, which is appropriate for Na^{24}. $Z=11$ would be scarcely distinguishable from $Z=0$.

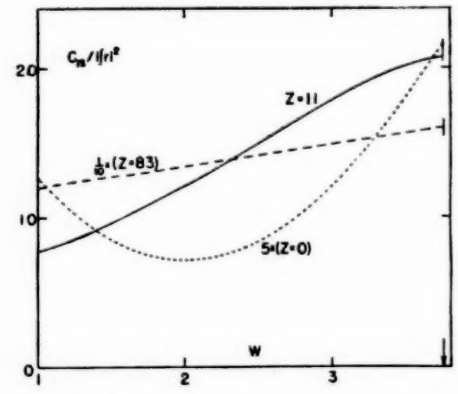

FIG. 2. The first forbidden correction factor for the scalar interaction divided by the square of the matrix element $\int\mathbf{r}$ as a function of the electron energy W. The arrow indicates the end point used, $W_0=3.75$, which is appropriate for Na^{24}. Expressions like $5\times(Z=0)$ signify that the actual ordinates were multiplied by five in plotting here. The pseudo-scalar interaction gives precisely the same dependence on the energy.

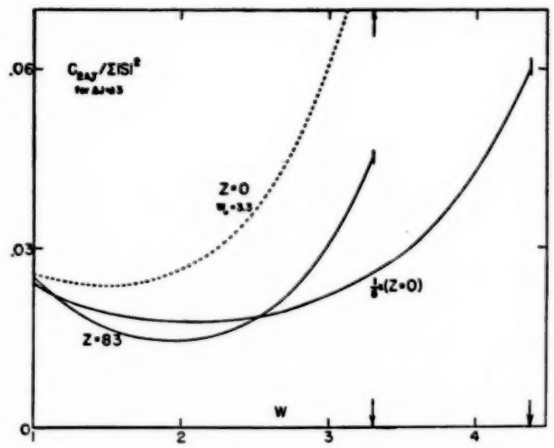

FIG. 3. The second forbidden correction factors C_{2A} and C_{2T}, for the axial vector and tensor interactions with $\Delta J=\pm 3$, divided by the nuclear matrix element expression $\Sigma|S_{ijk}|^2$, as functions of the energy W. The arrows indicate the end points used: $W_0=3.3$ (appropriate for RaE) for $Z=83$ and one curve with $Z=0$; $W_0=4.37$ (appropriate for P^{32}) for the other curve with $Z=0$. $Z=15$ gives results scarcely distinguishable from $Z=0$, here.

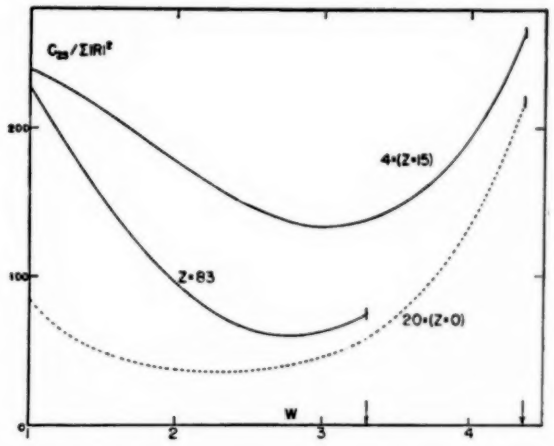

FIG. 4. The second forbidden correction factor C_{2S} for the scalar interaction divided by the nuclear matrix element expression $\Sigma|R_{ij}|^2$ as a function of the electron energy W. The arrows indicate the end points used: $W_0=4.37$ (appropriate for P^{32}) for $Z=0$ and $Z=15$; $W_0=3.3$ for $Z=83$.

expects it to be necessary to know something about the nuclear states before anything definite concerning the energy dependence of the correction factors can be concluded. However, one can try to make some estimates of the order of magnitude of the matrix elements. Fermi has already mentioned that matrix elements like $\int\boldsymbol{\alpha}$ and $\int\boldsymbol{\gamma}_5$ are of the order v/c smaller than $\int 1$ or $\int\boldsymbol{\sigma}$, v being the velocity of the nucleons. The ratio v/c is thought to be of the order 1/10, which is just about the same as the magnitude of $(p+q)\rho$ in Eq. (4a). This serves as an additional argument for combining the first term of (4b) with the second term in (4a), etc., besides the fact that these terms lead to the same selection rules. One is tempted to make a sharper estimate of such matrix elements as $\int\boldsymbol{\alpha}$, by making use of the symmetrical nuclear Hamiltonian. If one neglects the difference in the Coulomb energy in the initial and final nuclei, one can derive for example relations like

$$\int\boldsymbol{\alpha}=iW_0\int\mathbf{r},\quad A_{ij}=iW_0R_{ij}.$$

This would, for instance, make the energy dependence of the correction factor C_{1V} completely definite. However it seems unjustifiable to neglect the Coulomb energy. We prefer, therefore, to draw only such conclusions which are unaffected by using arbitrary ratios of the nuclear matrix elements.

Another outstanding characteristic of the forbidden formulas in contrast to the allowed is their sensitivity to the position ρ at which the wave functions are evaluated. Except for the very lightest nuclei, the dominant terms are those containing $\alpha Z/\rho$, as long as ρ is of nuclear dimensions. The assumption made by Fermi that ρ is to be set equal to the nuclear radius here becomes quite critical. Exceptions to this can be found in the tensor and axial vector interactions for cases in which ΔJ has the highest possible value; in the only contributing terms $\alpha Z/\rho$ does not appear.

More detailed conclusions which can be made regarding the first forbidden formulas follow:

(1*a*) For $\Delta J=\pm 2$, which is allowed in this approximation only by the axial vector and the tensor interactions, the energy dependence of the correction factors becomes completely definite since only a single matrix element does not vanish. This dependence is shown in Fig. 1 for two values of Z. It can be seen that the influence of Z is comparatively small, as is to be expected from the absence of terms in $\alpha Z/\rho$.

(1*b*) Also completely definite are the correction factors for the scalar and pseudo-scalar interactions. These are shown in Fig. 2 for three values of Z. This time, due to the presence of $\alpha Z/\rho$, the Coulomb influence is quite large.

(1*c*) All the interactions give the allowed form to first forbidden spectra with $\Delta J=0, \pm 1$ if the nuclear charge is large enough and the energy small enough. In such cases the α^2Z^2/ρ^2 term predominates in the correction factors and it is independent of energy. This tendency is displayed by the C_{1S} curve for $Z=83$ in Fig. 2.

(1*d*) It may happen that first forbidden spectra take the allowed form even for light nuclei according to the vector and tensor interactions. If it should happen that the matrix element $|\int \boldsymbol{\alpha}|^2$ in C_{1V} or C_{1T}, or $|\int \boldsymbol{\gamma}_5|^2$ in C_{1A}, has a dominant magnitude, then the correction factor becomes nearly independent of the energy.

(1*e*) A definite result is also possible for C_{1T} in $0\rightarrow 0$ transitions and for C_{1A} in $1\leftrightarrow 0$ transitions. In each case only a single matrix element does not vanish. The energy dependence in these cases is very similar to that of C_{1S} as illustrated in Fig. 2.

Concerning the second forbidden correction factors one can make the following statements:

(2*a*) A definite energy dependence is obtained for C_{2A} and C_{2T} in case $\Delta J=\pm 3$. It is shown in Fig. 3 for a large and a small value of Z. Again the Coulomb influence is comparatively small.

(2*b*) The scalar and pseudo-scalar correction factors are again completely definite and are shown in Fig. 4. As in the first forbidden transitions, the Coulomb influence is considerable.

(2*c*) Excepting $\Delta J=\pm 3$, all the interactions in general give for large Z a correction factor which decreases steeply with energy, approximately as $(W_0-W)^2$. This is illustrated for C_{2S} in Fig. 4.

(2*d*) For $0\rightarrow 0$ transitions, C_{2T} assumes a definite energy dependence much like that of C_{1S}. For $2\leftrightarrow 0$ transitions, C_{2A} is definite and very nearly like C_{2S}. Finally, C_{2V} becomes definite for $1\leftrightarrow 0$ transitions and gives a distribution much like C_{1S} again.

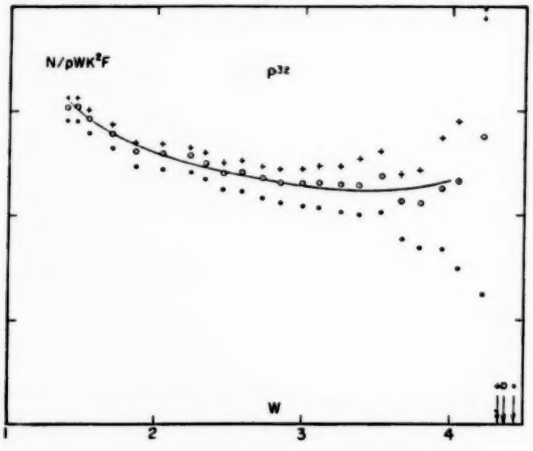

FIG. 5. The experimental number of electrons emitted by P^{32} per unit energy range in ratio to the relative numbers expected according to Fermi's allowed formula, $N\sim pW(W_0-W)^2F$. The data are Lawson's.[11] The blank circles indicate points computed for $W_0=4.37$, the value given by Lawson as most probably correct. The crosses are for $W_0=4.33$ and the solid dots for $W_0=4.44$; this shows the influence of small uncertainties in the upper limit. The curve is drawn to represent an average of the measurements. The ordinates are on an arbitrary scale which is the same for all the points.

§6. Comparison with Experiments

There seem to be available for comparison with the "forbidden" formulas only three reliable β-spectrum measurements, namely those of Na^{24}, P^{32} and RaE. By dividing the experimental number of electrons per unit energy range by $pW(W_0-W)^2F(Z, W)$, one obtains, according to (1). the energy dependence of the correction factor C. Since one divides by a quantity which becomes small at both ends of the spectrum, it is clear that great accuracy is needed to obtain a reliable correction curve. Small uncertainties in the value of the upper limit W_0 have great effect. All this is illustrated by Fig. 5.

Na^{24} is expected to be first forbidden according to the Sargent law.[19] The experimental correction factor, shown in Fig. 6, must accordingly be compared with the formulas for C_1. It seems impossible however for any of the C_1's to represent the data, whatever choice is made for the values of the nuclear matrix elements. This

[19] Compare Konopinski, reference 8.

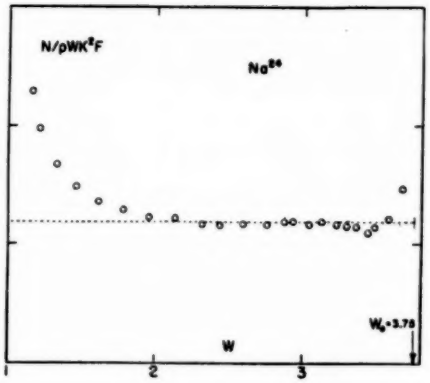

FIG. 6. The ratio of the number of electrons emitted by Na^{24} per unit energy range to the relative number expected according to Fermi's allowed formula. The data are due to Lawson.[11] The circles are the experimental points and the straight line is drawn on the hypothesis that the spectrum is complex with the main component of the spectrum having the allowed form as indicated by the experimental points for energy greater than $W=2$. The ordinates are on an arbitrary scale.

may not at all be a real difficulty, since it seems quite possible for the Na^{24} spectrum to be complex. The sudden rise of C toward low energies must then be interpreted as due to a superposed spectrum with an upper limit of around 1 Mev. Gamma-rays of about the right energy have been observed.[20] This conclusion is contradictory to that drawn by Langer, Mitchell and McDaniel[21] and by Feather and Dunworth[22] from their coincidence experiments. These experiments do not seem to be quite conclusive however, especially since they have not been extended to low enough energies. Accepting the conclusion that the spectrum is complex, one sees from Fig. 5 that, for the main component, the correction factor is constant over a large part of the spectrum. This already excludes the purely scalar and pseudo-scalar theories, as can be seen from Fig. 2. To explain the result with the vector or tensor correction factors, one must assume that the matrix elements $\int \alpha$ or $\int \gamma_5$ which have coefficients independent of the energy are much larger than all the others. This may very well be the case. Of course, the possibility still remains that Na^{24} is not first forbidden but allowed according to our selection rules, especially since the experimental form of the main component seems to be the allowed one. One then must explain the long lifetime by the violation of some further selection rule.

As has already been mentioned, P^{32} and RaE are most likely to be second forbidden and their spectra are almost certainly single. Comparison of Figs. 4, 5 and 7 shows that C_{2S} cannot explain the data. One can also exclude C_{2A}. This follows from the fact that S^{32} and RaF are even-even nuclei and so can be taken to have $J=0$ in their normal states. According to the axial vector theory, then, the transitions must be $2\rightarrow 0$ or $3\rightarrow 0$ in the second forbidden approximation. As mentioned in conclusions (2*a*) and (2*d*), both these cases lead to definite energy dependences for C_{2A}. The $2\rightarrow 0$ case is excluded for the same reason as C_{2S}, while in the $3\rightarrow 0$ case C_{2A} cannot explain the data either, as can be seen from Fig. 3. There remain now only the polar vector and the tensor interactions. For the first we can exclude the $1\rightarrow 0$ and for the second the $0\rightarrow 0$ and $3\rightarrow 0$ possibilities, since these are similar either to C_{1S} or to C_{2A}, as pointed out in conclusions (2*d*) and (2*a*). There is left now only the possibility of $2\rightarrow 0$ transitions for P^{32} and RaE. The energy distribution which C_{2V} and C_{2T} yield for the $2\rightarrow 0$ case depends on the

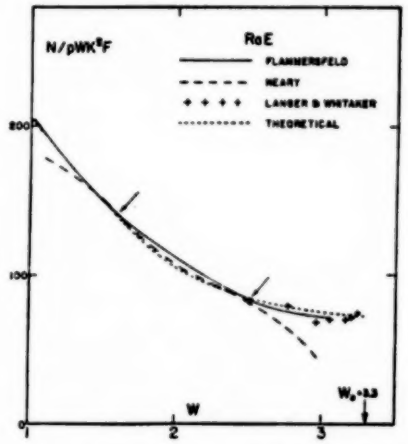

FIG. 7. The ratio of the number of electrons emitted by RaE per unit energy range to the relative number expected according to Fermi's allowed formula. The experimenters responsible for the data are indicated.[11] The dashed line gives $C_{2T}/\sum|T_{ij}|^2$ with the ratio of the matrix elements involved in C_{2T} adjusted to fit the experimental curves at the points indicated by the arrows. The adjusted ratio was $A_{ij}/T_{ij}=-5.8$, which does not seem implausible. The ordinates are on an arbitrary scale.

[20] J. R. Richardson and F. N. D. Kurie, Phys. Rev. **50**, 999 (1936).
[21] Langer, Mitchell and McDaniel, Phys. Rev. **56**, 962 (1939).
[22] N. Feather and J. V. Dunworth, Proc. Camb. Phil. Soc. **34**, 442 (1938).

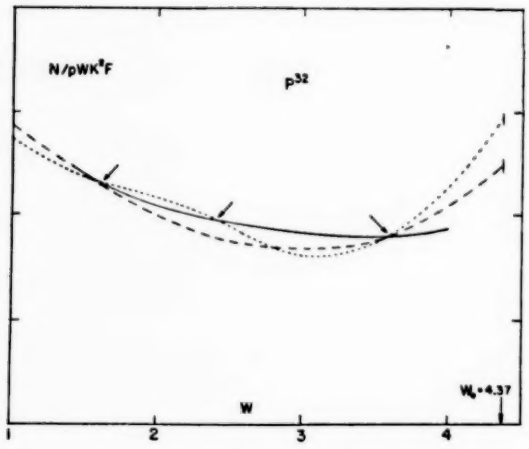

FIG. 8. The solid curve is the same as the curve in Fig. 5, representing an average experimental correction factor for P^{32}. The broken lines give $C_{2T}/\Sigma|T_{ij}|^2$, the correction factor according to the tensor theory. The dashed line was fitted to the experimental curve at two points indicated by arrows, leading to $A_{ij}/T_{ij}=-2.2$. The dotted curve was fitted at three points with $A_{ij}/T_{ij}=-1.5\pm i3.0$. Compare with Fig. 5.

ratio of two matrix elements. By adjustment of the ratio, C_{2V} and C_{2T} can be made to give an equally good account of the facts since two of the three terms in each depend on the energy identically and the third terms are very nearly alike. We have done the computations for C_{2T} since the tensor theory is, perhaps, to be favored over the polar vector theory, considering that there is some evidence that the Gamow-Teller selection rules are to be preferred to the original Fermi ones. The fitting of C_{2T} to the RaE and P^{32} experimental data is shown in Figs. 7 and 8.

The one encouraging feature of the application of the theory to the experiments is that the decided deviation of the RaE from the allowed form can be at all explained by the theory. According to statement (2*c*) of §5, the theory gives a correction factor approximately proportional to $(W_0-W)^2$ for an element like RaE. This accounts for the surprising agreements found by the experimenters between their data and the so-called K-U distribution.

The authors wish to express their appreciation for helpful discussions of the problem with Professors E. Wigner and O. Laporte.

AUGUST 15, 1941 PHYSICAL REVIEW VOLUME 60

A Dilatometric Study of the Order-Disorder Transformation in Cu-Au Alloys

F. C. NIX AND D. MACNAIR
Bell Telephone Laboratories, New York, New York

(Received June 26, 1941)

The order-disorder transformation in single crystals of Cu-Au alloys, containing 22, 25, and 30 atomic percent Au, has been studied by dilatometric means. The plots of true coefficient of thermal expansion *versus* temperature for previously well-ordered alloys display a slow rise from −190°C to about +50°C, followed by a flat plateau to about 250°C. From the flat plateau they rise rapidly to a peak at the critical ordering temperature T_c, followed by a fall to a second flat plateau which extends to at least 450°C above T_c. The lower portion, that portion below the flat plateau, can be well represented by a Grueneisen equation if one assumes additivity for the constants taken from the equation for the pure metals Cu and Au. The presence of the flat plateau above T_c is in disagreement with Bethe-Peierls' theory of the vanishing of short range order. Plots of true coefficient of expansion *versus* temperature, for specimens previously quenched from above T_c, display valleys similar to those in the comparable specific heat curves of Sykes and Jones.

THE transformation from a random or disordered state to an ordered state in Cu-Au alloys, containing 22 to 30 atomic percent Au, is accompanied by a decrease in volume. The greater the final degree of order attained, the greater the volume decrease. The contraction in volume on ordering for Cu_3Au, as deduced from the contrast between quenched and fully annealed alloys, has been found by x-ray measurements of lattice-constant to be 0.6 percent.[1] The volume change accompanying the redistribution of atoms over the lattice sites depends on the relative

[1] C. H. Johansson and J. O. Linde, Ann. d. Physik **25**, 1 (1936).

change in number of like and unlike pairs of atoms in the alloy and not on the size of the ordered domains, and is hence independent of the complications arising from the formation of out-of-step domains. In x-ray studies[2] of Cu_3Au alloys, it has been shown that superstructure lines are not detectable if the ordered domains have fewer than 18–20 atoms along an edge. On the other hand, energy and volume changes accompanying the ordering process produce a change in number of like and unlike pairs of atoms and, consequently, a measurement of either yields data on ordering processes where the ordered domains are too small to be detectable by the usual x-ray technique. The inherent defect in energy measurements—specific heat determinations—is that the heating rates required to obtain accurate thermal data are too great to permit thermal equilibrium to be established, except in cases, such as β-brass, where the time of relaxation of the ordering process is sufficiently small. In this research we have minimized this defect by using an interferometric dilatometer with photographic recording, permitting the use of extremely slow heating rates, to study the order-disorder process on single crystals of Cu-Au alloys. The dilatometric study has the further advantage of maintaining the same high degree of accuracy independent of the rate of heating or cooling and consequently permits one to obtain a very detailed study of any phase of the transformation. A detailed description of the apparatus and procedure used has recently been published in *The Review of Scientific Instruments*.[3]

Preparation of Specimens

The single crystals used in this investigation were prepared in a vacuum single-crystal furnace described by Nix.[4] The copper used in the preparation of the alloys, obtained from Adam Hilger, contained, according to their analysis, 99.979 percent Cu with an oxygen content of 0.02 percent. The gold, prepared by Handy and Harmon as spectroscopic standard, contained 99.99+ percent Au, the impurities consisting of traces of Ag, Cu, and Pd. The ingots were prepared in the vacuum single-crystal furnace and were subsequently homogenized in evacuated fused silica tubes immediately below their melting points. After an analysis to assure chemical homogeneity, they were rolled and swaged under extremely clean conditions to rods the size of the desired single crystals. The chemically homogeneous polycrystalline rods were then remelted in the vacuum furnace in high purity graphite crucibles. The crucibles with molten alloy were then lowered at a rate of about 2 in. per hour. The pressure in the furnace was 10^{-4} mm Hg. After solidification, the single crystals were annealed in evacuated fused silica tubes for 200 hours at a temperature about 50°C below the melting point, to eliminate any chemical inhomogeneities that might have arisen in the course of the formation of the single crystals. Subsequent chemical and x-ray analyses of the two ends of the single crystal rods showed them to be chemically homogeneous within 0.1 percent. The three samples used in the interferometric measurements were cut from the same end of a rod.

A high degree of *order* was obtained by following the procedure of Sykes and Evans,[5] in which the alloys are annealed for a prolonged period of time (about 70 hours) immediately below the critical ordering temperature T_c, and then cooled at the slow rate of about 5°C per hour down to 250°C. In order to obtain a high degree of *disorder* the specimens were subjected to an anneal of some 10 hours in evacuated glass tubes at 600°C (a temperature considerably above T_c), followed by a drastic quench in a low vapor pressure oil bath. The glass tubes were always broken under the oil surface, thus assuring a drastic quench with freedom from any substantial surface oxidation.

The x-ray studies were made on filings taken from the ends of the single crystal rods. The filings were annealed in evacuated fused silica tubes at about 900°C, in order to remove strain effects introduced by the filing operation. The strain-free filings were then subjected to the same thermal treatments as described above for the dilatometric specimens. The x-ray diffraction patterns were taken with a high dispersion back-reflection camera.

[2] C. Sykes and F. W. Jones, Proc. Roy. Soc. London **157**, 213 (1936).
[3] F. C. Nix and D. MacNair, Rev. Sci. Inst. **12**, 66 (1941).
[4] F. C. Nix, Rev. Sci. Inst. **9**, 426 (1938).
[5] C. Sykes and H. Evans, J. Inst. Metals **58**, 255 (1936).

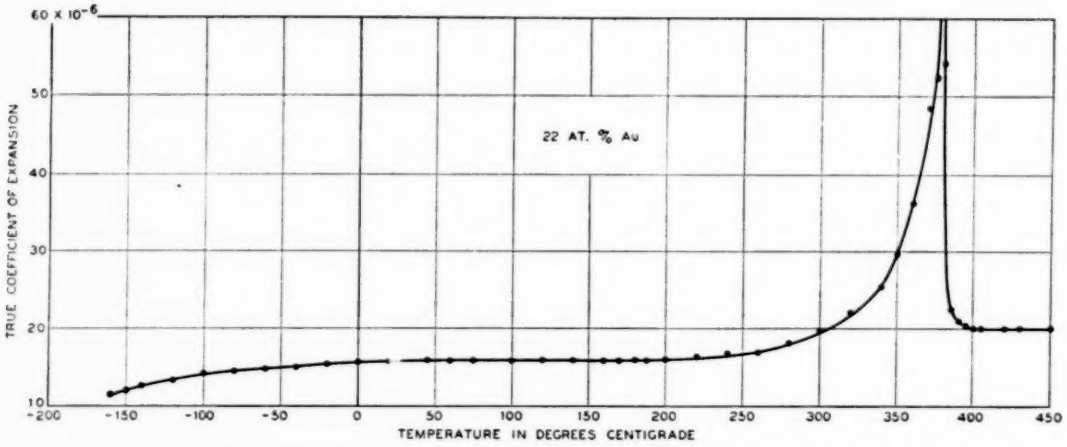

FIG. 1. True coefficient of expansion *versus* temperature for a previously highly ordered Cu-Au alloy containing 22 atomic percent Au. Heating rate 5°C per hour near T_c.

The exact analysis of the 22, 25, and 30 atomic percent Au specimens are as follows: 22.1, 24.8 and 30.2 atomic percent Au, respectively.

METHOD OF MEASUREMENTS

The measurements on well-ordered alloys were first made in the low temperature apparatus from room temperature up to +100°C and then cooled continuously at a rate of 10°C per hour down to −190°C in an atmosphere of helium gas at a pressure of 3 mm of Hg. In the case of disordered alloys the measurements were first made by cooling from room temperature to −190°C. The heating and cooling data for the region from room temperature to +100°C coincided within the experimental error. At the end of the cooling run the apparatus was held at a constant temperature for a period of two hours or more as a check on whether or not the refraction thermometer was in thermal equilibrium with the specimens. It was always observed that the contraction of the alloy ceased at the instant the temperature became constant. It was further observed that any accidental irregularities in the cooling rate—such as sometimes occurred in the temperature range below −150°C, causing either a short cessation in the fall of temperature or even an occasional heating of a few degrees—were accompanied by a complete unison of motion of the thermometer and dilatometer fringes: this also shows that thermal equilibrium existed between specimens and refraction thermometer. The portion of the curve from room temperature to +860°C was made in the high temperature apparatus described. Helium gas at a pressure of 3 mm of Hg was used, in most cases, up to +150°C, at which temperature the system was evacuated to a pressure of 10^{-5} mm Hg for the remaining portion of the high temperature run.

EXPERIMENTAL RESULTS

A plot of the true linear coefficient of thermal expansion β against temperature from −170°C to 450°C is given in Fig. 1 for a previously well-ordered Cu-Au alloy of 22 atomic percent Au. The coefficient of thermal expansion on heating from room temperature remains rigorously constant at 15.8×10^{-6} to 200°C; then it rises rapidly with increasing temperature, as the alloy begins to disorder; reaches a peak of 378°C with a value of 65×10^{-6}; then over a range of 22°C falls to a value 20.0×10^{-6} at 390°C; and thereafter remains rigorously constant up to the highest temperature in the run, namely 450°C. On cooling from room temperature, β continues to decrease with decreasing temperature with an accelerating pace, finally attaining a value of 11.5×10^{-6} at −170°C. The heating rates were 15°C per hour up to 300°, 5°C per hour from 300° to 400°C, and again 15°C per hour up to 450°C. The cooling rate was 15°C per hour from room temperature to −170°C. Measurements made on heating and cooling in the region from room temperature to +100°C failed to display any evidence of hysteresis. Excellent agreement was obtained with widely different heating and cooling rates.

Figure 2 is a plot of the thermal expansion *versus* temperature where l_0 is the length of specimens at 0°C, from 340°C to 400°C, for the same alloy at a heating rate of 5°C per hour. This curve is a portion of the curve from which the coefficients were obtained in Fig. 1. It is to be noted that even at this slow heating rate no indication of a vertical region is observed. Immediately following the rapidly rising region the curve becomes rigorously straight and remains so up to 450°C, the highest temperature used in this test.

Figure 3 depicts the results of similar studies on previously well-ordered "Cu_3Au" (Cu-Au alloy containing 25 atomic percent Au). The heating rate was 15°C per hour from room temperatures to 330°C, then 5°C per hour from 330 to 410°C and again 15°C per hour from 410° to 450°C. The cooling rate was 15°C from room temperature to −190°C. The true coefficient of thermal expansion β rises from a value of 9.2×10^{-6} at −180°C to a value of 15.75×10^{-6} at +30°C, and remains at this value up to *ca.* +180°C. From this level plateau, β rises to a value of 120×10^{-6} at 393°C, then immediately following the vertical portion, as is clearly to be seen from Fig. 4, at 394°C it falls over a temperature range of about 15°C to another plateau at 20.05×10^{-6} and remains at this value up to the highest temperature in this run, namely 450°C.

Figure 4 is again a plot of the experimental points of $\Delta l/l_0$ against temperature in the region around the critical ordering temperature T_c. The thermal expansion curve rises much more rapidly than in the case of the 22 atomic percent alloy and displays a sensibly vertical portion at 394°C. After passing through this rapidly rising region, the rate of expansion again becomes constant up to 450°C.

Figure 5 depicts studies similar to those illustrated in Figs. 1 and 3, for a Cu-Au alloy containing 30 atomic percent Au. The heating rate was 15°C per hour from room temperature to 700°C and the cooling rate was again 15°C from room temperature to −190°C. The curve is similar to that of the 22 atomic percent Au alloy except for the appearance of a secondary hump at about 275°C in this case. The true coefficient of expansion rises from the minimum value of 10×10^{-6} at −180°C to a value of 15.60×10^{-6} at +20°C and remains at this value up to 225°C. From the high temperature end of this plateau it rises to a peak value of 60×10^{-6} at 360°C and then falls over a range of about 20°C to another level plateau at a value of 20×10^{-6} which extends unchanged up to 680°C.

It was of great interest to determine whether or not alloys drastically quenched from a temperature considerably above the critical ordering temperature T_c would possess a true coefficient of thermal expansion differing from that displayed in the well-annealed or highly ordered alloys. In view of the extreme constancy in the magnitude of β over a wide temperature interval above T_c, it was thought probable that a sufficiently drastic quench from a temperature considerably greater than T_c might suppress the ordering process to such an extent that one could preserve the higher "plateau" values of β. It was, furthermore, of real interest to study the effect of the ordering process as manifested in the dependence of the true thermal coefficient of expansion on the temperatures of quench and rates of heating in the course of making the thermal expansion measurements.

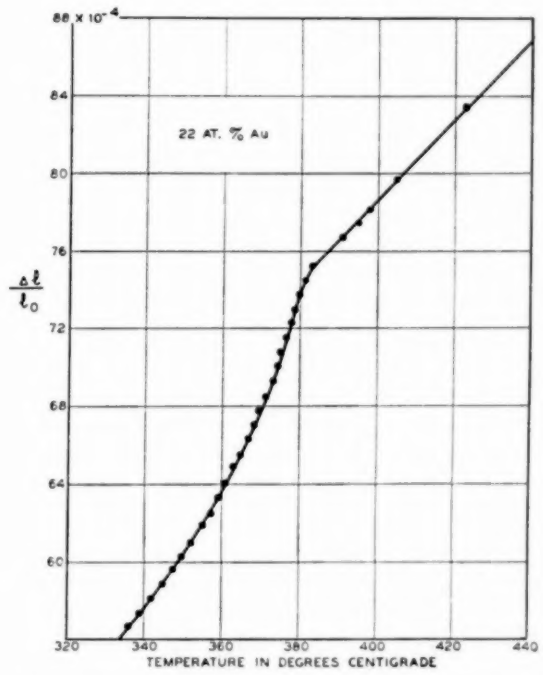

FIG. 2. A thermal expansion *versus* temperature curve for the region in the vicinity of T_c for the ordered 22 atomic percent Au, Cu-Au alloy. Heating rate 5°C per hour.

The ordering process should tend to produce a contraction in the alloy.

Figure 6 depicts the results obtained on a Cu-Au alloy with 22 atomic percent Au, after it was drastically quenched from 600°C in a previously cooled low vapor pressure oil bath. The low temperature run was made at a cooling rate of 15°C per hour, and the high temperature run at a heating rate of 30°C per hour. The true coefficient of thermal expansion β rises from a value of 11×10^{-6} at -160°C to 15.6×10^{-6} at about 30°C and remains constant to 125°C, at which temperature it begins to recede and passes through a series of three valleys at 175, 295, and 340°C, respectively. The curve then rises to the disordering peak of 56×10^{-6} at 377°C, and finally falls over a range of about 10°C to the high temperature plateau at 19.9×10^{-6}.

Figure 7 gives a typical curve of β *vs.* T for a Cu-Au alloy with 25 atomic percent Au, quenched from 600°C. The quenched alloy was first cooled to -170°C at a rate of 40°C per hour. The heating rate was 15°C per hour from room temperature to 350°C, then 5°C per hour from 350°C to 450°C. The coefficient of expansion rises from a value of 10×10^{-6} at -162°C to 15.4×10^{-6} at $+25$°C, where it remains constant until the recession sets in at *ca.* 175°C, whence it then falls to a value of 1×10^{-6} at $+285$°C, rises to a high disordering peak at 392°C and falls to the high temperature plateau over a range of 15°C. In other tests on quenched 25 atomic percent Au alloys, the number, position, and depth of the valleys varied considerably. In some instances, with slow rates of heating, the coefficient of thermal expansion takes on small negative values.

Figure 8 illustrates the effect of two different heating rates on a previously quenched Cu-Au alloy containing 30 atomic percent Au. The quenching temperature was 600°C for both tests. The full line represents the results with a cooling rate of 15°C per hour from room temperature down to -110°C and a heating rate of 30°C per hour from room temperature to 600°C. The dashed line depicts results obtained with a heating rate of 5°C per hour. It is of interest to note that, in this instance, the recession of β was more drastic in the case of the faster rate of heating, whereas the temperature of onset of the recession from the level plateau, at $\beta=15.6\times10^{-6}$, was the same for the two rates. Both rates of heating display two valleys preceding the disordering peak although there is no agreement as to position on temperature scale and depth. The level plateau above T_c again, as in *all* experiments, remains constant up to the highest temperature studied, namely 600°C. The position and magnitude of the peak for the 30°C per hour rate agrees well with the results obtained on the 15°C per hour rate for the previously ordered alloy.

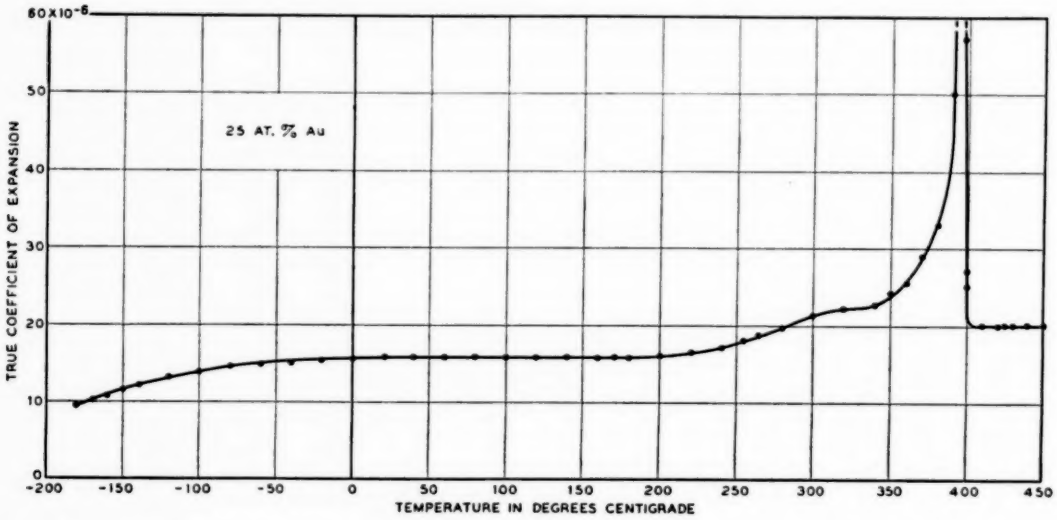

FIG. 3. True coefficient of expansion *versus* temperature for a previously highly ordered Cu-Au alloy containing 25 atomic percent Au (Cu_3Au). Heating rate near T_c 5°C per hour.

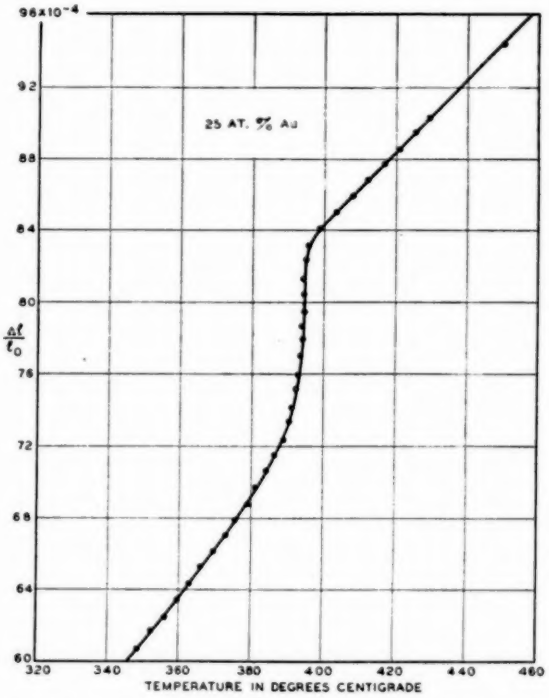

FIG. 4. A thermal expansion *versus* temperature curve for the region in the vicinity of T_c for the ordered 25 atomic percent Au, Cu-Au alloy (Cu_3Au). Heating rate 5°C per hour.

CONTRACTION ON ORDERING

The ordered Cu-Au alloys are denser than the quenched alloys at room temperature. Johansson and Linde[1] report the ordered Cu_3Au alloy to possess a 0.6 percent smaller volume than the quenched alloy as determined by x-ray measurements. In column 2, Table I, lattice constants are given for the quenched and annealed or ordered Cu-Au alloys as we determined them with a high dispersion back-reflection x-ray camera, using Cu $K\alpha$ radiation. Column 3 shows the linear contraction in percent on ordering thus determined. Column 4 of the table gives the percent contraction of the alloys as determined from the thermal expansion *versus* temperature plots for initially ordered and quenched alloys. In column 5 we give the percent in contraction on ordering as obtained from the thermal expansion *versus* temperature plots by assuming the contraction below T_c for each alloy to possess a coefficient of expansion characteristic of the low temperature plateau. The justification for this rather crude assumption will be discussed below in the "Discussion of Results."

DISCUSSION OF RESULTS

The temperature of onset of the disordering process in the 25 atomic percent Au alloys inferred from these curves is in reasonably good agreement with the temperature obtained from specific heat measurements. The corresponding temperature for the 22 and 30 atomic percent Au alloys falls in the same neighborhood, as might be expected. The slow heating rates possible with the dilatometer used in this investigation, along with the maintenance of the high degree of precision, common to interferometric measurements, permitted a rather detailed study of the alloys at temperatures immediately below the critical ordering region. The 25 and 30 atomic percent Au alloys displayed a small broad peak located about 100°C below the critical ordering temperature T_c, which is completely absent in the 22 atomic percent alloy. These peaks may arise from a cause similar to that of a comparable peak in Cu_3Pd,[6] where the cubic disordered structure is slightly distorted to a tetragonal lattice on ordering. The structure of the disordering peaks in the 22 and 30 atomic percent Au alloys are quite similar, as is to be seen from Fig. 1 and Fig. 5. The thermal expansion *versus* temperature plot of the 22 atomic percent alloy given in Fig. 2 clearly shows the complete lack of a vertical portion at T_c as the Bragg-Williams theory as extended by Shockley[7] demands. On the other hand, the 25 atomic percent Au, Cu_3Au, alloy as shown by Fig. 4 clearly shows a sensibly vertical region at T_c; however, the magnitude of the vertical portion relative to the preceding ex-

TABLE I. *Data on Cu-Au alloys.*

1	2		3	4	5
Au Content of Alloy in Atomic Percent	Lattice Constants in Angstrom Units		Percent Contraction on Ordering from Lattice Constants	Percent Contraction on Ordering Determined from Thermal Expansion Measurements	Percent Contraction on Ordering Assuming Coeff. of Expansion of the Low Temperature Plateau
	Quenched	Annealed			
22	3.729	3.725	0.080	0.152	0.127
25	3.746	3.739	0.187	0.165	0.187
30	3.770	3.768	0.053	0.081	0.087

[6] F. W. Jones and C. Sykes, J. Inst. Metals **65**, 419 (1939).
[7] W. Shockley, J. Chem. Phys. **6**, 523 (1938).

pansion caused by disordering is considerably less than one would be led to expect from the Bragg-Williams and Bethe theories.[8] This comparison of experiment with theory assumes that the heating rates used in these experiments are sufficiently slow to permit the establishment of an equilibrium condition while traversing the critical ordering region. In view of the recent results of Siegel[9] on the time necessary to attain equilibrium in his elastic constant measurements, amounting to as much as 50 hours at T_c, it is possible that the extremely slow rates used in this investigation are still too rapid to permit equilibrium to be established and the expansion may consequently have been spread over a greater temperature interval than it would have been at true equilibrium. This may account for the fact that the T_c values obtained both by Sykes and Jones[2] from specific heat studies, using a heating rate of 120°C per hour, and from these studies where a substantially slower rate (5°C per hour) was used, are higher than T_c values obtained from elastic constant and electrical conductivity studies. The T_c values for Cu_3Au are 391°C from specific heat studies, 394°C from our dilatometric data, 387.5°C (heating) and 385°C (cooling) from elastic constant measurements and 385°C from electrical conductivity measurements (cooling). The high value obtained from specific heat and dilatometric studies may be, in part, due to lack of equilibrium.

[8] F. C. Nix and W. Shockley, Rev. Mod. Phys. **10**, 1 (1938).
[9] S. Siegel, Phys. Rev. **57**, 537 (1940).

In Fig. 9, the solid curve is a plot of a Grueneisen theoretical curve of true coefficient of expansion *versus* temperature for a Cu_3Au alloy, it being assumed that the constants of the theoretical formula for pure Cu and Au are strictly additive for the alloy. The dashed curve is a replot of part of the data given in Fig. 3. It is of interest to note the excellent agreement between the theoretical curve obtained from the crude assumptions made and the data below 300°K: note that the fit involves no adjustment of any disposable constant! There is a disagreement between theory and experiment from 300°K to about 500°K, in the sense which indicates that forces are coming into play which tend to make the alloy contract. At 450°K the experimental curve begins to rise very rapidly with the onset of disorder and rises more rapidly as the disordering process progresses. After passing through the disordering peak, at T_c, β falls sharply but not all the way to the theoretical curve. The final part of the experimental curve is horizontal and lies above the Grueneisen curve.

We think of the experimental curve as being the sum of three components; first the component due to thermal vibrations, as conforming to the Grueneisen theory (β positive); secondly a "disordering component" due to the disappearance of order with increasing temperature, which dominates the rapidly rising portion of the curve starting at 450°K, and thirdly a component introduced to account for the horizontal portion from 300 to 450°K, this having a negative β-value which tends to counteract the vibrational com-

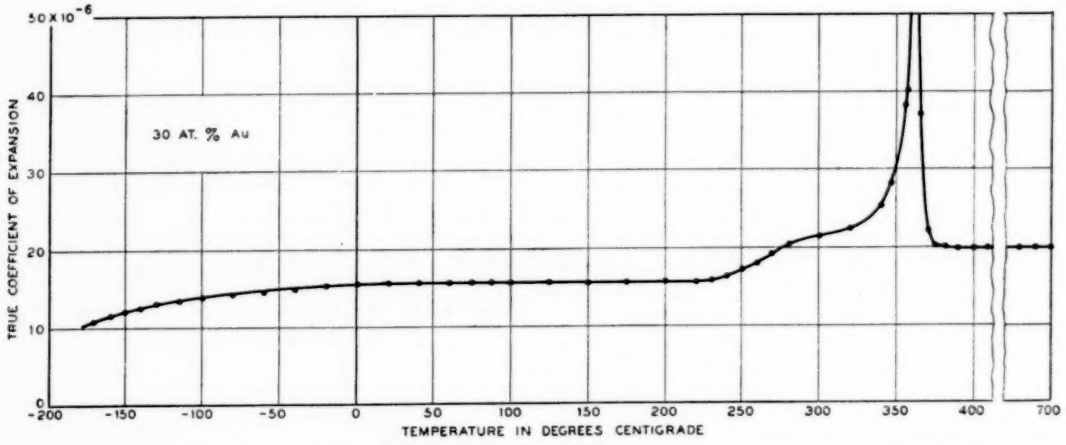

FIG. 5. True coefficient of expansion *versus* temperature for a previously highly ordered Cu-Au alloy containing 30 atomic percent Au.

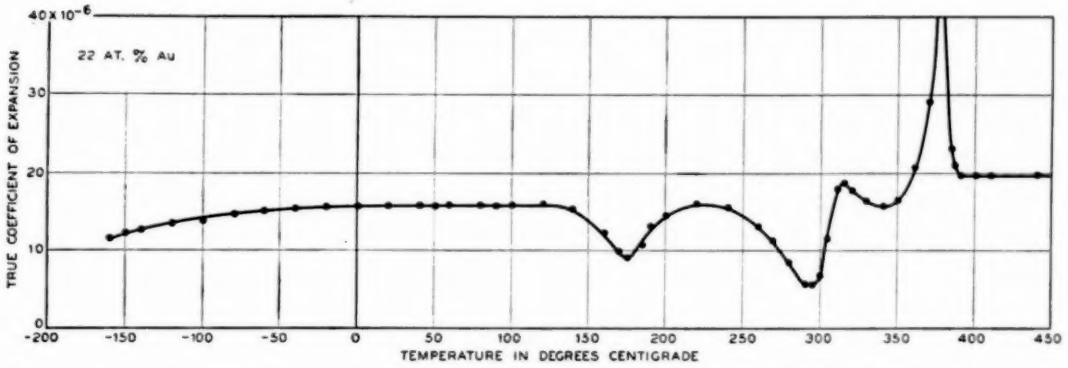

FIG. 6. True coefficient of expansion *versus* temperature for a 22 atomic percent Cu-Au alloy quenched in an oil bath from 600°C. Heating rate above room temperature 30°C per hour.

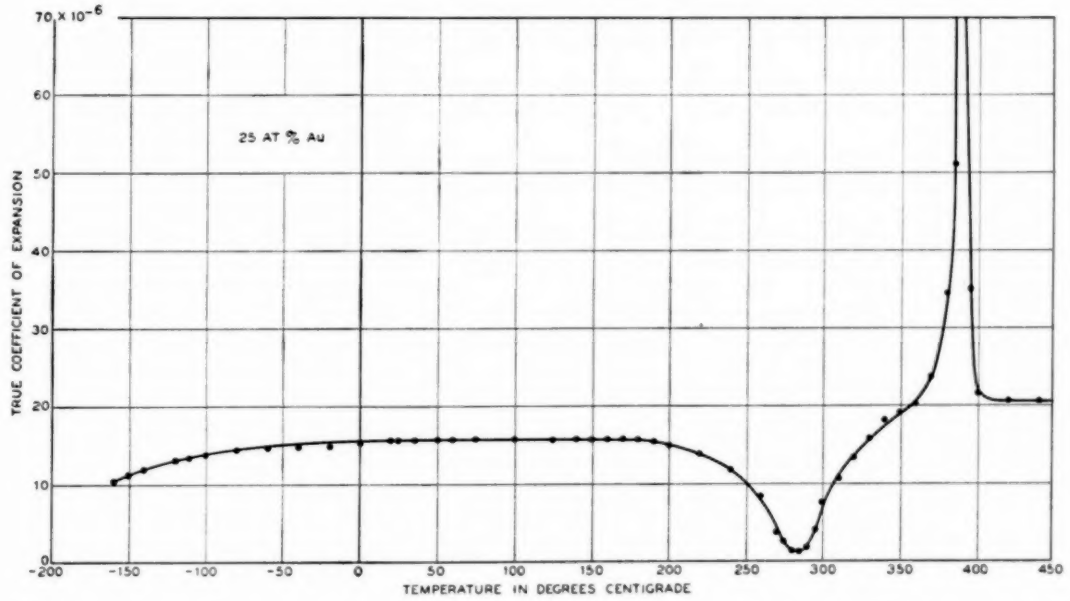

FIG. 7. True coefficient of expansion *versus* temperature for a 25 atomic percent Au, Cu-Au alloy quenched in an oil bath 600°C. Heating rate 15°C per hour from 25 to 350°C and 5°C per hour from 350 to 450°C.

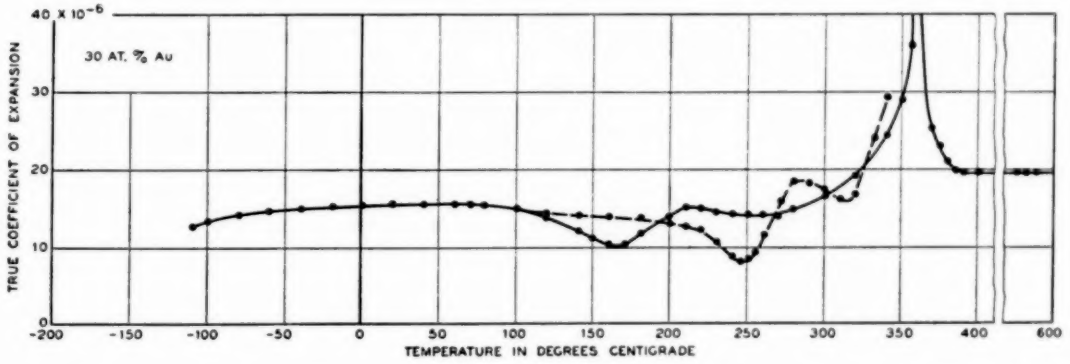

FIG. 8. True coefficient of expansion *versus* temperature for a 30 atomic percent Au, Cu-Au alloy quenched in an oil bath from 600°C. Solid line depicts results for a heating rate of 30°C per hour from 25 to 600°C. The dashed line depicts results for a heating rate of 5°C per hour.

ponent. According to the Bethe-Peierls[8,10,11] theory of short range order, the so-called disordering component should persist above T_c with the gradual disappearance of short range order. As the short range order vanishes, we would then expect the total expansion to approach that due entirely to thermal vibrations and approach the theoretical Grueneisen curve. The third component is, therefore, a supplement to the theory as heretofore conceived.

Figure 10 shows a similar theoretical curve and the data for a Cu-Au alloy with 30 atomic percent Au. The data for the temperature region from 90 to 300°K are in excellent agreement with the Grueneisen curve (calculated, as for the previous case, by assuming the constants for pure Cu and Au to be additive for the alloy). The agreement, as well as the divergence from theory, is similar to that of the 25 atomic percent Au alloy, but in this instance the data extend to a temperature considerably further above T_c. In the region above T_c the coefficient of thermal expansion remains rigorously constant, intersects the Grueneisen curve and continues to higher temperatures without displaying any tendency to approach the theoretical curve. In approximately 40 tests, a deviation from a rigorous straight line has never been observed.

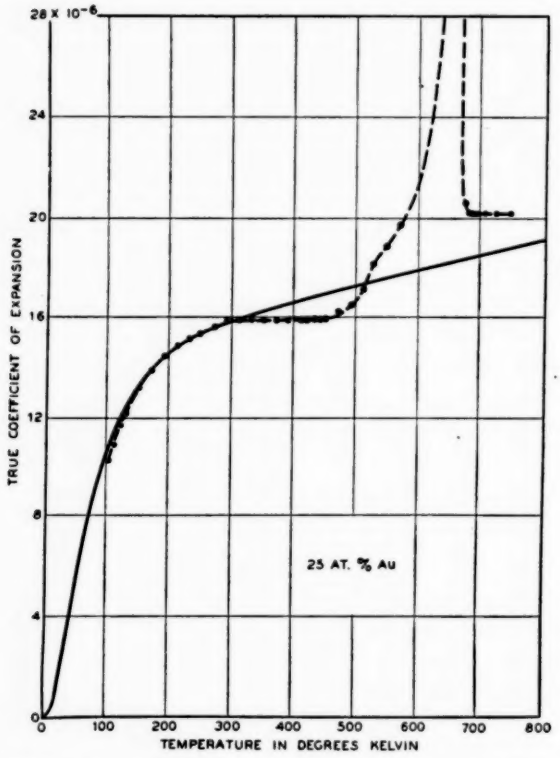

FIG. 9. True coefficient of expansion *versus* temperature for a previously highly ordered 25 atomic percent Au, Cu-Au alloy. Solid line gives a Grueneisen curve with a characteristic Debye temperature of 291°K.

According to the Bethe theory of short range order, as mentioned above, one would expect the experimental curve to be a sum of the normal vibrational expansion coefficient and that component arising from the vanishing of short range order. It seems highly improbable that the addition of these components, the vibrational component increasing at an almost constant rate with increasing temperature and the disordering component decreasing with increasing temperature, should add up to a horizontal line independent of temperature, over so wide a temperature region. The authors feel that the behavior of the true coefficient of thermal expansion curve above T_c cannot be satisfactorily explained on the assumption of the gradual disappearance of short range order above T_c and should be reexamined theoretically in view of the above data. Confidence in the reliability of the theoretical Grueneisen curve arises from the excellent agreement between theory and experiment in the case of the pure metals Cu and Au and the agreement in the case of the alloys for the low temperature region from 85 to 300°K.

From about 85°K to about 400°K, where a decrease occurs due to further ordering, the quenched alloys possess the same coefficient of expansion as the highly ordered alloys within the limits of accuracy of the measurements. The same is true of both quenched and annealed alloys above T_c, as might be expected. This rather surprising agreement in true coefficients of expansion near room temperature and below between the quenched and annealed alloys is undoubtedly due to the presence of sufficient short range order to control the magnitude of the true coefficient of expansion resulting from the extremely short relaxation times around T_c. This is confirmed to some extent by the agreement shown in Table I between the percent contraction on ordering as obtained by x-ray lattice constant measurements, on the one hand, and, on the other hand, the contraction obtained from

[10] H. A. Bethe, Proc. Roy. Soc. London **150**, 552 (1935).
[11] R. Peierls, Proc. Roy. Soc. London **154**, 207 (1936).

thermal expansion *versus* temperature curves by assuming the coefficient of expansion from T_c to room temperature to be that existing at room temperature. The lack of better agreement between the contraction on ordering values given in columns 3 and 4 of the table is probably due, in part, to the different degrees of order attained at room temperature resulting from different rates of cooling of the dilatometric specimens and the x-ray powders.

The valleys in the β *vs.* T plots of Figs. 6, 7, and 8 for the quenched alloys result from a further ordering over that occurring during the quenching process. These valleys are similar to those obtained by Sykes and his collaborators on Cu_3Au and other alloys in the quenched state. The authors were unable to obtain the reproducible results reported by Sykes and Jones[2] for Cu_3Au in their specific heat studies. This may be due to the fact that the small size of the specimens used in these experiments, as compared with the considerably larger ones necessary for the specific heat studies, greatly magnifies the unavoidable variations in cooling rates. The curves given in Figs. 6, 7, and 8 are typical of many experiments aimed at obtaining a correlation between temperature of quench, rate of heating, and position and depth of the valleys. Such variations are clearly illustrated in Fig. 8, depicting the β *vs.* T plot for two identically annealed and quenched samples with two rates of heating. One would have expected the slower rate of 15°C per hour to have given rise to a lower temperature of onset of ordering and to a greater degree of ordering, resulting in a larger decrease in the coefficient of expansion.

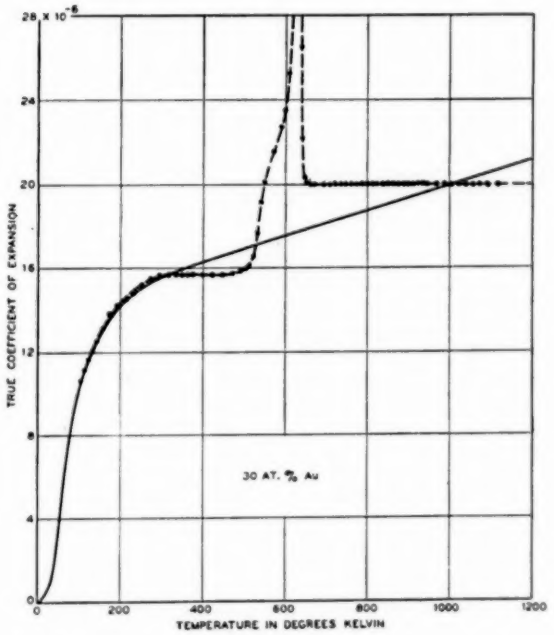

FIG. 10. True coefficient of expansion *versus* temperature for a previously well-ordered 30 atomic percent Au, Cu-Au alloy. Solid line depicts a Grueneisen curve with a characteristic Debye temperature of 284.5°K.

The Effect of Stress on Internal Friction in Polycrystalline Copper

A. W. Lawson
Randal Morgan Laboratory of Physics, University of Pennsylvania, Philadelphia, Pennsylvania
(Received April 23, 1941)

The internal friction of polycrystalline specimens of oxygen-free copper, subjected to compressive stress, increases and then decreases with continuously increasing stress. A complementary behavior of Young's modulus is found. Thus, while the internal friction increases 100 percent, Young's modulus decreases about 6 percent for a stress of 90 kg/cm². An increase of stress to 160 kg/cm² leaves a remnant increase of only 40 percent in the internal friction and a remnant decrease in Young's modulus of 4 percent. This effect is nearly independent of the temperature at which the stress is applied. Although the Taylor dislocation of plasticity is capable of explaining qualitatively the data obtained at any one temperature, no simple explanation of the temperature independence of the effect is available at the present time.

RECENT theoretical studies of phenomena associated with slip in single crystals have been based principally on a model proposed independently by Taylor,[1] and by Orowan[2] who suggested that the various irreversible processes occurring in stressed crystals originate in microscopic lattice irregularities which are termed dislocations. Numerous proposals[3] have been made concerning the nature and behavior of these dislocations, whose movement through the lattice is believed to be responsible for creep and strain hardening.

Recently, Read[4] reported some measurements of internal friction in single crystals. His results indicate that the irreversible work performed during the vibration of a single crystal is generated by the mechanism responsible for plastic flow. This relation is immediately suggested by the fact that the decrement of the vibrations is inversely proportional to the frequency of vibration. Further, Read finds that an increase in the amplitude of vibration augments the internal friction. He suggests that the explanation of the phenomena is as follows. The increase in amplitude of vibration generates dislocations whose motion contributes to the internal friction. The increase of internal friction accompanying application of an external stress supports this contention. The internal friction returns to a lower value after annealing, and, in fact, the more careful the anneal, the lower the internal friction. If it be assumed that dislocations can diffuse out of the lattice during the annealing process, it is reasonable to conclude that all internal friction in single crystals arises from the presence of dislocations. This statement must be qualified, of course, if the specimens are ferromagnetic or if the geometry is such that the vibration is neither adiabatic nor isothermal.

The object of this paper is to report some measurements on the increase in internal friction at different temperatures in polycrystalline copper due to the application of various external compressions. The range of stress here studied is about four times that covered by Read.[5] Such data should yield information concerning the ease with which dislocations may be generated at various temperatures.

Specimens

The study of polycrystalline specimens has the disadvantage that a certain amount of internal friction must arise from the irreversible flow of heat currents between variously oriented grains to neutralize the temperature gradients established by thermoelastic effects. Zener[6] has treated this type of internal friction both experimentally and theoretically and shown that the contribution of such heat currents to the internal friction is small if the time for the heat wave to flow across a grain is either very short (isothermal

[1] G. I. Taylor, Proc. Roy. Soc. **A145**, 362, 388, 405 (1934).
[2] E. Orowan, Zeits. f. Physik **89**, 614, 634 (1934).
[3] For a comprehensive review of plasticity and correlated subjects, the reader should consult F. Seitz and T. A. Read, J. App. Phys. **12**, 100 (1941).
[4] T. A. Read, Phys. Rev. **58**, 371 (1940).
[5] T. A. Read, Phys. Rev. **59**, 477A (1941).
[6] C. Zener, Phys. Rev. **52**, 230 (1937).

extreme) or very long (adiabatic extreme) compared to the period of vibration. The grain size of the specimens herein described is estimated visually after etching the copper with a concentrated solution of nitric and acetic acids. The linear dimensions of the grains are of the order of magnitude of several millimeters, and the contribution to the internal friction due to their random orientation is sufficiently small to permit a determination of internal friction due to the generation of dislocations by an external load.

The advantage of using polycrystalline specimens in this work is afforded by the availability of extremely pure polycrystalline samples of copper. This is important since it is well known that strain hardening is very structure sensitive, particularly with regard to the addition of small amounts of a foreign substance. The materials used in this work were prepared in the research laboratories of the American Smelting and Refining Company, in Barber, New Jersey, under the supervision of Dr. A. J. Phillips. The most refined chemical and spectroscopic analyses fail to reveal any impurities. In most cases, this indicates that the impurity in question is less than 0.0001 percent, and, though it is impossible to prove the oxygen content is less than 0.001 percent, other evidence indicates the oxygen content is also less than 0.0001 percent. In view of the extreme purity of the samples, it was decided to work on polycrystalline samples despite the disadvantage noted above, since it was felt that remelting would undoubtedly introduce impurities. The specimens therefore were machined directly from the supplied stock which consisted of a rolled rod $\frac{3}{8}''$ in diameter. These specimens are right cylinders approximately 3.2 cm in length and 0.476 cm in diameter.

Method

Internal friction is most conveniently described in terms of the decrement of the vibrations, which is defined as the ratio of the energy dissipated per cycle of vibration to twice the vibrational energy of the specimen. This quantity may be ascertained by observing the variation with frequency of the impedance of a composite piezoelectric oscillator constructed by cementing a rod of cylinder material to a suitably cut quartz crystal. Since the electric network equivalent to the piezoelectric oscillator is a capacitance C in parallel with a series circuit comprising an inductance L, capacitance K, and resistance R, the admittance A at a frequency $\Delta\omega$ from the resonant frequency may be written

$$A=\left\{\frac{1-4LC\omega\Delta\omega}{R^2+4L^2(\Delta\omega)^2}+\omega^2C^2\right\}^{\frac{1}{2}}, \tag{1}$$

where ω is the angular frequency. An analysis[7] of the admittance as a function of frequency reveals that, at constant voltage, the resulting current possesses a maximum and minimum value and frequencies near resonance. If one denotes the maximum and minimum observed currents by I_1 and I_2, respectively, and the frequencies at which they occur by f_1 and f_2, respectively, the resonant frequency f_0 is calculated from the relation:

$$f_0=f_1+(f_2-f_1)\frac{I_2}{I_1+I_2}. \tag{2}$$

The decrement of the composite oscillator δ is given in terms of the foregoing quantities by:

$$\delta=2\pi\{(f_2-f_0)(f_0-f_1)\}^{\frac{1}{2}}/f_0. \tag{3}$$

The decrement of the specimen Δ_1 may be calculated from a knowledge of δ and the decrement of the quartz crystal alone Δ_2, determined in the same manner as δ, with the aid of the relation:

$$\delta=\frac{m_1\Delta_1+m_2\Delta_2}{m_1+m_2}, \tag{4}$$

where m_1 and m_2 are the masses of the specimen and the quartz crystal, respectively.

When the resonance curve is very narrow, a precise determination of the quantity (f_2-f_0) appearing in Eq. (3) is difficult and the errors in δ are large. The value of δ is then best determined by an alternating-current bridge after the manner of Cooke and Brown.[8] When the resonance curve is broad, the precision of δ suffers due to the difficulty of locating f_1 and f_2 accurately. Fortunately, however, in this experiment we are interested in the *increase* in internal friction upon the application of an external stress. In other

[7] S. Siegel and S. L. Quimby, Phys. Rev. **49**, 663 (1936).
[8] W. T. Cooke and W. F. Brown, Phys. Rev. **50**, 1158 (1936).

words, relative values of internal friction are of primary interest. These may be determined by the simple method described below for all values of δ to a precision of about 2 percent.

If, in Eq. (1), we regard ω^2C^2 as constant over the width of a resonance curve, we find simply:

$$A_{\max}-A_{\min}=1/R, \tag{5}$$

where R, the resistance of the oscillator, is related to the decrement by the relation:[9]

$$R=\tfrac{1}{4}K(m_1+m_2)\delta f_0. \tag{6}$$

If the amplitude of the voltage applied to the quartz crystal is held constant, we obtain immediately from Eqs. (4), (5), and (6) the relations:

$$\frac{\delta'}{\delta''}=\frac{I_1''-I_2''}{I_1'-I_2'}, \tag{7}$$

$$\frac{\Delta_1'}{\Delta_1''}=\frac{I_1''-I_2''}{I_1'-I_2'}\left\{\frac{(i_1-i_2)-(I_1'-I_2')}{(i_1-i_2)-(I_1''-I_2'')}\right\}, \tag{8}$$

where I_1 and I_2 are the maximum and minimum currents, respectively, drawn by the composite oscillator, and i_1 and i_2 are the maximum and minimum values of the current drawn by the quartz crystal alone under the action of the applied voltage. The prime and double prime quantities refer to values observed in two different measurements on the same specimen. It is to be noted that the quantity in the brackets in Eq. (8) is, in general, a small correction term, since the contribution of the quartz crystal to the decrement of the composite oscillator is usually ten to a thousand times smaller than the contribution of the specimen.

The above theory is only applicable, of course, if the resistance of the device employed to measure the current through the quartz crystal is negligible compared to the resistance of the quartz. There seems to be no way of predicting from the geometry and physical constants of the quartz crystal the resistance of the oscillator. In general, the resistances of quartz crystals similar to those used in this work lie between several hundred and several thousand ohms. The resistance of the composite oscillators is a factor of ten to a thousand larger, since the resistance is proportional to the decrement. In order to measure the currents in these experiments, a resistance of 17 ohms is inserted between the crystal and ground, and the voltage developed across this resistor is amplified and measured. In order to ascertain the effect of the resistance on the accuracy of the measurements, the same experiments were repeated with a 50-ohm resistor. No systematic discrepancies between the two sets of data appeared. The alternating voltage applied to the quartz crystal is generated by a transitron oscillator which is decoupled from the crystal by means of two buffer stages of amplification. From a knowledge of the resonant frequency of free longitudinal vibration of the quartz crystal alone, and that of the composite oscillator, the frequency of free vibration of the specimen alone may be computed.[7] Twice the product of this quantity and the length of the specimen yields the velocity of longitudinal waves in the specimen material.

It may further be noted that, provided the crystal and specimens have resonant frequencies differing by less than ten percent, the effect of the adhesive is not discernible, nor is it necessary to have the areas of the crystal and the specimen congruent.

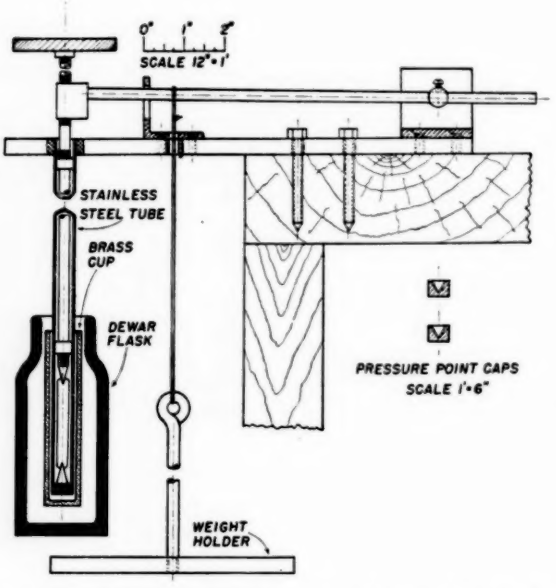

FIG. 1. The apparatus used for subjecting specimen cylinders to compressive stresses at various temperatures.

[9] In Eq. (6), $K=1/b^2\epsilon^2$, where ϵ is the appropriate piezoelectric constant for quartz, and b is the width of the metal electrodes plated on the quartz.

Procedure

The specimens are initially annealed by heating them in hydrogen at atmospheric pressure at a rate of approximately 100°C an hour to 600°C where their temperature is kept constant for several hours. The specimens are then cooled to room temperature over a period of ten hours.

The specimens are cemented to a quartz crystal whose resonant frequency for longitudinal vibrations is about 50 kc, by a thin film of beeswax and rosin under a compressive force of 0.2 kg at a temperature of 60°C. This procedure does not seem to affect the specimens appreciably, inasmuch as reproducible results are obtained after successive adhesions. A further justification of this technique will be discussed below.

The specimens are detached from the quartz crystal and subjected to compressive stresses in the device shown in Fig. 1. This device is designed in a manner calculated to facilitate the application of stresses over a wide range of temperatures. Thus, the specimen is supported at the bottom of a stainless steel tube on a pressure point cap which rests on a pointed screw. Slots cut in the side of the tube permit the insertion of the specimen. The load is transmitted from a mechanical lever system to a similar pressure point cap on the top of the specimen by a rigid steel rod which is threaded so that its length may be adjusted to fit with that of the specimen. Initially, the lever, from which the weights are hung, rests on a knife edge which bears the load until the steel rod is so adjusted in length that it just touches the cap on the top of the specimen. When it is desired to apply the load to the specimen it is merely necessary to advance the screw slightly. The angle of the cone of indenture in the pressure point caps is slightly greater than the angle of the conical points applying the compression. This fact, coupled with the fact that the ends of the specimen are ground accurately perpendicular to the cylinder axis, ensures that the surface traction will be normal to and uniform over the ends of the specimen.

The temperature of the specimen during loading is controlled by immersing the end of the stainless steel tube in a suitable temperature bath. In order to control the approximate rate of cooling or heating of the specimen when it is introduced to the bath, a brass cup to surround the end of the tube is provided. In practice, the Dewar flask containing the cryogenic fluid is raised around the cup at such a rate that the thermoelastic forces experienced by the specimen are negligibly small. When the temperature of the specimen has approached sufficiently that of the bath, the flask is raised further until the fluid spills over into the cup and actually comes into direct thermal contact with the specimen. This ensures that the specimen finally attains the temperature of the bath.

After the application of the load, the specimens are allowed to return slowly to room temperature and are removed from the press and reaffixed to the quartz crystal for the purpose of determining the increase in internal friction due to the application of the load. The results obtained seem to be independent of the time of duration of the stress for times greater than one second and less than one hour. No experiments were performed in which the duration of the stress was greater than one hour, and, in general, the duration of the stress was not greater than one minute. Since the recrystallization temperature of copper is about 200°C, the effect of any stress applied below this temperature is probably permanent. The increase in internal friction due to the stress may, therefore, be measured at leisure.

All the results reported in this paper were obtained from measurements on nine specimens. After the curve of increase in internal friction as a function of stress is obtained at one temperature, the specimens are subjected to another cycle of annealing and stressing to obtain similar data at another temperature.

Results

The base value of the decrement of the annealed specimens is approximately 2×10^{-3}. The increase of the decrement over the base value as a function of applied compressive stress is shown in Fig. 2, where the results obtained at 80°K are compared with those obtained at 298°K. The effect of decreasing the temperature is to increase the maximum in the internal friction and to displace it to somewhat higher stress values. In order to ascertain that the larger increase in internal friction observed at liquid-nitrogen

temperatures was not due to the existence of thermoelastic stresses, an annealed specimen was quenched directly in liquid nitrogen, removed and warmed to room temperature as rapidly as possible. This drastic treatment produced an increase of only 23 percent in the internal friction; a reasonable rate of cooling such as described above reduced the increase to 2 percent which is within the experimental error.

The average ratio of internal friction after applying a stress of 76.5 kg/cm² to the base value on nine annealed specimens was found to be at

80°K	2.06±0.08,	298°K	1.98±0.08,
193°K	2.02±0.06,	423°K	2.00±0.05.

An attempt to obtain data at temperatures above 200°C was unsuccessful. The data were quite irreproducible due, presumably, to the unpredictable effects of traversing the region of recrystallization. The fact that the data obtained at 150°C agree with those obtained at lower temperatures, however, tends to justify the procedure employed of affixing the specimen to the quartz at a temperature of 60°C.

The average velocity of longitudinal sound waves in the well-annealed specimens at 25°C is found to be 3.23×10^5 cm/sec. This value is considerably lower than that reported by Quimby,[10] who found the velocity of sound to be 3.65×10^5 cm/sec. This discrepancy might conceivably arise from two sources: first, the presence of impurities, although it is extremely doubtful that such a large difference can be explained in this manner; or, secondly, an anisotropic orientation of the crystallites. Annealing the specimens in oxygen produced no appreciable effect on the velocity of sound. In order to investigate more fully the second possibility, a specimen was severely cold-worked by hammering a cylinder into a parallelepiped. After annealing, the velocity of sound in this specimen evinced a normal value, namely 3.67×10^5 cm/sec. As a result of this test, it is concluded that the anomalously low values found for the velocity of sound in specimens employed in these experiments are due to a preferred orientation of the crystallites, arising, presumably, from a rolling or extruding operation used in their preparation.

[10] S. L. Quimby, Phys. Rev. **4**, 558 (1925).

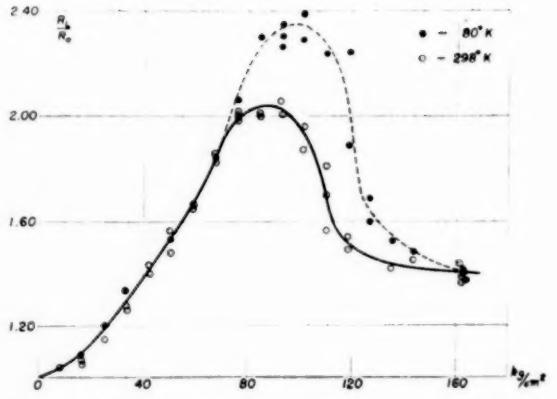

FIG. 2. The relative increase in internal friction as a function of compressive stress. The solid circles refer to data taken on specimens subjected to compression at 80°K. The open circles refer to data taken on specimens subjected to compression at 298°K.

The behavior of Young's modulus as a function of the applied stress is complementary to the behavior of the internal friction. Thus in several specimens investigated, Young's modulus decreases with increasing load until at the stresses which produced the maximum increase in internal friction, the value of Young's modulus reaches a minimum from 6 percent to 7 percent lower than the initial value. Application of still larger stresses then causes an increase in Young's modulus until after a stress of 162 kg cm² the value of the modulus is only from 4 percent to 5 percent lower than the initial value in well-annealed specimens.

The effect of oxygen impurity on the generation of dislocations was investigated in the following manner. The specimens were annealed in an atmosphere of air and then etched until a clean copper surface was exposed. The behavior of the internal friction in specimens prepared in this manner as a function of applied compressive stress differs from the behavior of specimens annealed in hydrogen in only one particular. The former specimens evinced a somewhat higher base value of internal friction in the annealed state and the maximum increase in internal friction was somewhat less than that observed in the hydrogen annealed specimens, and furthermore varied from specimen to specimen. The average maximum increase in internal friction in the oxygen annealed specimens was about 60 percent. The decrease in internal friction observed at high stresses was the same in all specimens and

equal to that observed in the specimens annealed in hydrogen.

Discussion

Errors in this experiment arise principally from two sources. The first of these is due to the effect of poor adhesion between the specimen and the quartz. Poor adhesion results in an anomalously high value of the decrement. The second source of error is mishandling of the specimen. Thus, when a specimen is dropped a quarter of an inch onto a hard surface, there is an increase in internal friction equivalent to the maximum increase in internal friction produced by the application of external static forces. Errors due to the first source may be corrected by reaffixing the specimen to the quartz crystal in any case in which the value observed for the decrement is suspiciously high. The only precaution which can be adopted to avoid errors from the second source is extreme care in the handling of the specimens to prevent any sudden jarring in their manipulation.

The initial increase in internal friction as a function of applied stress may be interpreted as due to the formation of dislocations which dissipate energy by virtue of irreversible work performed in moving them. The decrease in internal friction at higher stresses may be understood as due to the formation of a more stable array of dislocations. The term "locking" is introduced to describe this condition. Until a more concrete model of locking is proposed, no simple explanation of why more dislocations can be introduced into the lattice at low temperatures and why a higher stress is needed there to produce locking is justifiable until more data on creep at low temperatures is available.

It might be appropriate to mention at this juncture two further experiments, more or less qualitative in nature. A number of rocksalt crystals which had been standing in a desiccator over phosphorus pentoxide for over a year were subjected to a compressive stress of 25 kg/cm^2. The average observed increase in internal friction was about 10 percent. If the specimens were dipped in water for about 10 seconds just prior to or during the application of the stress, the average observed increase in internal friction was about 70 percent. The effect of a strong etch on the polycrystalline specimens of copper, however, was not detectable. This is not surprising in virtue of the fact that only a small part of the total crystal surfaces was exposed to the action of the etch. It is planned to repeat this experiment on single crystals of copper in the future.

In order to investigate the effect of the duration of the forces on the increase in internal friction for very small durations, the following crude experiment was performed. The specimens were rolled from a table top onto a cast iron plate whose height below the table top could be adjusted at various distances. It was found that the maximum increase in internal friction always occurred for distances of less than one inch but that the specimens had to fall about thirty inches before the decrease observed in the internal friction was comparable with that found in the experiments above. Inasmuch as the area of contact when the specimen struck the plate might vary considerably from experiment to experiment, no quantitative conclusions may be drawn. However, these results do suggest that while the formation of dislocations under the action of applied stress is practically instantaneous, duration as well as magnitude of load plays a role in the production of locked dislocations. Since, in some of the specimens which were dropped, increases in internal friction as much as fifty percent greater than any increase under static loads were observed, these experiments suggest that the higher maximum in internal friction and the shift of this maximum to higher stresses at low temperatures are due to a less rapid formation of locked dislocations at low temperatures than at high temperatures for a given stress. More experiments on the effect of rate of loading are being undertaken in an effort to settle this point.

In conclusion, the author desires to express his appreciation to the participants in the Works Progress Administration Project O.P. 65-1-23-2884 for much routine assistance, and to Professor Frederick Seitz and his colleagues Dr. Hillard Huntington and Dr. James Koehler for several stimulating discussions concerning the theoretical aspects of the problem.

Absolute Saturation Magnetization of Nickel-Antimony and Nickel-Tantalum Alloys

G. T. RADO AND A. R. KAUFMANN
Massachusetts Institute of Technology, Cambridge, Massachusetts

(Received June 18, 1941)

The absolute saturation magnetic moment per atom (M) was measured as a function of the atomic composition (τ) for nickel-antimony and nickel-tantalum solid solutions. Fields up to 40,000 gauss and temperatures down to 77.2°K were used. The initial slope $dM/d\tau$ was found to be -3.6 and -5.7 Bohr magnetons per substituted atom for Ni-Sb and Ni-Ta, respectively. The disagreement between the former result and the data of Sadron and of Marian is discussed in conjunction with "superposed paramagnetism." A complete summary of previous data on ferromagnetic binary alloys shows the present results to be additional exceptions to a surprisingly large range of applicability of the energy band theory. The "anomalous" behavior of the iron alloys is briefly discussed.

INTRODUCTION

THE intrinsic magnetic moment per atom of a ferromagnetic substance is determined experimentally by measuring the extrapolated value of the saturation magnetization at 0°K. Such measurements are of considerable theoretical interest. They supply information on the field-free distribution of the electrons and their spins in the *3d* and *4s* energy bands of a metal, thus contributing data to the theory of metallic structure as well as to that of ferromagnetism.

Most of the previous work was done at the University of Strasbourg, where the absolute saturation moments were studied as a function of the atomic composition for a great number of binary alloys of iron, cobalt and nickel. Many of the results were explained by Slater[1] on the basis of his energy band theory, while some of the others suggest relations which may also have theoretical significance. These are apparent from Figs. 3, 4 and 5 of the present paper, where the available data are summarized in a form which seems most amenable to theoretical discussions.

Further experiments are necessary in order to clarify and completely interpret the relations mentioned. As a first step toward this aim, additional measurements on nickel alloys appear to be most promising. The systems nickel-antimony and nickel-tantalum have been chosen for this investigation. The latter system offers a wide range of solubility of Ta in Ni and has not been previously studied, whereas the accuracy of the results available on Ni-Sb suggested a repetition of the measurements. It is to be noted that the "added elements" Sb and Ta are in the same column of the periodic system.

[1] J. C. Slater, Phys. Rev. **49**, 537, 931 (1936).

PREPARATION OF SPECIMENS

Five alloys of each system were prepared, ranging in composition up to an atomic fraction (τ) of about 7 percent for the added element. The maximum impurities of the nickel* and antimony* were 0.135 percent and 0.045 percent, respectively, while the purity of the tantalum† metal was 99.9+ percent. The alloys were melted in a hydrogen atmosphere and then cast in vacuum. No evaporation of the Sb was noticed and the Ta dissolved readily in Ni. A hydrogen atmosphere was used for anneals of suitable duration, the temperature being 900°C for the Ni-Sb and 1170°C for the Ni-Ta. It is believed[2] that no hydrogen compounds were formed and that no appreciable amount of hydrogen was adsorbed. Microscopic examination showed the alloys to be homogeneous solid solutions, as found by Therkelsen[3] for Ni-Ta and by Marian[4] for Ni-Sb. The specimens were prepared in the form of small spheres (1/16 of an inch in diameter) and the adjacent parts of the alloys chemically analyzed.

* Obtained from the Mallinckrodt Chemical Works.
† Kindly donated by the Fansteel Metallurgical Corporation.
[2] J. N. Friend, *A Textbook of Inorganic Chemistry* (Griffin and Company, London) Vol. VI, part V (1936) and Vol. VI, part III (1929).
[3] E. Therkelsen, Metals and Alloys **4**, 105 (1933).
[4] V. Marian, Ann. de physique **7**, 459 (1937).

Method of Measurement

The measurements of the magnetization were made with a Bitter type high field solenoid (magnet No. 1 of the M. I. T. magnet laboratory),[5] by using a nonhomogeneous field method (Curie) similar to that described by Bitter and Kaufmann.[6] The specimens fitted closely into a glass tube which was suspended by a silk thread from one arm of an analytical balance. A slight correction was applied for the weak paramagnetism of the holder. By using a position about $\frac{1}{3}$ of an inch from the center of the magnet, the lateral stability of the specimen was satisfactory even in the case of pure nickel. This arrangement permitted fields up to 40,000 gauss, which was sufficient to saturate every alloy. The sensitivity of the apparatus, however, was limited by the vertical restoring forces due to the fast change of the field gradient along the axis of the magnet. It was found convenient to redetermine the position of the specimen for each measurement by locating the center of the magnet, where the gradient and hence the force is zero, and then raising the specimen a fixed distance.

The method of determining the saturation at a given temperature seems worth mentioning because alloys of decreasing nickel content

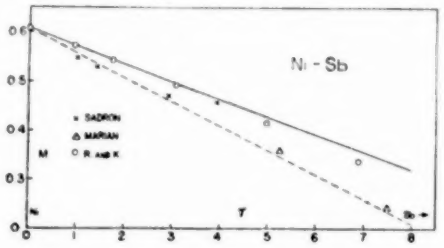

FIG. 1. The absolute saturation moment per atom in Bohr magnetons as a function of the atomic composition in percent for Ni-Sb alloys.

showed a "superposed paramagnetism" at higher temperatures, in general agreement with the Strasbourg results. On account of the high field strengths, no "law of approach" had to be used and, as shown in the following, even the calculation of the demagnetizing field could be omitted.

The force on a specimen is given by

$$F=\sigma m(dH/dx),$$

from which one obtains the magnetic moment per unit mass σ, if the mass m and the field gradient dH/dx are known. In these experiments, the gradient was determined by measuring the absolute saturation moment per atom (M) of pure nickel and assuming it to be 0.607 Bohr magnetons (μ_B). For pure nickel and some of the alloys, complete saturation within the experimental error could be reached. For other alloys, however, the magnetization curve at high fields was a slightly inclined straight line instead of being horizontal. In these cases we can let $\sigma=\sigma_s+xH_i$, where σ_s is the value of the "ferromagnetic component" of σ in an infinite field,‡ x is the paramagnetic susceptibility after normal saturation and $H_i=H-D\rho\sigma$ is the internal field, containing the density ρ and the demagnetization coefficient D. A combination of these equations gives

$$\sigma(1+xD\rho)=\sigma_s+xH,$$

which shows that if $xD\rho$ can be neglected in comparison to unity, then σ is a linear function of the external field with an intercept equal to the saturation. By using an approximate value of H and $D=4\pi/3$ (sphere), it was found that the numerical value of $xD\rho$ never exceeded 0.003, which made it possible to determine the saturation by extrapolating σ to zero magnet current, a quantity proportional to H.

By means of a Dewar flask which fitted in the magnet, measurements were made at 77.2°K (boiling N_2) and at 194.5°K (solid CO_2), in addition to room temperature (290°K). Curves of the saturation *versus* T^2 were sufficiently linear to allow the absolute saturation to be determined by extrapolation to 0°K. The accuracy of the measurements was not sufficient to decide whether a "$T^{\frac{1}{2}}$ law" would be better obeyed.

Results

The results of the measurements are shown in Figs. 1 and 2 and in Table I, where M is the absolute saturation moment per atom in Bohr magnetons (μ_B) and τ the atomic composition in percent. As was expected from the results of similar measurements, the experimental points

[5] F. Bitter, Rev. Sci. Inst. **10**, 373 (1939).
[6] F. Bitter and A. R. Kaufmann, Phys. Rev. **56**, 1044 (1939).

‡ σ_s may be regarded as the value of σ for a domain in zero field.

are in an excellent straight line for small values of τ, up to about $\tau=4$ percent. The slope of this initial portion of the curves is shown by the full lines and has a value of -3.6 and $-5.7\mu_B$ per substituted atom for Ni-Sb and Ni-Ta, respectively.

It is difficult to estimate the accuracy of these slopes but they are believed to be correct to better than 8 percent. The results for pure nickel and for the first alloy in each system are accurate to about 2 percent, but the error for the least magnetic alloy at room temperature may be as much as 10 percent. Only nickel and the first three alloys were used for the determination of the slope in each system. The principal sources of systematic error were as follows: (1) change of position of the specimen in the field, (2) diminished sensitivity due to restoring forces, as explained above, (3) uncertainty in the temperature extrapolations and (4) small forces in the case of weakly magnetic specimens.

The results on Ni-Sb alloys are seen to disagree with those of Sadron[7] and Marian.[4] It seems likely that Sadron's alloys were not completely saturated in the fields at his disposal because his values for the room temperature susceptibility after normal saturation are unusually high. This quantity increases with τ and he obtains 17.8×10^{-5} cm^3 g^{-1} at $\tau=3.94$ percent, as compared to our value of only about 6.0×10^{-5} at the larger fraction of 6.89 percent. The latter result is of the same order as the 8.3×10^{-5} found at $\tau=6.25$ percent for Ni-Ta alloys at room temperature.

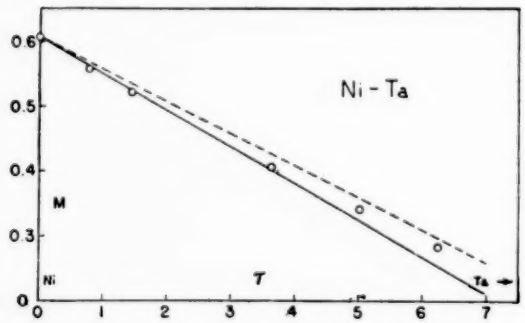

FIG. 2. The absolute saturation moment per atom in Bohr magnetons as a function of the atomic composition in percent for Ni-Ta alloys.

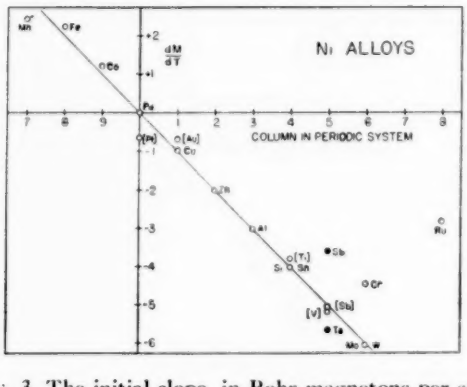

FIG. 3. The initial slope, in Bohr magnetons per substituted atom, of the absolute saturation *versus* composition curves for alloys of nickel.

TABLE I. *Values of the absolute saturation moment per atom for* Ni-Sb *and* Ni-Ta *alloys.*

Ni-Sb		Ni-Ta	
τ IN %	M IN μ_B	τ IN %	M IN μ_B
0.964	0.57	0.786	0.56
1.76	0.54	1.45	0.52
3.08	0.49	3.64	0.41
4.98	0.42	5.03	0.34
6.89	0.34	6.25	0.28

The initial slope $dM/d\tau$ measures essentially the rate at which the more loosely bound electrons of the added element fill up the holes in the *3d* band of nickel. On the basis of the work of Slater[1] it appears plausible, but by no means necessary, that this slope should be numerically equal to the number of valence electrons of the added element. This is borne out by the results of previous experiments (Fig. 3). It is seen that many elements, including some members of the transition series and even aluminum, do fit into this relation, while others, like chromium, do not. For this reason, the discrepancy between our measured slope values and the "theoretical" value of $-5\mu_B$ per substituted atom (dashed lines in Figs. 1 and 2) does not conflict with theory, but shows that a full explanation of the experimental results requires better approximations than those used for simple alloys like Ni-Cu and Ni-Zn.

PREVIOUS RESULTS AND DISCUSSION

It was pointed out by Stoner[8] that the initial slope $dM/d\tau$ of an M *versus* τ curve is more

[7] C. Sadron, Ann. de physique **17**, 371 (1932).
[8] E. C. Stoner, *Magnetism and Matter* (Methuen and Company, London, 1934), pp. 531–541.

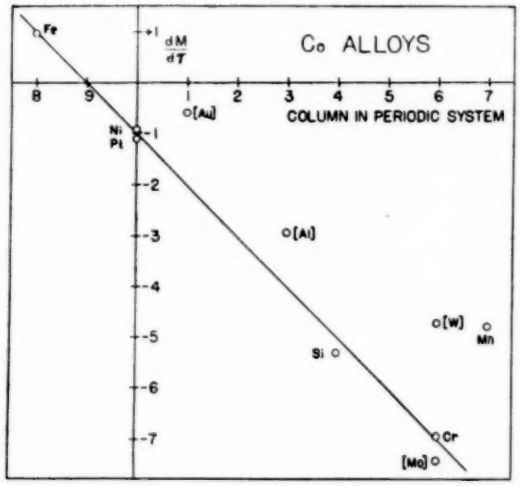

FIG. 4. The initial slope, in Bohr magnetons per substituted atom, of the absolute saturation *versus* composition curves for alloys of cobalt.

significant than the values of M over the whole composition range, because for a small concentration of the added atoms the change in the lattice dimensions of the solvent is minimized and complications due to limited solubility and changes of phase are eliminated. For these reasons, we have summarized the previous experimental results by plotting the values of this initial slope (in μ_B per substituted atom) for all the Ni, Co and Fe alloys (Figs. 3, 4 and 5) for which data could be found in the literature. Relatively uncertain measurements are indicated by brackets and the abscissae represent the number of valence electrons of the added element. The straight 45° lines in the figures have no fundamental significance. They show where the experimental points would lie if the number of valence electrons would determine the value of $dM/d\tau$ in a way similar to the ideal case of Ni-Cu.[1]

Elements alloyed with nickel include Al,[7,4] Si,[4] Ti,[4] V,[7,4] Cr,[7] Mn,[7] Fe,[9] Co,[10] Cu,[11] Zn,[7,4] Mo,[7,4] Ru,[7] Pd,[7] Sn,[7,4] Sb,[7,4] W,[7,4] Pt,[4] and Au.[4] Figure 3 shows that the "theoretical" relation is surprisingly well obeyed, a fact which makes the present results (full circles; Ni-Sb and Ni-Ta have different slopes) difficult to interpret.

[9] Peschard, Thesis, Strasbourg, 1925. See R. Forrer, J. de phys. et rad. **1**, 325 (1930) for quotations of Peschard's results.

[10] P. Weiss and R. Forrer, Ann. de physique **12**, 279 (1929).

[11] M. Alder, Thesis, Zurich, 1916.

Elements alloyed with cobalt include Al,[12] Si,[7] Cr,[12] Mn,[7] Fe,[10] Ni,[10] Mo,[12] W,[12] Pt,[7] and Au.[7] On account of experimental difficulties, due mainly to the magnetic hardness of cobalt alloys, the data of Fig. 4 are less accurate than those of Fig. 3.

Elements alloyed with iron include Al,[13] Si,[13] V,[13] Cr,[13] Mn,[7] Co,[10] Ni,[9] Zn,[14] Ru,[15] Rh,[15] Pd,[15] Sn,[13] Os,[15] Ir,[15] Pt,[15] and Au.[13] Figure 5 shows that a number of alloys have an initial slope of $-2.2\mu_B$ per substituted atom. This might partly be caused by the fact that iron is believed to have holes in the plus *and* minus spin bands of the 3*d* shell. It might also be interpreted as meaning that the loosely bound electrons of elements like Al, V, Cr, Sn and Au do not go into the 3*d* band of iron, as the following argument shows. Let M_F be the absolute saturation moment of the alloy per atom of the ferromagnetic element, and M, as before, the same quantity per atom of alloy. Then $M=M_F(1-\tau)$, which gives, at $\tau=0$, $dM_F/d\tau=dM/d\tau+M_F$. For pure iron, $M_F=2.2\mu_B$ and hence $dM_F/d\tau$ is zero for the alloys mentioned. This means that the absolute saturation moment per iron atom does not change after alloying, so that these particular elements simply dilute the iron without filling up* the holes in its 3*d* band. If data on

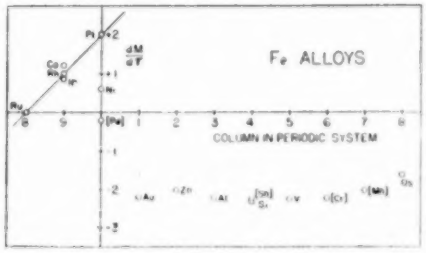

FIG. 5. The initial slope, in Bohr magnetons per substituted atom, of the absolute saturation *versus* composition curves for alloys of iron.

the soft x-ray emission spectra of these alloys were available, the above interpretation might be compared with the approximate band forms.

We thank Professor F. Bitter for suggesting the problem and Professor J. C. Slater for discussions.

[12] T. Farkas, Ann. de physique **8**, 146 (1937).

[13] M. Fallot, Thesis, Strasbourg, 1935.

[14] M. Fallot, Ann. de physique **7**, 420 (1937).

[15] M. Fallot, Ann. de physique **10**, 291 (1938).

* Or without "unevenly" filling up the holes corresponding to the two signs of spin.

Gamma-Rays from Sodium Bombarded by Protons

R. L. BURLING
University of Wisconsin, Madison, Wisconsin

(Received June 19, 1941)

The intensity of the γ-radiation emitted by sodium under proton bombardment has been studied as a function of the energy of the bombarding protons up to 1.9 Mev. Protons were accelerated by a 2-Mv pressure-insulated electrostatic generator, and were incident on a thin evaporated film of metallic sodium. The γ-ray intensities were measured by means of the counts produced by recoil electrons entering a single glass Geiger-Müller counter which actuated a scale-of-16 and mechanical recorder. Generator voltages were measured by a generating voltmeter, which was calibrated by means of the 0.862-Mev resonance in the $F(p, \gamma)$ reaction. The yield curve shows 21 well-defined resonances, whose half-widths (with one exception) are probably experimental.

INTRODUCTION

THE intensity of the γ-radiation emitted by sodium under proton bombardment has been studied as a function of the energy of the bombarding protons by Herb, Kerst, and McKibben;[1] Gentner;[2] and Curran and Strothers.[3] From Barkas' values of the atomic masses,[4] the only known proton reactions that are energetically possible (for incident protons of less than 2-Mev energy) are the radiative capture

$$Na^{23}(p, \gamma)Mg^{24},$$

in which 11 Mev are liberated, and the (p, α) reaction, in which the available energy is 1.4 Mev. That the (p, γ) reaction is responsible for the observed radiation is shown by the fact that measurements by Curran and Strothers,[3] of the absorption of the recoil electrons, indicate a quantum energy of the order of 10 Mev, which is several times as great as the energy that could be liberated in the (p, α) reaction.

The present paper is a more detailed study of the yield of γ-rays from a thin target of metallic sodium as a function of the proton energy, and covers the range of energies up to 1.9 Mev.

APPARATUS

Protons were accelerated by a two-million-volt pressure-insulated electrostatic generator.[5] The voltage was measured by means of a generating voltmeter of the type described by Parkinson, Herb, Bernet, and McKibben.[6] This was calibrated against the 0.862-Mev resonance in the $F^{19}(p, \gamma)$ reaction by using as a target a thick calcium fluoride crystal covered by nickel gauze.[7] The voltage of the fluorine resonance depends, in turn, upon that of the 0.440-Mev resonance in the lithium (p, γ) reaction measured by Hafstad, Heydenburg, and Tuve.[8]

The arrangement of the target chamber and recording counter is shown in Fig. 1. Protons, separated from molecular and other ions by a magnetic analyzer, enter the target chamber through a $\frac{7}{32}$-inch defining aperture in a tantalum sheet (A). The $\frac{1}{8}$-inch thick copper strip T, which served to cool the target by conduction, was faced on both sides with tantalum (used because of its low γ-ray yield under proton bombardment), and could be rotated through a ground brass joint. One of these faces was coated with a thin film of metallic sodium by evaporation from the Nichrome wire W, and the other was used to check background counting rate. During the preparation of an evaporated sodium film, the target was rotated into a horizontal position above the wire W.

Recoil electrons produced in the aluminum top of the target chamber by the γ-radiation, were recorded by means of the single glass

[1] Herb, Kerst, and McKibben, Phys. Rev. **51**, 691 (1937).
[2] W. Gentner, Zeits. f. Physik **107**, 354 (1937).
[3] S. C. Curran and J. E. Strothers, Proc. Roy. Soc. **A172**, 72 (1939).
[4] W. H. Barkas, Phys. Rev. **55**, 696 (1939).
[5] The generator is to be described in connection with some test work done with it. J. L. McKibben and R. L. Burling in a forthcoming issue of Rev. Sci. Inst.
[6] Parkinson, Herb, Bernet, and McKibben, Phys. Rev. **53**, 642 (1938).
[7] Bernet, Herb, and Parkinson, Phys. Rev. **54**, 398 (1938).
[8] Hafstad, Heydenburg, and Tuve, Phys. Rev. **50**, 504 (1936).

Geiger-Müller counter C, which actuated a scale-of-16 circuit and mechanical recorder. The proton current entering the target chamber was measured by means of the current integrator described by Herb, Kerst, and McKibben.[1] The entry of secondary electrons into the target chamber was prevented by applying a potential of minus 45 volts to it; and the escape of secondaries was prevented by the fact that the solid angle subtended by the opening of the chamber at the target was very small.

Results

The γ-ray yield curves obtained for sodium are shown in Fig. 2 in which γ-ray intensities are plotted against the energy of the incident protons. The abscissas are proton energies in Mev, and have been corrected for the energy imparted by the probe which draws the ions out of the arc source. The ordinates are γ-ray yields in arbitrary units. For curves A, B, and C, the ordinates are the numbers of counts produced in the Geiger-Müller counter for every 2×10^{14} protons incident on the target. In Curve A, which was taken with a single thin film, the ordinate is the actual number of counts recorded at each point, so that it may be used to estimate the probable statistical errors in the data. In curves B and C the actual number of counts recorded at any point was 1, 2, or 5 times as great as the ordinate of the point, the total number of incident protons having been increased for these points. Curve B was taken with two films, each only slightly thicker than that used for curve A, but is less accurate statistically because of the low yield in the low voltage region. Curve C is for a film of about the same thickness as that used for curve A, and is given merely to demonstrate the reproducibility of the data in curve A.

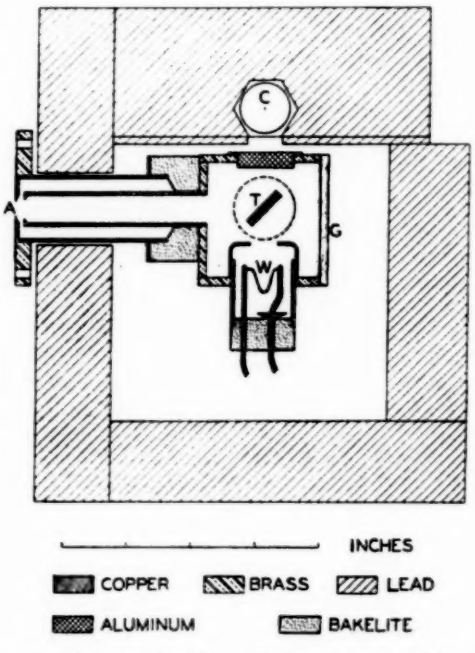

FIG. 1. Target chamber. Protons enter the target chamber through the $\frac{3}{32}''$ defining aperture A. Sodium is evaporated onto the tantalum-faced copper target T from the wire W. γ-rays are detected by the Geiger-Müller counter C. G is a glass window.

Curve D is for two films, each several times as thick as the films used for the other curves, and shows for this reason wide peaks shifted fifteen or twenty kev toward higher voltage relative to the curves taken with thinner targets. Its ordinates bear no relation to those of curves A, B, and C, since curve D was taken with a different geometrical arrangement of the Geiger-Müller counting tube (as in Fig. 2 of reference 9). For the portion of curve D above 1.1 Mev, the ordinates are actual numbers of counts, but for lower voltages, six times as much proton current was incident on the target, so that the ordinates must be multiplied by six to give the actual number of counts from which the probable statistical errors may be determined.

It was not necessary to extend the thin film data below 0.3 Mev, since a thick target yield curve showed (in agreement with the results of Gentner[2]) a sharp threshold at this energy, thus indicating that there could be no resonances of measurable intensity below this value.

With the same scale as was used for curve A, the yield of γ-radiation from a thick target of sheet Nichrome was 1600 at 1.65 Mev; or only 400 greater than the background yield from a tantalum target. Hence none of the observed resonances could have been due to a contamination from the Nichrome wire from which the sodium was evaporated.

The yield curves show twenty-one well-defined resonances, the approximate voltages of the peaks, listed in order of decreasing intensity,

[9] Plain, Herb, Hudson, and Warren, Phys. Rev. **57**, 187 (1940).

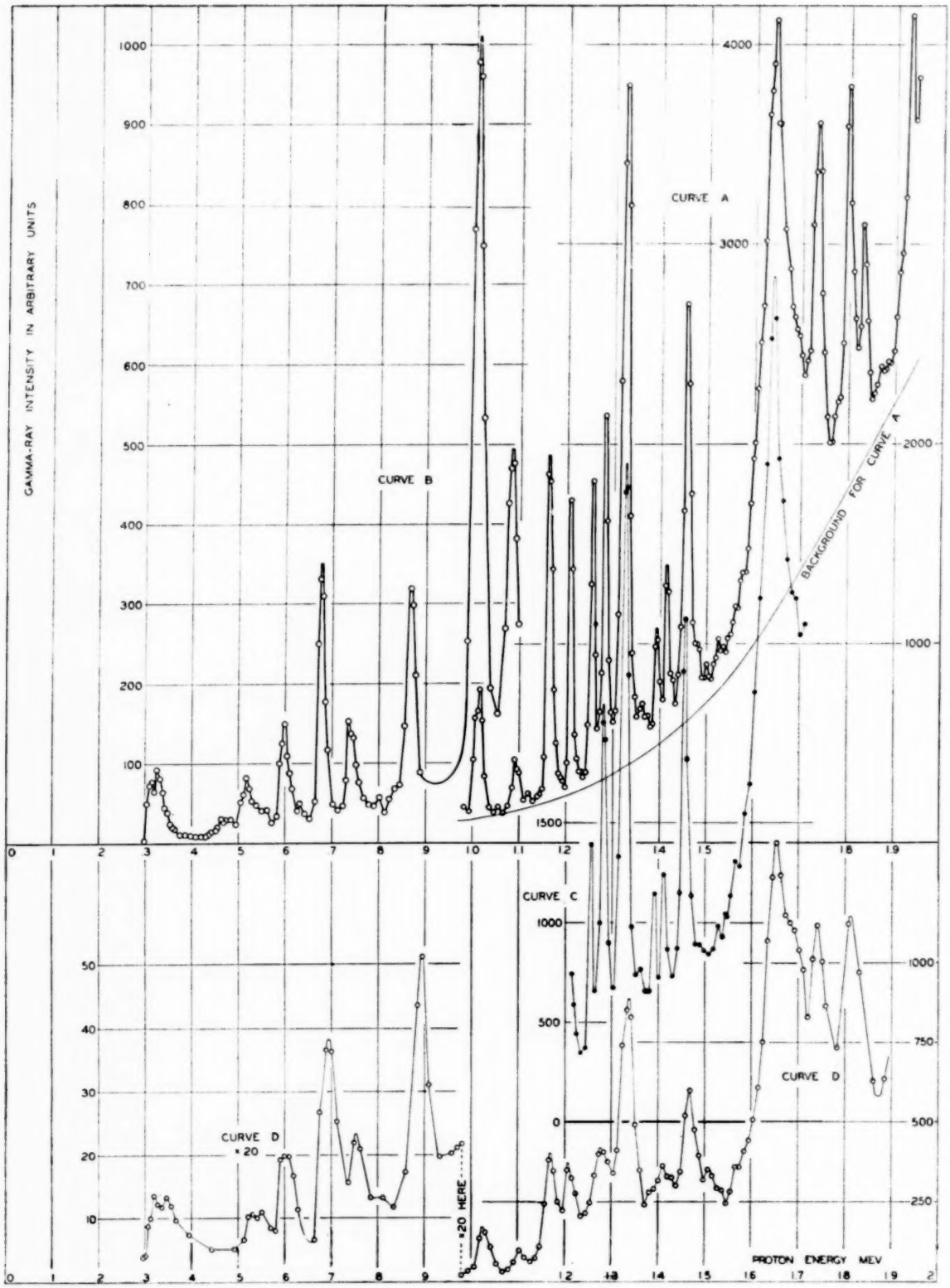

FIG. 2. Yield of γ-radiation from sodium as a function of the energy of the incident protons. Curves *A* and *B*: thin film data using three different target films. Curve *C*: comparison run with a different film to demonstrate reproducibility. Curve *D*: Thicker film.

being: 1.324, 1.638, 1.454, 1.795, 1.732, 1.93, 1.159, 1.281, 1.255, 1.206, 1.829, 1.412, 1.006, 1.392, 1.08, 0.576, 0.867, 0.735, 0.598, 0.31, and 0.515 Mev. These energies are in million electron volts, and have not been corrected for target thickness, so do not represent actual resonance energies. The peak at 0.31 Mev is due to a resonance reported by Gentner,[2] in whose work the resonance is more sharply defined. The resonances between 0.4 and 0.9 Mev have all been reported by Curran and Strothers,[3] although their work does not appear to resolve them as clearly as does curve *B*.

The half-widths of the resonance peaks (with the exception of that at 1.638 Mev) vary from 10 to 25 kev, and are to be regarded as largely experimental, since: (1) the generator voltage fluctuated by 5 or 10 kilovolts during any single observation; (2) there was a spread of energy in the proton beam due to ionization in the probe canal of the ion source and in the accelerating tube; and (3) no corrections have been applied for target thickness. However, the 1.638-Mev resonance has an observed half-width of 70 kev, so that it must be due either to a wide level, or to an unresolved group of closely spaced levels.

ACKNOWLEDGMENTS

The author wishes to express his indebtedness to Dr. R. G. Herb, under whose direction this work was done; to Dr. J. L. McKibben for assistance with the generator; and to the Wisconsin Alumni Research Foundation for financial support.

AUGUST 15, 1941 PHYSICAL REVIEW VOLUME 60

The Paschen-Back Effect

VIII. The Reality of the Distant Components

J. B. GREEN
Mendenhall Laboratory of Physics, Ohio State University, Columbus, Ohio
(Received June 23, 1941)

The helium line λ7066 has been investigated in order to show that the distant components, whose predicted intensities are extremely small, really do exist. Agreement between theory and experiment, as regards both position and intensities of these components, is excellent.

IN all elementary discussions of the Paschen-Back effect, we find statements to the effect that in very strong fields, the Zeeman pattern of a multiplet degenerates into a normal triplet. A more careful analysis of the problem shows, however, that the perpendicular components of this triplet should show structure, each of the lines consisting of a number of components equal to the multiplicity involved in the transition, when we are dealing with *LS* coupling. The reality of this structure has been shown in an earlier communication[1] and by Jacquinot.[2] But in addition to this so-called "normal" triplet, there should also be some components of twice the normal distance (for doublet spectra) and also at three times the normal distance (for triplet spectra). These far distant components have never been separated[3] and it is the purpose of this paper to complete the record. It may be shown quite simply that the most distant component is $\Delta\nu_{\text{norm}}\times$the multiplicity $(2S+1)$ if the full multiplicity of one of the groups of L levels has been reached. We must find the largest value of $(m_S+2m_L)-(m_S'+2m_L')$ subject to the condition that $(m_S+m_L)=(m_S'+m_L')\pm 1$ for the perpendicular components. This will obviously be

[1] J. B. Green and R. A. Loring, Phys. Rev. **49**, 630 (1936).
[2] P. Jacquinot, *Verh. Zeeman* (Amsterdam, 1935).
[3] Paschen and Back report weak components in the oxygen triplet, but this is really a quintet spectrum and should have more distant components.

$m_S - m_S' \pm 1$ and since the largest value of m_S is S and the smallest value of m_S' is $-S$, the largest value of $m_S - m_S' \pm 1$ is $2S+1$. If, however, neither of the levels has reached full multiplicity, then the values of m_S and m_S' for given $m = m_S + m_L$ and $m' = m \pm 1 = m_S' + m_L'$ may not have the full run from $+S$ to $-S$. If, for a given m' the values of m_S run from S to $S-2L$ (L being the larger L), then for the neighboring $m = m'-1$, m_S will run from $S-2$ to $S-2L$ and the largest value of $m_S - m_S' \pm 1$ is $2L+1$. For $m = m'+1$, m_S will run from S to $S-2L+2$, and again the largest value of $m_S - m_S' \pm 1$ is $2L+1$.

In a previous communication[4] the Paschen-Back[5] effect of the triplet spectrum of Be was studied to investigate the effect of the spin-spin interaction. It was not pointed out at the time that in the case of LS coupling, the only effect of the magnetic field would be the terms due to $(SLJM|L_z+2S_z|SL'J'M')$, the spin-spin terms affecting only the zero positions of the diagonal elements. This, indeed, is what was assumed in the earlier paper without any justification other than the pragmatic one that agreement existed between theory and experiment.

In our recent work on the rare gases, very intense sources have been produced and it was found possible to extend our investigations to determining whether these predicted distant components really existed. These lines should be extremely faint lines, and unless a very intense source is available, the inertia of the photographic plate would render their observation well-nigh impossible. The strong helium line at λ7066 was chosen and photographed on Eastman IN plates. Certainly, if for any spectrum, the assumption of LS coupling holds for He, since no interior combination lines between singlet and triplet levels are known to exist. Figure 1 shows the microphotogram and the calculated results for the above-mentioned line and the agreement between theory and experiment for the positions of the expected lines is excellent. The figure is the result of a 120-hour exposure, which was necessary in order to bring out the weak outside components to a sufficient density that they might be recorded against the very dense background of the stronger components. Such a great difference in intensity existed between the strong and weak components that it was thought advisable to indicate the logarithm of the intensity by the length of the line, and a difference in length of one centimeter is equivalent to a factor of 100. The polarizations were not separated, and hence the weaker parallel components (indicated by dashed lines) are lost in the background. But the weak perpendicular distant components are clearly evident and with the predicted intensity ratios. The great deal of overexposure required to make these components recordable is shown by the considerable fog density in their neighborhood. The ghosts on either side of the main line at the edges of the figure are approximately the correct density for good recording.

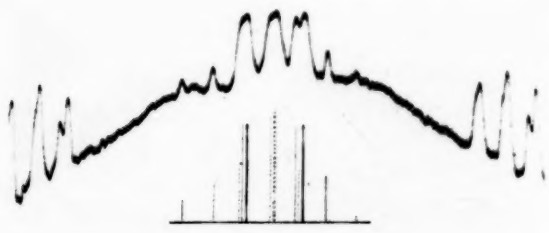

FIG. 1. The Paschen-Back effect of the helium line λ7066.

The attention of the reader is called to the fact that even at this high field strength, there is still considerable asymmetry in the spacing of the components. It is unfortunate that the low atomic number of He and the rather high temperature which probably existed in the discharge has precluded the possibility of resolving the triplet structure of the closest perpendicular components. However, the existence of the components at $3\Delta\nu_{\text{norm}}$ indicate that the levels involved have a multiplicity of at least 3, as indicated in the discussion.

[4] J. B. Green and R. A. Loring, Phys. Rev. **49**, 632 (1936).
[5] Paschen and Back, Ann. d. Physik **39**, 897 (1912).

The Velocities of Electrons in Hydrocarbon Bonds

A. L. HUGHES AND T. ENNS
Wayman Crow Laboratory of Physics, Washington University, St. Louis, Missouri

(Received June 19, 1941)

Fast electrons when scattered inelastically by gas molecules furnish information as to the *distribution of component velocities* (and therefore as to the distribution of resultant velocities) among the electrons in the molecules. An experimental determination of the distribution of energies among the electrons scattered inelastically from a beam of 8000-volt electrons by acetylene, ethylene, ethane, and methane has been made. The results give information as to the velocities of the bonding electrons, but not the K electrons of the carbon atoms. It is found that the distribution curves are substantially the same for acetylene and ethylene. The same statement applies also to ethane and methane. The curves for the distribution of component velocities for the first two gases lie above the corresponding curves for the last two gases. A convenient parameter to summarize the results is the value of the component velocity at "half maximum," which is closely analogous to the half width of a spectrum line. The values of the component electron velocities at half maximum for C_2H_2, C_2H_4, C_2H_6, and CH_4 are, respectively, 29.7, 29.7, 26.7 and 26.7, multiplied by 10^7, cm/sec. A short discussion is given of the bearing of these results on the various types of bonds in the molecules investigated.

INTRODUCTION

WHEN conditions are properly chosen, it is possible to use the results of experiments on electron scattering by gases to determine the distribution of velocities of the electrons in the molecules of the scattering gas. Results have been obtained for helium,[1] hydrogen,[2] nitrogen and methane.[3] In the case of helium and hydrogen the results agreed remarkably well with those obtained by DuMond and Kirkpatrick.[4] As these authors obtained their results from a study of the profile of the modified band in the Compton effect, which is a totally different approach from that involving electron scattering, one may have considerable confidence in the experimental results, for it is difficult to believe that the same type of error could occur in the two methods. No Compton effect results are available for nitrogen and methane, but since the electron scattering experiments were carried out in precisely the same manner with these two gases as with hydrogen and helium, it may be assumed that the results obtained are equally accurate. For helium, the experimental results for the atomic electron velocity distribution agreed very well with the theoretical calculations of Hicks, but the agreement was less satisfactory in the case of hydrogen.[5] No theoretical calculations have been made for the other gases.

In this paper we give an account of an investigation of the distribution of electron velocities in the molecules of methane, ethane, ethylene, and acetylene. The electrons involved are those in the carbon-hydrogen and the carbon-carbon bonds. The conditions were such that the electron energies were not high enough to tell us anything about the K electrons in carbon. The distance between the atoms in a molecule has been investigated very extensively during the last decade. The equally fundamental parameter, the distribution of the velocities or momenta of the electrons in the various bonds, has received very little attention in comparison. Except for the experimental investigations on hydrogen, nitrogen, and methane already referred to[2,3] and the theoretical discussions of Hicks on hydrogen and hydrocarbons[5,6] and those of Coulson[7] and Duncanson[8] on hydrocarbons, the field is untouched. It seemed therefore desirable to make an experimental study of the distribution of ve-

[1] A. L. Hughes and M. M. Mann, Jr., Phys. Rev. **53**, 50 (1938).
[2] A. L. Hughes and M. A. Starr, Phys. Rev. **54**, 189 (1938).
[3] A. L. Hughes and M. A. Starr, Phys. Rev. **55**, 343 (1939).
[4] J. W. M. DuMond and H. A. Kirkpatrick, Phys. Rev. **52**, 419 (1937); **54**, 802 (1938).
[5] B. L. Hicks, Phys. Rev. **52**, 436 (1937).
[6] B. L. Hicks, Phys. Rev. **57**, 665 (1940).
[7] C. A. Coulson, Proc. Camb. Phil. Soc. **57**, 55 (1941); **57**, 74 (1941).
[8] C. A. Coulson and W. E. Duncanson, Proc. Camb. Phil. Soc. **57**, 67 (1941).

locities among the bonding electrons in methane, ethane, ethylene, and acetylene in the hope that some light would be thrown on the momentum characteristics of the various bonds in these hydrocarbons.

METHOD

As a full discussion of the principles used in deriving the distribution of velocities among atomic electrons was given in an earlier paper,[1] only a summary will be given here. When an electron of energy 200 volts or less is scattered by an atom, the atom as a whole is involved. But if the energy be increased to a sufficiently high value, 2000 volts or more for hydrogen and helium and for the outer electrons of heavier atoms, the scattering observed at considerable angles is essentially due to the interaction of the incoming electrons with just one scattering center which may be either the nucleus or any one of the atomic electrons in the molecule. The scattering observed is to be thought of as Rutherford scattering by a center which attracts, or repels, the incoming electron with a force varying inversely as the square of the distance between the electron and the center. The "collision parameter," i.e., the distance between the scattering center and the prolongation of the path along which the incoming electron travels, determines the angle of scattering. For electrons of sufficiently high energy the collision parameter is so much smaller than the dimensions of the atom that we may safely ascribe any observed scattering to one and only one scattering center. The chances of the incoming electron passing sufficiently near to *two* scattering centers within an atom so that both contribute finite deflections are small enough to be neglected. Cases can arise in which the energy of the incoming electron is high enough to permit us to regard interaction between the incoming electron and the outer atomic or molecular electrons as "single center" scattering, but in which the energy is not high enough to treat the effects of the K electrons and the nucleus as separable. This in fact is the case in the experiments to be described in this paper.

When the electrons interact with nuclei they are deflected with no loss of energy; they are scattered elastically. When they interact with electrons in the atom or molecule they lose

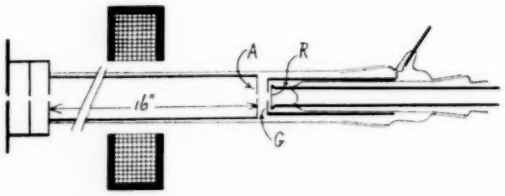

FIG. 1. The electron gun with magnetic focusing.

energy; they are scattered inelastically. The energy which an electron of initial energy V_0 retains after deflection by an atomic electron through an angle θ is $V = V_0 \cos^2\theta$. Thus there will be two distinct groups of electrons among those scattered through a certain angle, those scattered elastically and those scattered inelastically. The relation $V = V_0 \cos^2\theta$ is true only if the atomic electron is at rest before the collision. Actually it is in motion, and the energy with which an electron comes away from a collision in a direction θ differs from V by an amount V''' which is a function of the velocity and direction of motion of the atomic electron before the collision occurred. What we measure experimentally is the distribution of energies, $f(V'')$, among the electrons scattered through a selected angle θ. By means of a very important relationship first pointed out by Jauncey,[9] it turns out that $f(u)$, the distribution of *component velocities* among the electrons in the atom or molecule, has precisely the same shape as $F(V'')$, the distribution of *energies* among the electrons scattered at a selected angle. V''' is the difference between the actual value of the energy of the scattered electron and the value, $V = V_0 \cos^2\theta$, which it would have had, had the atomic electron been at rest. Thus an experimental investigation giving $F(V'')$, the distribution of energies among the scattered electrons, gives us at once the shape of $f(u)$ for the component velocities of the electrons in the atom or molecule. (If one needs the distribution of total velocities among the electrons in the atom or molecule, one can get it by plotting $V'''dF(V'')/dV'''$ against V''' and properly re-labeling the abscissas in terms of the resultant velocity.)

The scattering gas can be thought of as providing a mixture of nuclei and electrons all scattering independently of each other, the

[9] G. E. M. Jauncey, Phys. Rev. **50**, 326 (1936).

electrons, however, retaining the distribution of velocities characteristic of the atom or molecule to which they belong. Single scattering is secured by limiting the total number of molecules exposed to the electron beam, which in our apparatus is done by keeping the pressure below about 0.001 mm.

Experimental Details

The apparatus was identical with that described in a former paper,[1] except for the electron gun and a minor change in the electrostatic analyzer. In these experiments the accuracy of the experimental results is limited by the fact that only a minute fraction of the primary beam is scattered through a finite angle. In our previous experiments, the maximum electron current scattered in the inelastic group did not amount to more than about 2×10^{-15} amp. It is desirable to measure this current, and also the smaller currents found on both sides of the maximum of the inelastic band, with as high a degree of accuracy as possible. We increased the opening of the slit just in front of the Faraday cylinder located at the exit end of the electrostatic analyzer by a factor of about four to increase the number of electrons collected. Increasing this slit opening impairs the resolution somewhat. This is of little importance in the present experiment since we are concerned not so much with absolute electron velocity distributions as with the change in these as we go from one hydrocarbon molecule to another. To secure better "single center" scattering conditions the energy of the incident electron beam was increased from 4000 volts, the maximum used in previous experiments, to 8000 volts. This increase, however, automatically diminishes the number of scattered electrons by a factor of four. The sensitivity of the electrometer tube circuit was such that a one-mm deflection on the scale meant a current of 2.5×10^{-17} amp. The maximum inelastic scattered current was of the order 5×10^{-15} amp. As the readings were somewhat unsteady at the high sensitivity used, one could not determine any individual reading to better than four or five percent. This situation was met by taking the average of a great many observations.

The new electron gun is shown in Fig. 1. The source of electrons is a tungsten ribbon, R, 0.002″ thick, 0.04″ wide, and 0.19″ long. At a distance of 0.06″ in front of it is a "grid," G, which is a tantalum sheet with a central hole 0.12″ in diameter. The anode, A, is a tube of brass 16″ long, closed at one end with a copper disk in the center of which is a hole of 0.08″ diameter. The distance between the grid and the end of the anode is 0.31″. A magnetic lens is located about 5″ from the end of the anode nearest the electron source. A potential difference of 8000 volts is applied between the filament and the anode. The current in the coil forming the magnetic lens and the voltage on the grid is varied until the maximum electron current into the collision chamber is obtained. Currents through the set of 1.5-mm diameter holes into the collision chamber as high as 2.0 ma have been obtained, but it was found more convenient to carry out the experiments described in this paper with a current of 0.6 ma. (This is a current about four times as strong as that used in previous measurements on electron scattering.)

The gases, methane, ethane, and ethylene, were obtained under pressure in steel cylinders

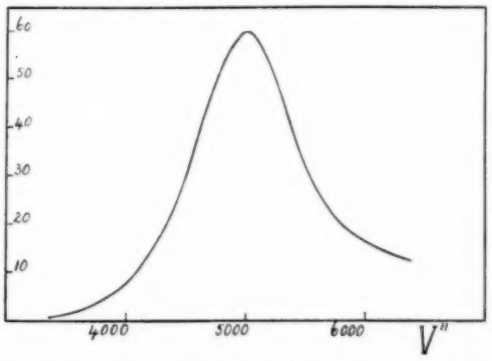

Fig. 2. The distribution of energies among the electrons scattered inelastically by acetylene through 34.2°.

from the Ohio Chemical Company. The methane was said to be 86 percent pure. A certain amount of it was liquefied. The first third was allowed to boil away, the second third was led into a reservoir supplying gas through a capillary leak into the collision chamber, and the last third was rejected. The same procedure was applied to the ethane and the ethylene, which were stated to be 95 and 99.5 percent pure, respectively. The acetylene was prepared by dropping water on

commercial calcium carbide. A bulletin issued by the Linde Air Products Company stated that the acetylene evolved was 99.5 percent pure, except for water vapor which was removed by a drying agent.

The tungsten filament had to be replaced frequently during the experiments on ethylene and very frequently during those on acetylene.

Experimental Results

The distribution of energies among the electrons scattered inelastically by acetylene is shown in Fig. 2. (The height of the elastic peak, which is omitted as it is of no importance in this investigation, is 1240, while the height of the maximum of the inelastic band is 60.) Similar curves were obtained for the other gases.

To determine $f(u)$, *the distribution of component velocities* among the electrons in the molecule, we proceed as described in the first paper in the series.[1] The curve in Fig. 2 is, by definition, $F(V'')$ where V'' is measured from the center of the band in either direction. We shall use only the left side of the inelastic band as the lower part of the right side is distorted somewhat by the "foot" of the elastic peak. As was shown in previous papers,[1-3] $f(u)$ is obtained by taking the $F(V'')$ curve and changing the abscissas in V'' into abscissas in u or β, which are related through $u/c=\beta$, by the equation

$$\beta(=u/c)\times 10^3 = V'' \div (0.5782)\, V_0^{\frac{1}{2}}, \qquad (1)$$

where V_0 is the velocity of the electrons before collision. The same curve also gives the distribution of intensity across the Compton modified band for a primary wave-length of 695 x.u. and a scattering angle of $\theta=90°$, if we use the relation

$$\lambda''=\beta\times 10^3 \qquad (2)$$

to give wave-length abscissas in x.u.'s. Thus the experimental curve $F(V'')$ gives simultaneously the distribution of *energies* among the electrons scattered inelastically when we use V'' as abscissas, the distribution of *component velocities* among the electrons in the molecule when we replace V'' by u by means of Eq. (1), and the *profile of the Compton modified band* (for 90° scattering of a primary wave-length $\lambda=695$ x.u.) when we replace u by λ'' by means of Eq. (2).

The final values of $f(u)$ were obtained as follows. Each individual point of $f(u)$ calculated from the corresponding experimental reading for $F(V'')$ was plotted on a large sheet of accurately ruled graph paper. A smooth curve was drawn through the points to give as equal weight as possible to all the points. Values for selected abscissas were read off this curve, which was then obliterated and the process repeated several times. A final curve was obtained by taking the mean values of the ordinates from these curves for the selected abscissas. Final curves for ethane, ethylene, and acetylene are shown in Fig. 3. The values from which these curves were plotted are given in Table I. Just as the breadth of a spectrum line is often arbitrarily indicated by its breadth at half maximum, so we find it convenient to give in Table II the values of the abscissas at half maximum and also at quarter maximum.

There are several ways of roughly summarizing our information about the motion of electrons in molecules. Because it is natural to express our results in the form of a curve giving the distribution of component velocities, we can associate with this as a convenient parameter the component velocity value at half maximum. Other equally good parameters would be the average component velocity, the average resultant momentum (or velocity), as used by Coulson and Duncanson, and the most frequent resultant momentum (or velocity). These parameters are approximately proportional to each other for the sort of distributions we meet in these experiments, and so the sequence in magnitude of any one parameter in a set of distributions

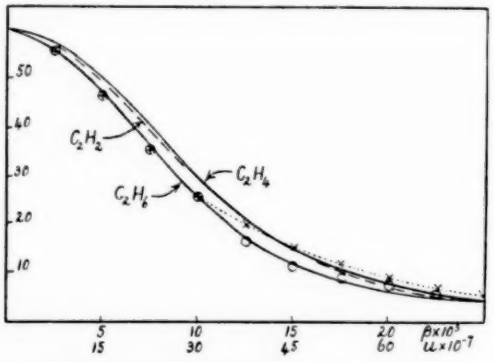

Fig. 3. The distribution of component velocities among the electrons in the molecules of acetylene, ethylene, ethane, and methane. The curve for acetylene is shown as a broken line except where it is indistinguishable from that for ethylene. The curve for methane is indicated by crosses which are joined by a dotted line where the methane curve breaks away from the ethane curve. The circles indicate the curve for methane when corrected in the manner suggested in the text.

is the same as that for any other parameter. Any generalization relating to the "component velocity at half maximum" will also apply to the "average component velocity," since they are approximately proportional to each other. We shall usually use the latter parameter in the discussion to follow merely because its implication is more readily grasped.

The degree of accuracy of the final curves may be indicated by the fact that the successive "best" curves drawn through the points representing values of $f(u)$ all passed through the "half maximum" ordinate at abscissa values within about ± 0.9 of the values given in Table II.

TABLE I. *The distribution of component velocities for the bonding electrons in acetylene, ethylene, ethane, and methane. $f(u)$ is identical in shape with $f(\lambda'')$, the profile of the associated Compton modified band. Values in parentheses for methane are alternative values obtained as described in the text.*

$\beta\times10^3$ AND λ'' (X.U.)	$u\times10^{-7}$ CM/SEC.	$f(u)$ (OR $f(\lambda'')$) C_2H_2	C_2H_4	C_2H_6	CH_4	
0.0	0.0	60.0	60.0	60.0	60.0	
2.5	7.5	56.8	57.1	55.6	57.7	
5.0	15.0	49.1	49.9	47.0	46.6	
7.5	22.5	39.4	40.0	36.4	35.4	
10.0	30.0	29.5	29.5	25.4	25.7	
12.5	37.5	21.0	21.1	16.9	19.4	(16.1)
15.0	45.0	14.7	14.9	11.8	15.2	(12.3)
17.5	52.5	10.0	10.7	8.6	12.0	(9.4)
20.0	60.0	7.1	7.8	6.6	9.4	(7.8)
22.5	67.5	5.2	5.7	5.3	7.0	(5.8)
25.0	75.0	3.9	4.5	4.2	5.0	(4.2)
27.5	82.5	2.9	3.1	3.5	3.3	(3.7)
30.0	90.0	2.2	2.5	2.9	2.0	(1.7)
35.0	105.0	1.3	1.7	2.0		
40.0	120.0	0.8	1.4	1.5		

Two conclusions may be drawn from these experimental results. (1) The average velocities of the bonding electrons in ethylene and acetylene are substantially identical and greater than the average velocity of the bonding electron in ethylene. (2) The abscissas at about one quarter maximum indicate the ethane has considerably fewer fast electrons than acetylene and ethylene.

The results for methane call for comment. This was the first gas investigated in the present research and as it had been investigated before,[3] not so much time was spent on it as on the other gases. This turned out to be unfortunate. The $f(u)$ curve for methane in this investigation is wider than the one in the earlier investigation. The width at half maximum in the earlier investigation was 22.5 as against 26.4 here. It is probably to be explained by the fact that to secure higher currents we opened the slit in front of the Faraday cylinder and thus impaired the resolution, which made the curve wider. This introduces an error in the absolute values of $f(u)$, but this is of little importance because in this research we are concerned more particularly with a *comparison* of curves obtained for different gases under identical experimental conditions.

We find that the $f(u)$ curves for methane and ethane are indistinguishable from $u=0$ to $u=30\times10^7$. At $u=30\times10^7$ the methane curve breaks away rather abruptly from the ethane curve. Unfortunately few observations were available for these points, and it was not possible to make further measurements when the collected results on all the gases pointed to the need for a new set of measurements on methane especially in the high velocity region. If we take the trend of the methane curve as established in a former paper[3] and use it to extrapolate the present methane curve beyond $u=30\times10^7$, we get a curve which differs but little from the ethane curve in the high velocity part as well as in the low velocity part. If this doubtful procedure is accepted, then we can say that the $f(u)$ curves for methane and ethane are substantially equal. It would have been much more satisfactory to re-investigate methane than to attempt to fit together two investigations as we have done, but circumstances prevented our doing so. For the present we can say that the methane and ethane curves are identical up to $u=30\times10^7$ and possibly beyond.

DISCUSSION

There are no quantitative theories available with which we can compare our experimental results. The next best thing to do is to make use of qualitative considerations. Let us suppose, as a tentative hypothesis, that the velocity distributions of the electrons in the C−H bonds in all the four gases investigated are identical, but that the velocity distributions of the electrons in the CC bonds change in such a way that the average velocities increase as we go from C−C in C_2H_6 to C=C in C_2H_4 and finally to C≡C in C_2H_2. (A reasonable assumption would be that the average velocities are approximately inversely proportional to the square root of the separation of the carbon atoms. This results in the average velocities of the electrons in the CC bonds in C_2H_6, C_2H_4, and C_2H_2 being in proportion to 1.00, 1.08, and 1.13.) For each molecule the contribution of the different bonds to the experimental velocity distribution curve is in proportion to the number of electrons involved in each bond. In C_2H_6, the contribution of the C−H bonds to that of the C−C bonds should be weighted in the ratio of 6 to 1, which means that, unless the electron velocity distribution for the C−C bond differs considerably from that of the C−H bond, the distribution for the molecule as a whole will be

nearly identical with that for the C−H bond alone. This is in line with our experimental result that the electron velocity distribution curves for CH_4 and C_2H_6 are substantially identical. (This is true for the lower velocities, but, as was mentioned earlier, there is some doubt as to the accuracy of that part of the distribution curve representing the scattering of the faster electrons in methane.) In C_2H_4, the ratio of the contribution of the C−H bond to that of the C=C bond is 2 : 1, while in C_2H_2 the corresponding ratio is 2 : 3. The assumption we have made leads to the conclusion that the average velocities of the electrons should increase as we follow the sequence ethane, ethylene, acetylene. This prediction is supported by our experimental results for ethane and ethylene, but we do not find any substantial change as we go from ethylene to acetylene. So long as we treat the C−H bond as identical in all three molecules, there seems to be no way of accounting for the change in average velocities from ethane to ethylene and the absence of a change from ethylene to acetylene.

It is possible that one is not justified in assuming that the electron velocity distributions are identical in the C−H bonds, when the adjacent CC bonds differ as they do in the three molecules considered. In a very recent paper, Coulson and Duncanson[10] published a theory from which it may be inferred that the mean momenta of the electrons in the C−H bonds in ethane, ethylene, and acetylene are in proportion to 1.00, 0.98, and 0.93. It will be observed that this sequence for the C−H bond is just the reverse of that assumed for the CC bonds in the same molecules. The result is that as we go from ethane to ethylene and then to acetylene the diminution in the average velocities in the C−H bonds will more or less offset the increase in the average velocities in the CC bonds. In view of these considerations one perhaps would not expect to find differences in the average velocities of the electrons in ethane and in ethylene as large as those implied in Table II. It is also difficult to see why there is no substantial difference between the curves for ethylene and acetylene when there is a difference between ethylene and ethane.

TABLE II. *Abscissa values for f(u) at half maximum and quarter maximum. (Values when multiplied by 10^7 are in cm/sec.) The value in parentheses for methane is an alternative quarter maximum value obtained as described in the text.*

	C_2H_2	C_2H_4	C_2H_6	CH_4
half max.	29.7	29.7	26.7	26.7
quarter max.	44.7	44.7	39.6	45.3 (39.6)

The senior author takes pleasure in acknowledging grants from the Penrose Fund of the American Philosophical Society and the Bache and Joseph Henry Funds of the National Academy of Sciences.

[10] C. A. Coulson and W. E. Duncanson, Proc. Camb. Phil. Soc. **37**, 67 (1941).

Compressions and Polymorphic Transitions of Seventeen Elements to 100,000 kg/cm²

P. W. BRIDGMAN
Research Laboratory of Physics, Harvard University, Cambridge, Massachusetts
(Received July 16, 1941)

IN the following I give the numerical results of the first measurements above 50,000 kg/cm² made by the method, already anticipated in a brief note,[1] in which the entire pressure apparatus is immersed in a liquid which is itself exposed to a hydrostatic pressure between 25,000 and 30,000 kg/cm². The details of the method are only briefly indicated here; I expect to publish in another place a fuller description and discussion.

The piezometer in which the material is compressed is shown in Fig. 1; it consists of a cylinder completely pierced with an axial hole. The compression is applied by two Carboloy pistons acting from each end. The piezometer is compound, consisting of an inner core of Carboloy, made slightly tapering on the outside, forced into an outer sleeve of heat-treated alloy steel. By this means the Carboloy cylinder starts under an initial compression in addition to the compression of 25 or 30,000 kg/cm² exerted by the confining liquid. The additional compression afforded by the steel sleeve is further increased by the external hydrostatic pressure because of the differential compressibility of steel and Carboloy, steel being about three times more compressible than Carboloy. The piezometer is six-tenths filled with the material to be measured A; this is prevented from leaking past the Carboloy pistons by conical steel retaining rings. The assembled piezometer is placed inside the cylinder of the apparatus for reaching 30,000 kg/cm², which is filled with an amount of isopentane, determined by preliminary trial, such that the piston of the 30,000 apparatus just makes up on the double pistons of the piezometer when the pressure in the 30,000 apparatus has reached approximately 25,000 kg/cm². Further motion of the piston of the 30,000 apparatus now produces the double result of increasing the pressure in the fluid of the 30,000 apparatus and at the same time increasing the pressure on the material in the piezometer. Because of the small amount of this material, compared with the total amount of fluid in the 30,000 cylinder, a motion of the piston sufficient to increase the pressure on the contents of the piezometer to 100,000 kg/cm² increases the pressure in the surrounding liquid by a much smaller amount. The precise increase of pressure in the surrounding liquid depends on the compressibility of the contents of the piezometer; for the materials described below it averaged something of the order of 3000 kg/cm², and might on occasion rise to 5000 kg/cm².

The extra force required to push the piston of the piezometer is measured electrically from the change of resistance of a hardened steel grid. This has already been described to some extent[2] and will be further described in the detailed paper. The compression coefficient of the grid was determined by independent measurement, as was also the pressure coefficient and the pressure coefficient of the compression coefficient. The compression coefficient is about 15 percent less at 25,000 than at atmospheric pressure. The confining pressure exerted by the liquid of the 30,000 apparatus was independently measured with a manganin gauge, which has already been described.[3] The piston displacement of the piezometer was obtained from a measurement of the piston displacement of the 30,000 apparatus, made with a jeweled Ames gauge, graduated to 0.0001 inch and reading by estimation to 0.00001

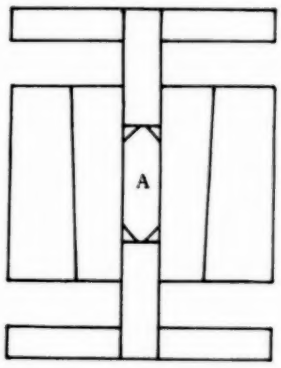

FIG. 1. Scale drawing of the high pressure piezometer. The outside diameter is 7/16 inch.

[1] P. W. Bridgman, Phys. Rev. **57**, 342 (1940). See also R. W. Goranson and E. A. Johnson, Phys. Rev. **57**, 845 (1940).

[2] P. W. Bridgman, J. App. Phys. **12**, 461 (1941).
[3] P. W. Bridgman, Proc. Am. Acad. **74**, 1 (1940).

inch. The method is a differential method; the difference of piston displacement is determined when the piezometer is filled with the material under investigation and when filled with some standard reference material. In this way most of the various distortions in the apparatus are eliminated. The reference material should have a small compressibility; for this purpose gold was chosen, which is as incompressible as iron and has the further advantage of mechanical softness, thus reducing hysteresis effects due to friction. To convert differential compressions to absolute compressions the compression of gold must be assumed; this was extrapolated from my measurements up to 12,000 kg/cm², corrected for my improved values for iron, by Murnaghan's formula. This formula has shown itself surprisingly good at high pressures, and in view of the small absolute value of gold in comparison with that of the substances listed here, the error in the absolute values introduced by the extrapolation should not be important. The assumed compressions for gold are 0.0255 at 50,000 and 0.0483 at 100,000. The results thus obtained are differential in another sense, because they are for the compressions taken from 25,000 as zero. The total compressions have to be obtained by combining the measurements here with previous measurements up to 25,000 kg/cm². Such measurements have been made for most of the materials of the following.

It is not possible to eliminate all correction for distortion by making the method differential, but the differential displacements must be corrected by the fractional change of cross section of the piezometer. Here appears a great advantage in making the piezometer of Carboloy instead of steel, because its elastic constants are three times higher. The correction was determined by calculation from the independently determined elastic constants and was 3.3 percent at the maximum. There was practically no permanent set of the piezometer under this distortion—another advantage of Carboloy.

The magnitude of the piston displacement for the range 25,000 to 100,000 kg/cm² varied from 0.020 inch for gold to 0.063 inch for barium. The readings lie on smooth curves to within 0.0002 or 0.0003 inch. The principal error in the method arises from friction; the effect of friction was eliminated as far as possible by taking the mean of increasing and decreasing readings. Because of friction a higher pressure has to be applied to the Carboloy pistons than can be applied, on the average, to the contents of the piezometer; the pressure on the piston was often pushed beyond 110,000 to get 100,000 in the piezometer. The error from friction is relatively small for the highly compressible softer metals, but for metals much less compressible than zinc becomes serious enough to limit the applicability of the method. In nearly all cases the results are the mean of two independent set-ups. A check on the results is afforded by the agreement of these results, and also by the agreement of the results between 25,000 and 50,000 with those previously obtained. I believe that, in general, the final accuracy is between one and two percent.

A number of the substances have new polymorphic transitions in the range; the establishment of such transitions is the most positive of the results obtained. If the volume discontinuity of the transition is less than 0.15 percent of the initial volume, however, it would escape detection, as also if the transition is too sluggish.

The numerical results are given in a table of compressions (Table I); that is, fractional changes of the initial volume at atmospheric pressure, at pressure intervals of 10,000 kg/cm². The results are for room temperature, which averaged 23°. The data for the transitions are given as footnotes; the difference of the two compressions is the volume change at the transition. Thus the volume change at the transition of calcium, which occurs at 64,000 kg/cm², is 0.013, or, otherwise expressed, the volume at 64,000 of the low pressure modification of that amount of calcium which occupies 1 cm³ at atmospheric pressure at 23° is 0.771 cm³, and the volume at the same pressure of the same number of grams of the high pressure modification is 0.758 cm³.

Because of their simple structure, which makes them amenable to theoretical treatment, perhaps the most interesting of the substances are the alkali metals. It is unfortunate, therefore, that the accuracy is materially less for them than for the other materials. The reason is that the usual technique could not be followed. These metals chemically attack and rupture the piezometer,

so that it was necessary to enclose them completely in a sheath of copper, which occupied two-thirds of the total volume. The rigidity of copper is so high that the accuracy is materially reduced, particularly at the lower pressures. The results given in Table I were obtained by a graphical compromise, in which much weight was given to the former results up to 45,000 or 50,000 kg/cm². The previous results differ principally from the present ones in the same range in their greater decrease of compressibility with pressure, the compressions now found being greater than would be found by an extrapolation of the previous results. The compression of copper enters these results. This was assumed as given by Murnaghan's formula; the assumed compressions were 0.0325 and 0.0608 at 50,000 and 100,000 kg/cm², respectively.

An attempt was made also to get the compressibility of caesium, but the results were incomplete because of rupture of the apparatus. It is probable that the compression is of the order of 15 percent greater than that of rubidium, but this statement must be used with some reserve.

An interesting question in connection with the alkali metals is whether any of them have high pressure transitions analogous to the transition of caesium at 23,000 kg/cm². None was found. The fractional change of volume at the transition of caesium is 0.006; this is small, but not smaller than several found and tabulated above. It is, therefore, highly probable that, if there are transitions of the other alkali metals, their volume change is materially smaller than the change of caesium.

In the case of three metals of the table, cadmium, thallium, and arsenic, there are no sufficient measurements of the compressions at low pressures; the values given for 10,000 and 20,000 were obtained by estimation from comparison with similar elements or from the initial compressibility in the first few hundred kg/cm². The results for arsenic are obtained from only a single run. The piezometer fractured on the next filling in a way to suggest chemical attack.

Seven new transitions have been found above 50,000 kg/cm². The transition of antimony had been looked for because of the close similarity of the crystal structures of antimony and bismuth; the magnitude of the change of volume at the new transition of antimony is not far from that of the first transition of bismuth, so that the behavior of antimony may be parallel to that of bismuth but on a much extended pressure scale. Bismuth has two new transitions at high pressure, making now six modifications in all. There is a rather close parallelism between the transitions of bismuth and those of water. Each of the alkali earth metals has two transitions; the low pressure transition of calcium is somewhat obscure and has been smoothed over in the table. The parallel-

TABLE I. *Compression of seventeen elements.*

PRESSURE KG/CM²	Li	Na	K	Rb	Ca	Sr	Ba	Zn	Cd	In	Tl	Sn	As	Sb	Bi	Se	Te
10,000	0.074	0.117	0.183	0.233	0.058	0.075	0.086	0.016	0.022	0.023	0.023	0.018	0.047	0.025	0.028	0.089	0.045
20,000	.125	.182	.268	.316	.103	.122	.159 (d)	.031	.042	.045	.043	.034	.083	.047	.052	.149	.079
30,000	.164	.232	.329	.371	.139	.172 (b)	.211	.046	.060	.064	.061	.049	.109	.066	.158 (h)	.187	.111
40,000	.201	.273	.377	.419	.168	.209	.253	.061	.076	.081	.079(f)	.064	.132	.083	.174	.208	.138
50,000	.237	.310	.419	.462	.195	.239	.288	.075	.091	.097	.103	.077	.152	.098	.192 (i)	.227	.214 (l)
60,000	.272	.343	.457	.501	.220	.266	.318(e)	.088	.104	.112	.119	.091	.171	.112	.205	.243	.225
70,000	.305	.372	.492	.539	.252 (a)	.298 (c)	.361	.100	.116	.126	.132	.103	.188	.124	.222 (j)	.258	.234(m)
80,000	.336	.397	.522	.575	.268	.317	.382	.111	.127	.140	.145	.114	.204	.136	.232	.271	.250
90,000	.366	.419	.549	.608	.284	.335	.402	.122	.138	.153	.157	.125	.219	.185 (g)	.240(k)	.283	.258
100,000	.394	.440	.573	.638	.298	.352	.420	.132	.148	.165	.169	.136	.233	.197	.261	.295	.267

(*a*) Transition at 64,000. Compressions: 0.229 and 0.242.
(*b*) Transition at 25,000. Compressions: .143 and .152.
(*c*) Transition at 65,000. Compressions: .279 and .287.
(*d*) Transition at 17,000. Compressions: .135 and .141.
(*e*) Transition at 60,000. Compressions: .318 and .337.
(*f*) Transition at 40,000. Compressions: .079 and .086.
(*g*) Transition at 85,000. Compressions: 0.142 and 0.179.
(*h*) Two transitions at 25,000. Extreme compressions: .064 and .150.
(*i*) Transition at 45,000. Compressions: .180 and .186.
(*j*) Transition at 65,000. Compressions: .211 and .216.
(*k*) Transition at 90,000. Compressions: .240 and .252.
(*l*) Transition at 45,000. Compressions: .152 and .207.
(*m*) Transition at 70,000. Compressions: .234 and .241.

ism between the alkali earth metals cannot be as close as superficially appears, because at atmospheric pressure calcium and strontium are face-centered cubic, whereas barium is body-centered. It is surprising that these simple cubic structures permit so many other forms.

Selenium is probably a mixture of amorphous and crystalline material. On the initial application of pressure it experiences some permanent change, but a single application apparently forces it into a more or less well-defined condition. The results obtained now agreed well in the common range with the former measurements to a pressure maximum of 50,000 kg/cm². The very sharp drop of compressibility of selenium in the neighborhood of 25,000 is to be noted. The curve of compression of selenium against pressure is quite different in character from that of all the other elements, dropping off with pressure at a much more rapid rate. The amorphous material doubtless functions more like a liquid than a crystalline solid.

As in all this work, I am indebted to the Carboloy Company for the Carboloy. I have received financial assistance from the Milton Fund of Harvard University, and the skillful assistance of my mechanic Mr. Charles Chase was essential.

AUGUST 15, 1941 PHYSICAL REVIEW VOLUME 60

Heat Transfer and Superfluidity of Helium II

P. L. KAPITZA
Institute for Physical Problems, Academy of Sciences USSR, Moscow, USSR
(Received June 23, 1941)

IN our recent researches, when studying the heat transfer of helium II in capillaries, we established the existence of a counter current in the liquid.[1] An analysis of the experimental results indicated that the transfer of heat into the kinetic energy of the current might take place in a thermodynamically reversible way. From these experiments it was suggested that the helium II flowing in thin films could be in a different energy state.

In the present experiments we studied the flow of helium through a narrow slit, about 10^{-5} cm, obtained by means of two optically polished quartz disks in the same way as in the viscosimeter by the aid of which we originally established the superfluidity of helium II.[2] By making the helium flow through this slit under the influence of a temperature gradient in a container with a good heat insulation it was possible to show that the flowing helium has zero entropy. The difference of the heat content Q(cal./g of free helium and helium flowing through the slit obtained at a number of temperatures is plotted by crosses in Fig. 1.

From a simple thermodynamic analysis of this phenomenon it follows that if the helium II is forced through a narrow channel under a pressure p; then in the case of thermohydrodynamically reversible phenomena a temperature difference ΔT will be caused which can be determined from the following expression.

$$p = A\rho Q(\Delta T/T), \tag{1}$$

where ρ is the density of the helium and A the mechanical heat equivalent.

By means of the same apparatus the existence of the temperature difference ΔT was established and measured. In such a way we have an independent means of determining the value of Q from expression (1). On the curve in Fig. 1 these values of Q are plotted by circles. The coincidence of Q determined by two different methods shows that the thermohydrodynamic processes of helium II are reversible.

The reversibility of the thermohydrodynamical processes in helium II must evidently be attributed to the lack of the sources of energy

[1] P. L. Kapitza, J. Exp. Theor. Phys. **11**, 1 (1941); J. Phys. USSR **4**, 177 (1941).
[2] P. L. Kapitza, Rec. Acad. Sci. USSR [18] **28** (1938); Nature **74**, 141 (1937).

dissipation. This shows once more that helium II is a superfluid and a poor heat conductor.

The former experiments made to study the viscosity of helium II when flowing through narrow channels did not take into account the influence of a possible temperature difference which, according to Eq. (1) would cause an additional pressure. Therefore, all the data obtained when studying the possibility of a viscous flow of helium II through a slit or through capillaries must be revised. By taking into account this extra pressure, we found that the limit of a possible viscosity for helium II is less than 10^{-11} poise. This is about 100 times less than the limit found with the same viscosimeter in our original experiments[1] and also much smaller than that established by other research workers.[3]

The reversibility of the thermohydrodynamic phenomena in helium II gives the research worker the possibility of establishing a method for attaining very low temperatures. As there are, at present, no experimental or theoretical reasons for supposing that helium II changes its thermohydrodynamical properties on approaching zero, this method for obtaining low temperatures—as distinguished from the magnetic method—will *a priori* permit us to approach as near to absolute zero as our technical means will permit.

This method is now being worked out by us, and in the preliminary experiments temperature drops of 0.4°K have already been easily obtained.

A possibility of helium II flowing with zero entropy has already been put forward in the theoretical views of London[4] and Tisza.[5] The

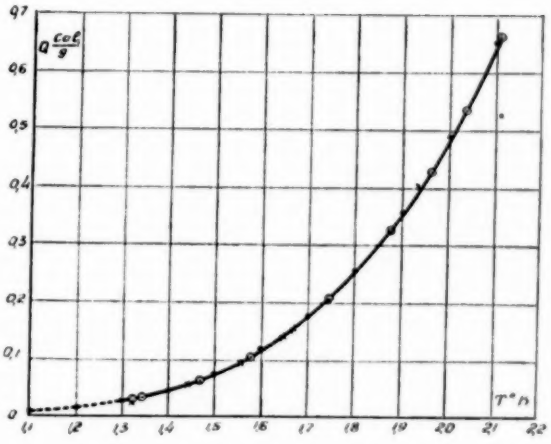

FIG. 1. Heat content of helium.

recently proposed theory of Landau[6] establishes a quantum basis for the phenomena of superfluidity and also permits us to make a qualitative calculation of the heat content of helium II at low temperatures. According to these theories

$$Q = ST, \tag{2}$$

where S is the entropy of helium II.

The results as calculated by Professor Landau from his theory are plotted by dots on the curve in Fig. 1 and coincide well with the independent experimental data from the experiments made to ascertain the values of Q. This theory also gives an interesting quantum interpretation of the counter current of helium observed during heat conductivity.

A detailed account of these experiments will be found in one of the next issues of the *Journal of Physics, USSR.*

[3] J. F. Allen and A. D. Misener, Proc. Roy. Soc. **172**, 467 (1939).

[4] W. F. Giauque, J. W. Stout and R. E. Barieau, Phys. Rev. **54**, 147 (1938); J. Am. Chem. Soc. **61**, 654 (1939); H. London, Proc. Roy. Soc. **171**, 484 (1939).

[5] L. Tisza, Nature **141**, 913 (1938); Comptes rendus (Paris) **207**, 1035, 1186 (1938).

[6] L. Landau, J. Phys. USSR, in press; Phys. Rev. **60**, 356 (1941) (this issue).

Theory of the Superfluidity of Helium II

L. LANDAU
Institute of Physical Problems, Academy of Sciences USSR, Moscow, USSR
(Received June 23, 1941)

IT is well known that liquid helium at temperatures below the λ-point possesses a number of peculiar properties, the most important of which is superfluidity discovered by P. L. Kapitza.[1] As to the theoretical interpretation of these phenomena, Tisza's[2] well-known attempt to consider helium II as a degenerate Bose gas cannot be accepted as satisfactory—even putting aside the fact that liquid helium is not an ideal gas, nothing could prevent the atoms in the normal state from colliding with the excited atoms; i.e., when moving through the liquid they would experience friction and there would be no superfluidity at all.

Consider the quantization of an arbitrary system of interacting particles (a liquid) from a general point of view. This can be done by means of introducing operators of the density of the mass ρ, the density of the flow of the mass (momentum density) $\mathbf{j}$ and the velocity $\mathbf{v}$ of the liquid according to:

$$\rho=\sum_a m_a\delta(\mathbf{r}_a-\mathbf{R}),$$

$$\mathbf{j}=\tfrac{1}{2}\sum_a[\mathbf{p}_a\delta(\mathbf{r}_a-\mathbf{R})+\delta(\mathbf{r}_a-\mathbf{R})\mathbf{p}_a], \qquad (1)$$

$$\mathbf{v}=\frac{1}{2}\left(\frac{1}{\rho}\cdot\mathbf{j}+\mathbf{j}\cdot\frac{1}{\rho}\right) \quad \left(\mathbf{p}_a=\frac{h}{i}\nabla_a\right),$$

$\mathbf{R}$ being the radius vector of an arbitrary point, $\mathbf{r}_a$ the radius vector of the particle m_a. (It must be emphasized that such a description is based on a microscopical picture and does not involve any statistical averaging.) The calculation leads to the following commutation rules:

$$\rho_1\rho_2-\rho_2\rho_1=0, \quad \mathbf{v}_1\rho_2-\rho_2\mathbf{v}_1=\frac{h}{i}\nabla\delta(\mathbf{R}_1-\mathbf{R}_2),$$
$$v_{1i}v_{2k}-v_{2k}v_{1i}=\frac{h}{i}\delta(\mathbf{R}_1-\mathbf{R}_2)\frac{1}{\rho_1}(\text{rot }\mathbf{v})_{ik} \qquad (2)$$

(here $i, k=x, y, z$; $(\text{rot }\mathbf{v})_{ik}=(\partial v_k/\partial x_i)-(\partial v_i/\partial x_k)$ and the indexes 1 and 2 refer to the points $\mathbf{R}_1$ and $\mathbf{R}_2$ in space). By applying the relations (2) to the macroscopic motion of the liquid, we find, as it should be, the usual hydrodynamic equations written in an operational form (in a macroscopic consideration the internal energy of a liquid is considered as a function of its density only).

From (2) it can be seen that rot $\mathbf{v}$ commutes with ρ and $\mathbf{v}$ and, therefore, also with the Hamiltonian in that case only when rot $\mathbf{v}=0$ over the whole volume of the liquid. This means that rot $\mathbf{v}=0$ is conserved, i.e., a quantum liquid always possesses stationary states in which rot $\mathbf{v}=0$ ("potential motion"). States in which rot $\mathbf{v}\neq 0$, but is arbitrarily small over the whole volume, do not exist. In other words, there is no continuous transition between the states of the potential (rot $\mathbf{v}=0$) and the vortex (rot $\mathbf{v}\neq 0$) motions of a quantum liquid. Therefore, between the lowest energy levels of vortex and potential motion there must be a certain energy interval Δ. (It must be emphasized that we do not here refer to the levels for single helium atoms but to the levels corresponding to the states of the whole liquid.) One may question which of these levels lies lower; apparently both cases are logically possible. The supposition that the normal level of potential motions lies lower than the beginning of the spectrum of vortex motions leads to the phenomenon of superfluidity. Hence we must suppose that this very case exists in liquid helium.

Every weakly excited state must be considered as a combination of simple "elementary excitations." In the case of potential internal motions, these excitations are quanta of longitudinal (sound) waves, i.e., phonons. The energy ϵ of the phonons, is, as is well known, a linear function of their momentum: $\epsilon=cp$ (c being the velocity of sound). The "elementary excitations" of the vortex spectrum can be called "rotons." Their energy is a quadratic function of the momentum:

[1] P. L. Kapitza, Nature **141**, 74 (1937); Comptes rendus Acad. Sci. USSR **18**, 28 (1938).
[2] L. Tisza, Nature **141**, 913 (1938).

$\epsilon=\Delta+p^2/2\mu$ (μ being the "effective mass" of a roton and the energy is measured from the normal state of the liquid). If the number of rotons and phonons per unit volume is not too large (sufficiently low temperatures) their aggregate can be considered as a mixture of two ideal gases. The phonon gas obeys Bose statistics. For the rotons we can apply (for $kT\ll\Delta$) the Boltzmann distribution independently of their statistics (probably Bose) owing to the assumed large term Δ (as compared with kT) in their energy.

From these properties of the energy spectrum the heat capacity of helium II must consist of two parts: the "phonon part," i.e., the normal Debye heat capacity proportional to T^3, and the "roton part," depending on the temperature exponentially ($\sim e^{-\Delta/kT}$). A comparison of the calculated phonon heat capacity with that measured experimentally[3] shows that right down to the lowest temperatures ($<1°$K) the roton part plays the dominant role in the heat capacity. If it is expressed through μ and Δ and compared with the experimental values, we get $\Delta/k=8$–$9°$, $\mu=7$–8 masses of a helium atom.

At absolute zero, helium is in its normal unexcited state. If such a liquid is considered when flowing as a whole along a capillary, it can be easily shown that the interaction between it and the walls of the capillary cannot lead (when the velocity of the flow is not too great) to an excitation of internal motion, i.e., to an energy dissipation; in other words, the liquid will disclose no viscosity. Owing to the presence of the energy gap in the spectrum the rotons can be excited only at velocities $V>(2\Delta/\mu)^{\frac{1}{2}}$, and the phonons—because of the linear dependence of their energy on the momentum—only at $V>c$.

At temperatures higher than absolute zero there are a certain number of phonons and rotons in helium II. If we consider helium II in a rotating vessel, a statistical investigation leads to the result that a statistical equilibrium must be established in the vessel which is distinguished from the equilibrium in a vessel at rest in that the gas of rotons and phonons rotates with the vessel as if it were carried along by the walls. If the angular momentum of the helium in the rotating vessel is calculated from the corresponding statistical distribution, at absolute zero, i.e., in the entire absence of rotons and phonons, we would get simply zero. At higher temperatures the angular momentum will be non-zero, but the moment of inertia will be, at sufficiently low temperatures, much lower than the usual one (which corresponds to the usual rotation of the whole liquid together with the vessel).

Thus, when the walls of the vessel are in motion, only a part of the mass of liquid helium is carried along by them, and the other part "remains stationary." Therefore we might regard liquid helium as if it consisted of a "mixture" of two liquids—one is "superfluid" without viscosity and not carried along by the walls of the vessel, and the other is "normal." When these two "liquids" move through each other there is "no friction" between them, i.e., there is no transfer of momentum from one to the other. It must be emphasized that when we talk about helium as being a "mixture" of two liquids it is no more than a means of expression convenient for describing the phenomena in helium II. Actually, it should be said that two motions can exist simultaneously in a quantum liquid, each of which is connected with its own effective mass. One of these motions is "normal" and the other is "superfluid." It must be particularly stressed that we have here no real division of the particles of the liquid into "superfluid" and "normal" ones—in a definite sense one can speak only of the "superfluid" and "normal" parts of the mass of the liquid as of masses connected with two simultaneously possible motions, but this does not mean that the liquid can be really divided into two parts.

At every temperature liquid helium is characterized by a definite value for the ratio of the densities ρ_n and ρ_s of the "normal" and "superfluid" liquids ($\rho=\rho_n+\rho_s$ is the true density of helium). At $T=0$ the ratio $\rho_n/\rho=0$; if the temperature is raised it increases. The temperature at which ρ_n/ρ becomes unity, i.e., the "superfluid" part vanishes, is the λ-point of helium. The ratio ρ_n/ρ can be measured experimentally in a direct way by measuring the moment of inertia of the rotating vessel filled with helium II.

The ratio ρ_n/ρ can be calculated for low temperatures when the aggregate of phonons and

[3] W. H. Keesom and A. P. Keesom, Physica **2**, 557 (1935).

rotons can be regarded as an ideal gas; one gets:

$$\frac{\rho_n}{\rho}=\frac{4}{3}\frac{E^{(\mathrm{ph})}}{c^2}+\mu N^{(\mathrm{rot})} \tag{3}$$

($E^{(\mathrm{ph})}$ is the energy of the phonon gas per 1 g of helium, $N^{(\mathrm{rot})}$ is the number of rotons in 1 g of helium; $E^{(\mathrm{ph})}\sim T^4$, $N^{(\mathrm{rot})}\sim e^{-\Delta/kT}$). In view of a very rapid exponential increase of $N^{(\mathrm{rot})}$, this formula can be approximately applied to the calculation of the temperature of the λ-point; with the values of μ and Δ given above we get 2.3°K for the λ-point, which is in sufficiently good agreement with the known value 2.19°K.

It can be shown that the motion of the "superfluid" liquid is always "potential." Besides this, the motion of the "superfluid" part of helium II does not carry heat. Therefore, a motion of helium II in which only the superfluid part takes part is thermodynamically reversible. When helium II is flowing through a narrow slit it is just the superfluid part which flows through without disclosing any friction. The outflowing helium ought to be at a lower temperature than the helium II in the initial vessel—in the ideal case at absolute zero.

For the heating of the liquid in the vessel when helium flows out through a narrow capillary, and for the temperature gradient of the pressure dp/dT, the formulae are obtained which were given by H. London[4] starting from Tisza's ideas, the verbal formulation of which coincides at this point with the theory here advanced. These formulae are fully confirmed by P. L. Kapitza's experiments.[5]

A temperature gradient along the capillary gives rise to two currents—the current of the "normal" liquid which carries heat from the hot to the cold end and the oppositely directed current of "superfluid" liquid; this mechanism leads to a very large heat transfer.

A complete system of hydrodynamic equations can be advanced describing the macroscopical motion of helium II. At every point the motion is described by two velocities—the "superfluid" $\mathbf{v}_s$ (for which $\mathrm{rot}\,\mathbf{v}_s=0$) and the "normal" $\mathbf{v}_n$; on a hard surface $\mathbf{v}_s$ must fulfill the boundary conditions of an ideal liquid and $\mathbf{v}_n$ that of a viscous one. If the values of $\mathbf{v}_s$ and $\mathbf{v}_n$ are not too large, the equations are found to be of the form:

$$\rho=\rho_s+\rho_n,\quad \mathbf{j}=\rho_s\mathbf{v}_s+\rho_n\mathbf{v}_n, \tag{4}$$

$$(\partial\rho/\partial t)+\mathrm{div}\,\mathbf{j}=0, \tag{5}$$

$$\frac{\partial j_i}{\partial t}+\sum_k\frac{\partial \Pi_{ik}}{\partial x_k}=0,$$

$$\Pi_{ik}=p\delta_{ik}+\rho_n v_i^{(n)}v_k^{(n)}+\rho_s v_i^{(s)}v_k^{(s)}, \tag{6}$$

$$\frac{\partial \mathbf{v}_s}{\partial t}=-\mathrm{grad}\left\{\varphi+\frac{v_s^2}{2}-\frac{\rho_n}{2\rho}(\mathbf{v}_n-\mathbf{v}_s)^2\right\}, \tag{7}$$

$$(\partial\rho S/\partial t)+\mathrm{div}(\rho S\mathbf{v}_n)=0 \tag{8}$$

(s and φ being the entropy and thermodynamic potential per 1 g of helium, p the pressure); in (6) and (8) the terms connected with the viscosity of the normal liquid are left out.

The application of these equations to the propagation of sound leads to the result that two velocities of sound must exist in helium II which are approximately equal to

$$u_1=(\partial p/\partial\rho)^{\frac{1}{2}},\qquad u_2=(Ts^2\rho_s/C\rho_n)^{\frac{1}{2}} \tag{9}$$

(C is the heat capacity). At the λ-point u_2 becomes zero. At $T\to 0$ these velocities tend to the limits $u_1=c$, $u_2=c/\sqrt{3}$.

A detailed paper will be published in one of the issues of the *Journal of Physics USSR*.

[4] H. London, Proc. Roy. Soc. **A171**, 484 (1939).
[5] P. L. Kapitza, Phys. Rev. **60**, 354 (1941) (this issue).

Letters to the Editor

PROMPT publication of brief reports of important discoveries in physics may be secured by addressing them to this department. Closing dates for this department are, for the first issue of the month, the eighteenth of the preceding month, for the second issue, the third of the month. Because of the late closing dates for the section no proof can be shown to authors. The Board of Editors does not hold itself responsible for the opinions expressed by the correspondents.

Communications should not in general exceed 600 words in length.

On the Isotopic Constitution of Cobalt

JOHN J. MITCHELL, HARRISON S. BROWN AND ROBERT DUDLEY FOWLER
Department of Chemistry, The Johns Hopkins University, Baltimore, Maryland
July 23, 1941

THE question as to whether the cobalt isotope Co^{57} is stable or radioactive is one of considerable interest. Sampson and Bleakney[1] reported the existence of this isotope in 1936, after a mass spectrometric study of $CoCl_2$ vapor. The abundance of Co^{57} was estimated to be about 1 part in 600 of Co^{59}. Their work and the experimental fact that cobalt gives rise to two distinct water-sensitive activities upon neutron irradiation[2] were accepted as quite conclusive proof of the existence of Co^{57} as a stable or very long-lived nuclear species. The deduction that the 36-hour nickel activity[3] is due to Ni^{57} would appear to lend weight to the spectrometric measurements, as the Ni^{57} presumably decays to stable Co^{57}.

However, several rather puzzling features connected with the existence of Co^{57} seemed to warrant a reinvestigation with a mass spectrometer. Co^{57} possesses a stable neighboring isobar Fe^{57}. While this would not be unusual among the heavier nuclei, it is quite unusual among the lighter species. Only one such case exists in the region of low atomic number, namely that of radioactive K^{41}. This particular feature of Co^{57} becomes still more striking when one realizes that the two similar nuclei V^{49} and Mn^{53} are non-existent in nature. It might be well to point out, also, that the existence of Co^{57} proved to be one of but three exceptions to the interesting considerations of Dickinson and Konopinski in their empirical correlation of half-lives.[4]

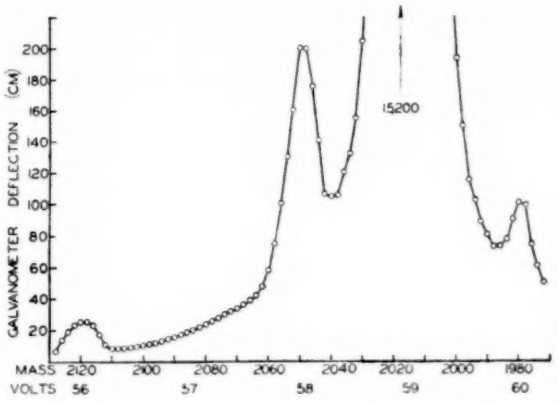

FIG. 1. A typical mass spectrum of cobalt containing a small amount of nickel and iron impurities.

The experimental evidence against the existence of Co^{57} is meager but suggestive. The 70-day Co^{58} has never been observed by slow neutron irradiation of cobalt. It has been produced only by cross bombardment of neighboring elements. The 7-year $(n-\gamma)$ product is quite definitely Co^{60}. The 11-minute $(n-\gamma)$ product is either an isomer of Co^{60} or of Co^{58}. It is to be noted that the existence of nuclear isomerism renders unnecessary the hypothesis of a stable Co^{57} in order to explain the existence of two neutron-induced activities.

We consequently analyzed cobalt with a 180° Dempster-type mass spectrometer of 15-cm radius of curvature.[5] Anhydrous $CoCl_2$ was vaporized in the ion source. The ions were formed by electron bombardment. They were then accelerated through about 2000 volts before entering the magnetic field. Both the Co^+ and the $CoCl^+$ ions were studied. Figure 1 shows a typical mass spectrum of the Co^+ ions. As the $CoCl_2$ contained an appreciable amount of nickel and a small amount of iron, peaks at 60, 58, and 56 can be seen, besides the large peak at 59 corresponding to cobalt. No trace of a peak was observed at mass number 57. Because of the steadiness of the spectrometer, we would be able to detect a peak as low as 2 percent of background. Using this figure, one can see that if Co^{57} exists it must exist to less than 1 part in 30,000 of Co^{59}. The iron impurity was low enough so that the Fe^{57} present in no way interfered with the evaluation of the above limit.

A study of the $CoCl^+$ ions showed no trace of a peak at mass 92, although there were peaks at 91, 93, 94, 95 and 96. Because of the low ion intensities, the limit with the $CoCl^+$ ions could be set at only 1 part in 2000.

From the low limit of 1 part in 30,000 set for the abundance of Co^{57}, one can see that it is quite impossible for the 11-minute cobalt activity to be due to Co^{58}. Consequently, the activity is probably isomeric with the 7-year activity ascribed to Co^{60}.

We wish to thank Dr. H. A. B. Dunning whose financial support made this work possible.

[1] M. B. Sampson and W. Bleakney, Phys. Rev. **50**, 732 (1936).
[2] (a) J. R. Risser, Phys. Rev. **52**, 768 (1937); (b) J. J. Livingood and G. T. Seaborg, Phys. Rev. **53**, 847 (1938); (c) F. A. Heyn, Physica **4**, 160 (1937); (d) Livingood, Seaborg and Fairbrother, Phys. Rev. **52**, 135 (1937).
[3] J. J. Livingood and G. T. Seaborg, Phys. Rev. **53**, 765 (1938).
[4] G. R. Dickinson and E. J. Konopinski, Phys. Rev. **58**, 949 (1940).
[5] Brown, Mitchell, and Fowler, Rev. Sci. Inst. (in press).

Note on the Beta-Ray Energy of H^3

R. D. O'NEAL
University of Illinois, Urbana, Illinois
July 22, 1941

BROWN[1] has recently published a value of 9.5 ± 2 kev for the maximum energy of the beta-rays from H^3. Although this is in disagreement with O'Neal and Goldhaber's[2] previously reported value of 15 ± 3 kev, his experimentally determined range is in essential agreement with

theirs, and the discrepancy is in the use of the range-energy relations.

Since only the result of the latter's measurements, 15 ± 3 kev, has been reported, a few details will be given here. The range was determined simply by varying the pressure of Trost mixture (argon and alcohol in the ratio 9 to 1) in a chamber containing a screen-wall Geiger counter and a previously bombarded beryllium target used as a source of H^3 electrons. This admittedly rough measurement gave as a range for the H^3 electrons 0.46 ± 0.05 mg/cm² of Trost mixture. Data[3,4] of atomic stopping powers for α-particle absorption were used to convert this range into a range in aluminum. Unfortunately, these atomic stopping powers are not particularly well known at this low energy, but by using what seemed the most likely values, a range of 0.48 ± 0.06 mg/cm² of aluminum was found.

Brown's measurements gave a range of 0.23 mg/cm² of helium for these beta-rays. Upon taking, from α-particle data,[3,4] the atomic stopping powers referred to air of 1.25 for aluminum and 0.40 for helium, it was found that this range corresponded to a range of 0.50 mg/cm² of aluminum, a value in good agreement with the above. This treatment for helium seems well justified since Alper,[5] comparing air and helium, showed experimentally, for low energy electrons, that the relative stopping powers for α-particles and for electrons are the same to within the limits of error of his experiment, about 5 percent.

The range of 0.48 mg/cm² of aluminum corresponded, according to the range-energy curve for aluminum in Rasetti's[6] *Elements of Nuclear Physics*, to an energy of 15 ± 2 kev. A plot of Schonland's[7] data for the absorption of homogeneous cathode rays in aluminum showed that this range corresponded to a maximum energy of the beta-rays of about 16 kev. However, since Schonland's data are for extrapolated ranges, one might expect this value to be somewhat high. It may, therefore, be concluded that 15 ± 3 kev is a reasonable value for the maximum energy of the beta-rays from H^3.

[1] S. C. Brown, Phys. Rev. **59**, 954 (1941).
[2] R. D. O'Neal and M. Goldhaber, Phys. Rev. **58**, 574 (1940).
[3] G. Mano, Ann. de physique **1**, 407 (1934).
[4] H. Geiger, *Handbuch der Physik* (1927), Vol. 24, p. 165.
[5] T. Alper, Zeits. f. Physik **76**, 172 (1932).
[6] F. Rasetti, *Elements of Nuclear Physics* (Prentice-Hall, 1936), p. 68.
[7] B. F. J. Schonland, Proc. Roy. Soc. **A108** (1925).

Electrets Made from Dry-Mixed Components

WELLESLEY J. DODDS AND J. D. STRANATHAN
Department of Physics, University of Kansas, Lawrence, Kansas
July 21, 1941

PERMANENT electrets are ordinarily made by mixing the wax and rosin components while in the melted state, and it is known[1] that the thoroughness of mixing affects the subsequent behavior of the electret. A method has been developed for making these electrets from dry-mixed components. The resulting electrets are strong, smooth, and physically uniform. They exhibit the usual electrical characteristics. It appears somewhat easier to duplicate these characteristics by the present method of manufacture than by the usual method.

The "Selected Flora" carnauba wax and the "WG" grade[2] rosin used in making these electrets were first pulverized with a mortar and pestle. Each component was then sifted through a series of sieves with meshes conforming to U.S.B.S. specifications. Equal portions by weight of a chosen size of each powdered component were then mixed in a mechanically driven mixer, the time of mixing being the same in all cases. The desired amount of the dry-mix was weighed out in a tinned pan and placed in an electrode-and-tank system[1] which was immersed in an oil bath. The melting and cooling times for the electret were carefully controlled, and a uniform procedure adopted for all electrets.

Proper choice of particle size is necessary to eliminate two faults which otherwise appear in the resulting electrets. If too large particles are used, stratification into two component layers occurs during melting. If too small particles are used, numerous small bubbles, probably of air, appear on the raised surface of the electret next to the movable electrode.[1] These bubbles can be removed by holding the material at a temperature slightly above its melting point for a longer time, but this procedure causes stratification for still smaller particles. Both stratification and air bubbles can be avoided by using particle sizes smaller than U.S.B.S. #30 but larger than #200.

Electrets made after the method described show the same general shape of reversal curve[1,3-5] as those made by other methods, and are closely reproducible both physically and electrically. Preliminary work indicates a slight particle-size effect on the shape of the reversal curve. The general shape of the reversal curve is given by a simple mathematical relation[5] of exponential form. The reversal times of electrets made in the present investigation were considerably shorter than many of those reported in the literature for electrets of similar composition. This is due to the grade of carnauba wax and rosin used, rather than to the method of manufacture.

[1] W. M. Good and J. D. Stranathan, Phys. Rev. **56**, 810 (1939).
[2] B. A. Brice, J. Opt. Soc. Am. **30**, 152 (1940).
[3] Crumrine, master's thesis, University of Kansas (1933).
[4] G. E. Sheppard, master's thesis, University of Kansas (1941).
[5] W. J. Dodds, master's thesis, University of Kansas (1941).

Effect of Pressure on the Surface Charge of an Electret

GLENN E. SHEPPARD AND J. D. STRANATHAN
Department of Physics, University of Kansas, Lawrence, Kansas
July 30, 1941

PERMANENT electrets[1,2] made of equal parts by weight of "Selected Flora" carnauba wax and "WG" grade[3] rosin have been studied under air pressures from 10 to 228 cm of Hg. The electrets were manufactured under atmospheric pressure by the method described by Good and Stranathan,[4] except that the two components were powdered and mixed dry, as suggested by Dodds and Stranathan.[5] An electric field of 11,000 volts/cm was used

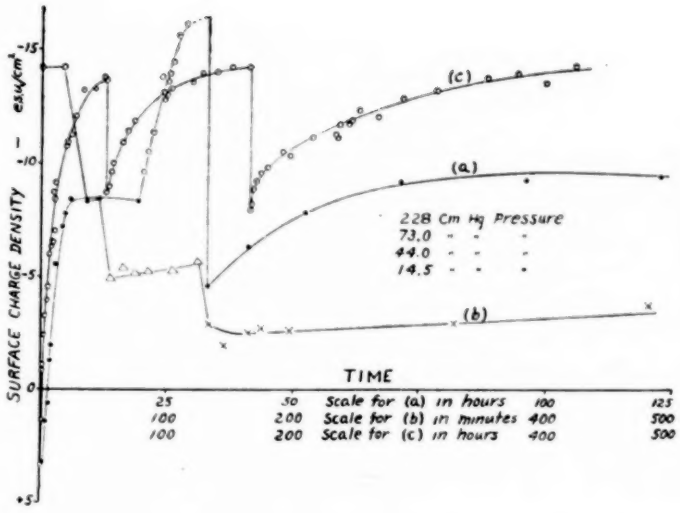

FIG. 1. Surface charge densities on electrets.

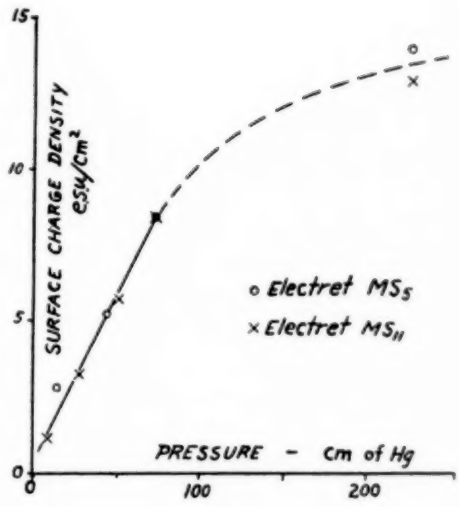

FIG. 2. Surface charge as a function of pressure.

in the manufacture. Immediately after manufacture the electret was placed in a pressure tank in which the pressure could be maintained indefinitely at any desired value. The induction plate used in measuring the surface charge on the electret, along with the mechanism which raised this plate from the electret surface, was housed in this tank. The raising mechanism was controlled electrically from without.

The authors wish to report the following findings: (1) The limiting surface charge density finally appearing on an electret depends upon the air pressure surrounding the electret. Whereas the charge on an electret at atmospheric pressure is roughly 10 e.s.u./cm², the charge is less on the electret if held under reduced pressure, and is greater if held under pressures higher than atmospheric. Figure 1(a) represents the behavior of an electret held originally at atmospheric pressure for 19 hours, then at a pressure of 228 cm of Hg for 14 hours, and finally again at atmospheric pressure. Figure 1(b) represents the surface charge densities attained by an electret held successively at the pressures 228 (P_1), 73.0 (P_2), 44.0 (P_3), and 14.5 (P_4) cm of Hg. The system was changed as rapidly as possible from any one to the next lower pressure. (2) Any newly manufactured electret held at a given pressure gradually acquires a surface charge density characteristic of the pressure. If the pressure is changed, the time required for the electret to build up to the new charge density increases with the age of the electret, or perhaps with the number of changes it has been made to undergo. This is illustrated by Fig. 1(c) for which the pressure was maintained at 228 cm of Hg except for two short intervals. At the end of 51 hours, and again at the end of 166 hours, the pressure was reduced momentarily to atmospheric and increased immediately again to 228 cm of Hg. The manner in which the surface charge builds up along the three sections of the curve illustrates this "aging" effect. That this is truly an effect of age rather than of previous changes which the electret has undergone is shown by the fact that not one of several electrets which had been kept at atmospheric pressure for six weeks or more showed any appreciable increase in surface charge over a period of a week after it was placed under a pressure of 228 cm of Hg. (3) For the electrets studied, the limiting value of the surface charge density is a function of the pressure, as shown in Fig. 2. This function is essentially linear at pressures less than atmospheric.

Electrets made in sufficiently high electric fields finally build up in the normal atmosphere to a surface charge density of about 10 e.s.u./cm², approximately the density corresponding to the break-down of air next a plane surface. If it is the break-down of air that limits the charge density, then one might expect a linear relation between this limiting density and pressure. A straight line could reasonably be drawn in Fig. 2 to represent all the points below atmospheric pressure. The authors would not be surprised if the shape of the curve at higher pressures is influenced by the strength of the electric field used in making the electret. Crumrine[6] has shown that a saturation effect exists at atmospheric pressure in the limiting charge attained by electrets made in stronger and stronger fields. The field of 11,000 volts/cm used in making the present electrets is not far above that for which this saturation effect occurs. Failure of the surface charge to build up proportional to the pressure at higher pressure may well be connected with this saturation effect. One of the authors hopes to observe soon the behavior of electrets made in much larger fields.

[1] M. Eguchi, Phil. Mag. **49**, 178 (1925).
[2] A. Gemant, Rev. Sci. Inst. **11**, 65 (1940).
[3] B. A. Brice, J. Opt. Soc. Am. **30**, 152 (1940).
[4] W. M. Good and J. D. Stranathan, Phys. Rev. **56**, 810 (1939).
[5] W. J. Dodds and J. D. Stranathan, Phys. Rev. **60**, 360 (1941) (this issue).
[6] Crumrine, master's thesis, University of Kansas (1933).

Energies of Gamma-Rays from Br^{82}, I^{131}, I^{130} Mn^{56}, Mn^{54}, As^{74}

MARTIN DEUTSCH AND ARTHUR ROBERTS
Massachusetts Institute of Technology, Cambridge, Massachusetts
July 31, 1941

IN many cases, the best method available for the determination of gamma-ray energies is a study of the energy distribution of secondary electrons by means of a magnetic spectrometer. The "short magnetic lens" spectrometer[1] has been found to be very well suited for this purpose because of the great distance between source and counter, the high transmission factor, and the use of circular sources. The gamma-ray source strengths required are about the same as those needed for reasonably good absorption measurements, namely, from two to ten micrograms radium equivalent per gamma-ray line present, depending on the energy range. With appropriate precautions, very much weaker activities could undoubtedly be measured. Sources weighing as much as several hundred milligrams can readily be used if necessary.

For energies up to about 1.4 Mev the photoelectrons produced in thin (8 to 100 mg/cm²) radiators of high atomic number (Sn, Pt, Au, Pb) permit accurate determination, even if several gamma-rays are present. Above 1 Mev the maximum energy of the Compton electrons can be measured,[2] but only the hardest gamma-ray can be determined accurately by this method because of the low energy tail on the Compton secondary distribution.

The estimated probable error is now about 3 percent of the gamma-ray energy, in the range from 0.3 Mev to 1 Mev, and slightly larger outside this range. About half of this allows for systematic errors, mainly uncertainty about the effect of energy losses in the radiator, and can certainly be greatly reduced by studying these factors. The rest of the error is due to uncertainty in picking the peak of a line in the presence of secondaries from other gamma-rays and can be reduced by adjusting the spectrometer for better resolution.

TABLE I. *Energies of gamma-rays.*

ISOTOPE	PERIOD	GAMMA-RAYS (MEV)	METHOD	REFERENCE
Br^{82}	36 hr.	0.547 0.787 1.35	*P* *P*, *C*? *C*, *P*?	1
I^{131}	7.8 days	0.367 ±0.007	*IC*, *P*, *C*	2
I^{130}	12.6 hr.	0.417 0.535 ±0.01 0.670 0.740	*P* *IC*, *P* *P*, *IC*? *P*	3
Mn^{56}	2.6 hr.	0.832 2.20	*P* *C*	4
Mn^{54}	310 days	0.850 0.120	*P*, *C* *P*	5
As^{74}	17 days	0.582	*P*	6

[1] These gamma-rays have been shown to be in cascade and associated with the entire beta-spectrum by J. R. Downing and A. Roberts, Phys. Rev. **59**, 940A (1941).
[2] This gamma-ray accompanies the entire beta-spectrum [M. Deutsch, Phys. Rev. **59**, 940A (1941)]. Mr. J. R. Downing has shown it to be in cascade with another gamma-ray of 0.080 ±0.002 Mev by critical absorption (private communication).
[3] Previous absorption measurements gave 0.6 Mev for these gamma-rays [J. J. Livingood and G. T. Seaborg, Phys. Rev. **54**, 775 (1938)].
[4] Previous measurements by Curran, Dee, and Strothers (reference 2 of text), in a semi-circular focusing spectrometer gave 0.91 ±0.05 and 2.03 ±0.05 Mev.
[5] The assignment at 0.120 Mev, obtained with a radiator of Sn assumes the observed absorption to be in the *K* shell. If it were in the *L* shell, the *K* line would not have been observed, due to counter window thickness.
[6] The annihilation radiation was also observed.

In this series of measurements we have not, in general, attempted to measure energies less than 0.18 Mev. The letters following the energy values in Table I indicate the method of measurement, in the order of accuracy, *IC* indicating internal conversion, *P* photoelectrons, *C* Compton electrons. A question mark signifies that the particular method confirmed the existence of the gamma-ray but did not yield adequate accuracy. The probable errors are those given in the preceding discussion unless otherwise indicated. Because of uncertainty as to how to correct for the momentum interval with radiators giving line widths comparable to the momentum interval, we can say little concerning intensities at present.

These investigations have been supported in part by a grant from the John and Mary R. Markle Foundation for physiological studies with radioactive iodine. It is a pleasure to acknowledge the friendly interest of Professor Robley D. Evans in these experiments.

[1] M. Deutsch, Phys. Rev. **59**, 684A (1941).
[2] S. C. Curran, P. I. Dee and J. E. Strothers, Proc. Roy. Soc. **A174**, 546 (1940).

Degenerate Non-Ideal Gases and Liquid Helium

L. I. SCHIFF
Randal Morgan Laboratory of Physics, University of Pennsylvania, Philadelphia, Pennsylvania
July 14, 1941

IN two recent papers,[1] the theory of degenerate non-ideal quantum gases was developed in an approximation that considered binary collisions, and an application was made to a simplified model of liquid helium. The present note corrects an error in the evaluation of an integral in I, and discusses an alternative solution for the particle distribution function in II.

The G_1 integral defined by I (29) actually contains a residue as well as a principal value part when expressed as in integral over k'. Thus I (34) should have added to it a term: $(8\pi/\Omega)\sum_{\text{even } l}(2l+1)(\beta\hbar^2/m)(\sin 2\delta_k{}^l)/2$. Similarly, I (35) should have added to it a term: $4\pi\beta\hbar^2\Delta/m\Omega$, where: $\Delta \equiv \lim_{k\to 0}(\sin\delta_k{}^0)/k$. These residue terms dominate in the perturbation theory limit ($V\to 0$),[2] and also in the low temperature limit considered explicitly in II.

In the application to liquid helium, there exists a temperature $T_c > T_0$ below which an alternative solution of the particle distribution equation II (5) appears. Since this solution has lower free energy than I (19), it must be regarded as the appropriate description of the equilibrium state. The calculation is particularly simple in the low temperature limit, in which the range of the two-particle interaction $\ll \hbar/(mkT)^{\frac{1}{2}}$. The leading term in G_1 is then the residue term given above, and condensation takes place if $\Delta < 0$, that is, if there is no bound state of the He_2 molecule ($\Delta = -a$ for a rigid sphere interaction). The parameter x

introduced in I may be taken equal to $|\Delta|\hbar^2N/mkT_0\Omega$; it is assumed that $x \ll 1$. The condensation temperature is then T_c rather than T_0, where $(T_c-T_0)\sim xT_0$. There is a latent heat $\sim x^2RT_0$, and a discontinuity in the specific heat $\sim xR$ (C_v is greater below than above T_c). The specific heat vanishes as $T\rightarrow 0$. These results are in general agreement with those obtained by Lamb and Nordsieck[3] from a perturbation treatment of the inter-particle interactions.

Since the calculation can claim validity only to terms of order x, it appears that a consistent treatment of binary interactions predicts results that are at least in qualitative agreement with experiment. However, in view of the great difficulties encountered in extending such a treatment to higher order collisions (higher orders of x), calculations based on liquid-type models[4] would still seem to be of considerable interest.

It is a pleasure to thank Drs. W. E. Lamb and A. Nordsieck for access to their results prior to publication, and for pointing out the existence of the alternative distribution function.

[1] L. I. Schiff, Phys. Rev. **59**, 751, 758 (1941); referred to here as I and II, respectively. The present notation follows these references.
[2] The writer is indebted to Drs. L. Tisza and E. Teller for pointing out to him that the perturbation theory evaluation of I (29) disagrees with that obtained from I (34) without the residue term.
[3] W. E. Lamb, Jr. and A. Nordsieck, Phys. Rev. **59**, 927 (1941).
[4] L. I. Schiff, Phys. Rev. **59**, 839 (1941).

Vibrational Analysis of CD and CH Bands in the Region of 2260–2500A

L. Gerö and R. F. Schmid
Physical Institute of the Royal Hungarian University of Technical and Economic Sciences, Budapest, Hungary.
June 18, 1941

IN a short note in this journal McDonald[1] reported two red-degraded bands lying at λ2264A and λ2367A and excited by condensed discharges in methane. No further details were known about them up to the present time.

Table I. *Vibrational scheme for* CD.

	$v''=$ 0	1	2	3	4	5	6		
$v'=0$	44,187	42,194	41,440					1092	
1			42,532	41,224				1021	71
2				42,245	40,979			931	90
3					41,910	40,687			
4							40,318		
	1393	1354	1308	1266	1223				
	39	46	42	43					

Table II. *Vibrational scheme for* CH.

	$v''=$ 0	1	2	3	
$v'=0$	44,156	42,234	40,395		1469
1			41,864	40,102	
	1922	1839	1762		
	83	77			

During a more thorough investigation of the entire CD and CH spectrum[2] plates were taken from condensed discharges (with a rotating spark gap in series) in helium containing small amounts of vapor from heavy paraffin and ordinary benzol. They show, in the region mentioned, several faint bands of similar structure. All of the heads could be arranged in the vibrational scheme shown in Tables I and II.

While the vibrational structure is rather narrow in respect to the known CD and CH bands, the first and second vibrational differences are related as the ratio of the reduced mass (i.e., its square root) of the isotopic molecules CD and CH. This fact and the circumstances of excitation, together with the apparently singlet structure of the bands, suggest that the ions CD^+ and CH^+ are the emitters.

[1] F. C. McDonald, Phys. Rev. **29**, 212 (1927).
[2] Cf. L. Gerö and R. F. Schmid, Phys. Rev. **59**, 528 (1941).